SYNTHESIS OF ORGANIC-INORGANIC HYBRIDS FOR THE ELECTROCATALYTIC DETECTION OF BIOLOGICALLY ACTIVE MOLECULES

By

ADEGUNLOYE AJIBOLA VINCENT

(Student Number: 218097981)

A thesis in fulfilment of the requirement for the degree

DOCTOR OF PHILOSOPHY

In

CHEMISTRY

In the

DEPARTMENT OF CHEMICAL SCIENCES

FACULTY OF SCIENCE

UNIVERSITY OF JOHANNESBURG

Supervisor: DR ORPAH ZINYEMBA

Co-Supervisor: PROF KAUSHIK MALLICK

JULY 2021

DECLARATION

I hereby declare that this Thesis, which I herewith submit for the research qualification.

PHILOSOPHIAE DOCTOR IN CHEMISTRY

to the University of Johannesburg, Department of Chemical Science, is, apart from the recognized assistance of my supervisors, my own work and has not previously been submitted by me to another institution to obtain a research diploma or degree.

_____ on this _____ day of _____

(Candidate)

_____ on this _____ day of _____

(Supervisor)

_____ on this _____ day of _____

(Co-supervisor)

DEDICATION

This work is dedicated to God, the Father of my Lord Jesus Christ, who has been everything to me in life. Also, to my lovely wife Mojirade Francisca Adegunloye, my parents, Dr & Mrs F.O Adegunloye, and my siblings, Busayo, Richard, and Toyin.

ACKNOWLEDGEMENTS

I want to express my sincere gratitude to the following people and organizations for their assistance, support, insight, and dedication to this work's success.

- I want to express my profound gratitude to my supervisors, Dr. Orpah Zinyemba and Prof Kaushik Mallick, for their supervision, advice, kind assistance, encouragement, and guidance throughout this work.
- I want to thank the Material Science Research group members for the precious time we had together.
- My heartfelt gratitude goes to every member of my family who stood by me during this period of my study: Dr. and Mrs. Francis Adegunloye, Engr and Mrs. Festus Adegunloye, Engr and Mrs. Asuku, Dr. and Dr. Mrs. Arawomo, and Mr. Emmanuel Akinnagbe for their prayers, love, and encouragement.
- I am grateful to every member of the association of Catholic students and Peace House Discipleship center, University of Johannesburg.
- My affectionate appreciation to my dearest Queen, Adegunloye Mojirade, for her understanding and contributions to realizing this goal. My friends, Dr. Gbenga Peleyeju, Ngulde Waziri, Oseghale Charles, Dr. Akinnawo Christianah, Dele Peter, Akinbile Babatunde, Dr. Habtegiorghies Yonas, Dr. Venkata Kishore and Awe Babatunde, are also appreciated for their support.
- I wish to thank all the academic, administrative, and technical staff of the Department of Chemical Science, University of Johannesburg, who contributed to my Ph.D. programme's success.
- Above all, I am eternally grateful to God Almighty for His grace and mercy upon my life throughout this period and forever.
- I greatly acknowledge the financial support from the National Research Foundation/The World Academy of Science (NRF/TWAS) of South Africa with grant-specific unique reference number SFH170710250936, NRF (UID: 110949), and the University of Johannesburg, South Africa.

PUBLICATIONS

The following are the journal articles published (or submitted for publication) as a Ph.D. student. Articles 1, 2, and 3 form chapters 4, 5, and 6, respectively, of this dissertation.

1. Adegunloye, Ajibola, Venkata K. Perla, Sarit K. Ghosh, Orpah Zinyemba, and Kaushik Mallick. "Electrochemical and electrical response of bismuth-aniline complex under the exposure of organic and inorganic environment." *SN Applied Sciences* 2, no. 12 (2020): 1-10. (***Published***).

2. **Adegunloye, Ajibola**, Ibrahim Ngulde, Sarit K. Ghosh, Venkata K. Perla, Orpah Zinyemba, and Kaushik Mallick. "Electric field induced polarization and electrochemical sensing performance of nickel based organic-inorganic hybrid system." (**Manuscript under review**).

3. Adegunloye, Ajibola, Orpah Zinyemba, and Kaushik Mallick. "Electrochemical recognition of uric acid and dopamine using cobalt-sulfide aniline complex within an organic and inorganic complex." (Manuscript to be submitted).

4. Adegunloye, Ajibola, Orpah Zinyemba, and Kaushik Mallick. "Biological synthesis of silver nanoparticles reduced graphene oxide using *Aloe ferox* plant for dopamine detection." (Manuscript to be submitted, not part of the thesis).

ABSTRACT

Biomedical diagnosis and testing are often accompanied by inefficiencies, including high-priced tests, high detection limits, and interference from other biologically relevant molecules. To overcome such inefficiencies, the construction of electrochemical sensors has attracted interest due to their promising nature. They are simple to fabricate, and they offer high sensitivity and selectivity and low detection limits. In this research work, aniline and some transition metals were used to form complex materials as tools in electrochemical biosensor fabrication. In general, cyclic voltammetric (CV), square wave voltammetric (SWV), and chronoamperometric techniques were employed to model the aniline metal complexes electrochemical reactivities on working glassy carbon electrodes. Fourier transformed infrared spectroscopy (FTIR), Transmission electron microscopy (TEM), Scanning electron microscopy (SEM), X-ray photoelectron spectroscopy (XPS), X-ray diffraction (XRD), Nuclear magnetic resonance (NMR), and Elemental analyzer (EA) were used for further characterization. Furthermore, the materials were employed for electrocatalytic detection of biologically active molecules.

In this regard, aniline-based metal complexes of bismuth, nickel, and cobalt were synthesized, characterized, and applied for the electrocatalytic detection of biologically active molecules. The complexes were synthesized by a simple complexation method using aniline as a ligand. The as-prepared complexes were deposited on the glassy carbon electrode (GCE) using the drop and dry method and investigated as an electrocatalyst for the efficient and sensitive detection of dopamine, iodine, uric acid, and cysteine. The hybrid materials showed good voltammetric sensor application for the detection of biologically active molecules. The results indicated that the electrodes modified with the complex materials could detect micromolar concentrations of dopamine, iodine, uric acid, and cysteine. The bismuth aniline complex (BAC) indicated 12.3 μM and 23.17 μM low detection limits for dopamine and iodine, respectively. The nickel aniline complex (NAC) revealed a 2.09 μM limit of detection and a wide linear range of 2.5 μM-220 μM for cysteine detection. The cobalt-aniline complex (COAC) indicated 9.26 μM and 9.52 μM limit of detection for uric acid and dopamine respectively, with linear ranges of 20 – 280 μM and 10 – 200 μM. The developed sensors could eliminate the interference of other biomolecules such as ascorbic acid, glucose, and histamine, to mention a few. The sensors were only selective to the analytes of interest. The electrochemical sensors developed in this work demonstrate good potential for the molecular diagnosis of neurological disorders such as Parkinson's disease.

TABLE OF CONTENTS

LIST OF FIGURES

LIST OF TABLES

LIST OF SCHEMES

LIST OF ABBREVIATIONS

5HT	Serotonin
BAC	Bismuth-aniline complex
BAM	Biologically active molecules
CA	Chronoamperometry
CCD	Charge-coupled device
CE	Capillary electrophoresis (CE)
CE	Counter electrode
COAC	Cobalt aniline complex
CV	Cyclic Voltammetry
CWES	Coated Wire Electrodes
Cys	Cysteine
DA	Dopamine
DMSO	Dimethylsulfoxide
EA	Elemental analysis
EC	Electrochemical
EEG	Electroencephalography
Ef	Final potential
Ei	Initial potential
EIS	Electrochemical impedance spectroscopy
E_{pa}	Anodic peak potential
E_{pc}	Cathodic peak potential
FETS	Field Effect Transistors
FTIR	Fourier Transform Infrared Spectroscopy
FWHM	Full width at half maximum
GCE	Glassy carbon electrode
HPLC	High-pressure liquid chromatography
HR-TEM	High Resolution-Transmission electron microscopy
ICP-MS	Inductively coupled mass spectrometry
IES	Ion-selective electrodes
I_{pa}	Anodic current
I_{pc}	Cathodic current
IR	Infrared
JCPDS	Joint committee on powder diffraction standards

KI	Potassium Iodide
L-DOPA	Levodopa
LOD	Limit of detection
MRI	Magnetic resonance imaging
MS	Mass spectroscopy
NAC	Nickel-aniline complex
NMR	Nuclear Magnetic Resonance Spectrometry,
NTs	Neurotransmitters
PBS	Phosphate buffer saline
PD	Parkinson's disease
POC	Point of care
RC	Resistor-capacitor
RE	Reference electrode
SE	Secondary electrons
SEM	Scanning electron microscopy
SK	Sandell-Kolthoff
SWV	Square wave Voltammetry
TEM	Transmission electron microscopy
UHV	Ultra-High Vacuum
UMEs	ultra-micro electrodes
UV-vis	Ultraviolet visible spectroscopy
WE	Working electrode
WHO	World Health Organization
XPS	X-ray photoelectron spectroscopy
XRD	X-ray diffractometry

CHAPTER 1
INTRODUCTION

1.1 Background Information

The development of cheap, easy-to-use, yet sensitive biosensing devices for early detection of disease biomarkers has become significant due to their wide application in the environment [1], foods [2,3], disease monitoring [4], monitoring of drugs [5], agriculture [6], and industries [7], etc. Most importantly, in disease monitoring, biosensors are of immense use to monitor and detect diseases that have infected human blood. The root cause of these diseases has been through industrialization, which has caused resource depletion and impaired humans health by exposing them to new conditions through pollution. These diseases can also be traced to the imbalance of essential biological molecules in the body. Diagnostic tests are usually conducted to monitor and detect these molecules in human fluid with the aid of conventional techniques such as capillary electrophoresis [8], fluorescence spectrometry [2], colorimetry [9], high-performance liquid chromatography (HPLC) [10,11,12]; just to mention a few. However, these techniques are accompanied with a handful of drawbacks that includes high-priced test, the requirement of experts to conduct analyses, the laborious task, coupled with the time consuming [13]. Therefore, it is pertinent to pursue user-friendly, faster, miniaturized, and convenient techniques that could complement existing analytical methods and assure good quality results to resolve these challenges.

Point-of-care (POC) diagnostic devices hold a lot of promise for diagnostic testing. POC devices such as the glucose biosensor used to monitor patients' blood glucose levels can fulfill the requirements expected from a present-day analytical device. POC devices are flexible, highly adaptive, versatile, and useful in health and environmental applications. The POC devices market has soared, constituting 85% of the world market for biosensors [14]. As a result, hybrid material /nanomaterial-based electrochemical sensors have gained attention due to their promising nature. They are simple to fabricate, and they offer high sensitivity and low detection limits [15]. These sensors can serve as a firm foundation for the detection of diseases. They can convert biological or chemical responses into such an analytically measurable signal.

Electrochemical-based sensors consist of three main components; a chemical recognition element, a transducer, and a data acquisition device. The chemical recognition element is

made up of an active sensing material such as a polymer, carbon nanotubes, graphene, and metal nanoparticles, which can interact with the target molecule. The transducer component transforms the recognition occurrence to an analytically measurable signal. The last component of an electrochemical sensor is the signal processing system, which transforms the measurable signal into a visual format.

The main focus of this work is the synthesis of aniline-based transition metal complexes and their applications for electrochemical sensing of biologically active molecules. Aniline transition metal complexes could successfully detect electrochemically active molecules. Furthermore, the aniline-based metal complexes electrode modifiers could serve as platforms for developing the next-generation sensors/biosensors.

1.2 Problem Statement and Research Motivation

Specific biological molecules play important functions in the human body and brain. For example, the biological molecules sometimes act as neurotransmitters (NTs) in the cardiovascular, hormonal, and central nervous systems. These molecules perform functions including metabolism, mental activity, emotional expression, cell growth, thyroid hormones, and neurotransmission. Examples of such biological molecules are ascorbic acid and dopamine. However, the imbalance of these molecules in the body can be detrimental to health; for example, low dopamine levels may lead to Parkinson's disease associated with slowed movement, tremors, impaired posture, and imbalance; to mention a few [16,17].

In contrast, high dopamine levels may lead to schizophrenia (a chronic psychiatric disorder) and obesity [14,16]. Also, iodine is required in the human body in trace amounts, but it is essential for producing thyroid hormones such as thyroxine (T4) and triiodothyronine (T3). These hormones assume a crucial role in a broad range of bodily functions, including bone health, immune response, metabolism, and the central nervous system. Iodine deficiency may lead to goiter, hypothyroidism, and possibly intellectual disabilities in infants, while severe cases can worsen hyperthyroidism and hypothyroidism [18,19]. The World Health Organization (WHO) has estimated the number of individuals affected globally and die annually owing to irregular neurological activity, approximately 6.8 million [20]. Hence, the rapid and selective detection of these biologically active molecules is imperative.

Electroanalytical Chemistry has established an analytical substitute for the analysis of neurochemicals using electrochemical-based sensors. These electrochemical sensors have

advantageous properties such as high selectivity and sensitivity, swift responses, simplicity, reproducibility, good controllability, and real-time detection [21,22]. To achieve sensitivity in electrochemical sensors, the surface of the electrodes needs to be improved by modification. In the current project, aniline-based transition metal complexes were chosen to act as modifiers. Aniline has an amine site for potential metal coordination such that its interaction with some selected metal ions gave rise to novel catalytic, luminescence, and other properties of the complexes formed. Aniline also has proficient redox behavior especially when oxidized. Furthermore, it can mediate the electron shuttling between the reaction sites to the electrode surface, making it an efficient conducting platform for electrochemical sensors [21]. The transition metal ion also imparted some desirable properties to the aniline complex, such as good thermal stability and mechanical strength. This research work addressed developing a protocol for incorporating the metal ions into the organic matrix and the strategy to fabricate an electrochemical sensor platform. The electrochemical sensors fabricated using metal-aniline complexes have exciting prospects for the analysis of biological molecules.

1.3 Justification

The need for quick and selective detection of biologically active molecules for humankind's health and economic prosperity cannot be overemphasized. The effective fabrication of highly sensitive and selective electrochemical sensors to satisfy this need is a definite necessity. The justification for the proposed study is the need for a moderately low cost, miniaturized, and convenient nano-sensor system with sample integrity for onsite application. Aniline-based metal complexes have been indicated to hold a huge potential for improving the working electrode's performance in sensor fabrication, thereby increasing the chances of sensing the biological molecules. The integration of transition metal with aniline offers a significant impact on biosensing. Transition metals salts of bismuth, cobalt, and nickel can provide a large surface area, electrochemical stability, and catalysis behavior. Thus, these transition metals could make a significant contribution to the advancement of electrochemistry technology.

The design and construction of transition metal-based biosensors are an exciting area of research in healthcare applications. Hybrids containing transition metals are suitable supportive materials for electrocatalytic processes as they have intriguing surface structure, excellent electrical and mechanical properties, limited aggregation, high stability, and outstanding performance. Composites made with aniline monomer and transition metals of Bi

[23,24], Co [25], and Ni [26,27] have previously been constructed for sensing applications, but no evidence on the synthesis of aniline metal complexes using the oxidized species of Bi, Co, and Ni for sensing applications. There are some pieces of evidence that Bi, Co, and Ni preferentially formed a metal-ligand complex with aniline with tetrahedral geometry. The synergistic properties of aniline and the transition metals provided a good electrochemical response for the detection of biological molecules. The proposed sensor was also free from coexisting molecules that could act as interferences.

1.4 Aims and objectives

1.4.1 Aims

This study aims to develop improved electrochemical sensors for the electrochemical detection of some biologically active molecules using aniline-based transition metal complexes synthesized with a simple complexation method.

1.4.2 Objectives

The specific objectives of this project are as follows:

I. To prepare suitable aniline complexes of bismuth, cobalt, and nickel for the fabrication of a biosensor.

II. To fabricate the complexes into the working electrodes.

III. To investigate the morphology, structural pattern, binding ability, and the interaction between the transition metals and the aniline moiety.

IV. To carry out the optical and electrochemical characterization of the synthesized aniline metal complexes.

V. To investigate the catalytic sensor responses for the aniline metal complexes electrodes.

VI. To apply the fabricated electrodes for the detection of biologically active molecules.

1.5 Thesis Statement

Electrochemical sensor platforms for detecting biologically active molecules with enhanced and good sensor performance can be developed using aniline and transition metals complexes as fabrication materials.

1.6 Thesis Outline

The thesis comprised seven chapters:

Chapter 1: This chapter presents a general introduction, research problem, motivation, justification, thesis statement, aim and objectives of the proposed research, and an outline of the thesis.

Chapter 2: This chapter entails reviewing some biologically active molecules, electrochemical sensors, and their market value, transition metal complexes, and their role in the fabrication of sensors.

Chapter 3: This chapter discusses the materials, methodology, design, and apparatus used in this work. The different characterization and electrochemical techniques used are discussed, as well.

Chapter 4: This chapter contains a report on the synthesis and application of the bismuth aniline complex for the electrochemical detection of iodine and dopamine.

Chapter 5: This chapter discusses the synthesis, characterization, and application of nickel aniline complex for cysteine electrochemical sensing.

Chapter 6: This chapter reports on the electrochemical recognition of uric acid and dopamine using the cobalt-aniline complex.

Chapter 7: This chapter presents the general conclusion and recommendation and future projects established on the findings obtained in this current research.

1.7 References

[1] Pisoschi, A. M. (2016). Potentiometric biosensors: concept and analytical applications-an editorial. *Biochem Anal Biochem*, *5*(3), 19-20.

[2] Safardoust-Hojaghan, H., Amiri, O., Hassanpour, M., Panahi-Kalamuei, M., Moayedi, H., & Salavati-Niasari, M. (2019). S, N co-doped graphene quantum dots-induced ascorbic acid fluorescent sensor: Design, characterization and performance. *Food Chemistry*, *295*, 530-536.

[3] Singh, A., Poshtiban, S., & Evoy, S. (2013). Recent advances in bacteriophage based biosensors for food-borne pathogen detection. *Sensors*, *13*(2), 1763-1786.

[4] Wang, Q., Liu, F., Yang, X., Wang, K., Wang, H., & Deng, X. (2015). Sensitive point-of-care monitoring of cardiac biomarker myoglobin using aptamer and ubiquitous personal glucose meter. *Biosensors and Bioelectronics*, *64*, 161-164.

[5] Garzón, V., Pinacho, D. G., Bustos, R. H., Garzón, G., & Bustamante, S. (2019). Optical biosensors for therapeutic drug monitoring. *Biosensors*, *9*(4), 132.

[6] Antonacci, A., Arduini, F., Moscone Dinia, D., Palleschi, G., & Scognamiglio, V. (2016). Commercially available (Bio)sensors in the Agrifood sector. In *Comprehensive Analytical Chemistry*; Elsevier: 74, 315–340.

[7] Dhall, P., Kumar, A., Joshi, A., Saxsena, T. K., Manoharan, A., Makhijani, S. D., & Kumar, R. (2008). Quick and reliable estimation of BOD load of beverage industrial wastewater by developing BOD biosensor. *Sensors and Actuators B: Chemical*, *133*(2), 478-483.

[8] Wang, W., Xu, G., Cui, X. T., Sheng, G., & Luo, X. (2014). Enhanced catalytic and dopamine sensing properties of electrochemically reduced conducting polymer nanocomposite doped with pure graphene oxide. *Biosensors and Bioelectronics*, *58*, 153-156.

[9] Leng, Y., Xie, K., Ye, L., Li, G., Lu, Z., & He, J. (2015). Gold-nanoparticle-based colorimetric array for detection of dopamine in urine and serum. *Talanta*, *139*, 89-95.

[10] Saetre, R., & Rabenstein, D. L. (1978). Determination of cysteine in plasma and urine and homocysteine in plasma by high-pressure liquid chromatography. *Analytical Biochemistry*, *90*(2), 684-692.

[11] Carvalho, F. D., Remião, F., Valet, P., Timbrell, J. A., Bastos, M. L., & Ferreira, M. A. (1994). Glutathione and cysteine measurement in biological samples by HPLC with a glassy carbon working detector. *Biomedical Chromatography*, *8*(3), 134-136.

[12] Cole, D. E., Lehotay, D. C., & Evrovski, J. (1998). Simplified simultaneous assay of total plasma homocysteine and methionine by HPLC and pulsed integrated amperometry. *Clinical Chemistry*, *44*(1), 188-190.

[13] Anajafi, Z., Naseri, M., Marini, S., Espro, C., Iannazzo, D., Leonardi, S. G., & Neri, G. (2019). $NdFeO_3$ as a new electrocatalytic material for the electrochemical monitoring of dopamine. *Analytical and Bioanalytical Chemistry*, *411*(29), 7681-7688.

[14] Newman, J. D., & Turner, A. P. (2005). Home blood glucose biosensors: a commercial perspective. *Biosensors and Bioelectronics*, *20*(12), 2435-2453.

[15] Nekrassova, O., Lawrence, N. S., & Compton, R. G. (2003). Analytical determination of homocysteine: a review. *Talanta*, *60*(6), 1085-1095.

[16] Noroozifar, M., Khorasani-Motlagh, M., & Taheri, A. (2010). Preparation of silver hexacyanoferrate nanoparticles and its application for the simultaneous determination of ascorbic acid, dopamine and uric acid. *Talanta*, *80*(5), 1657-1664.

[17] Baccarin, M., Santos, F. A., Vicentini, F. C., Zucolotto, V., Janegitz, B. C., & Fatibello-Filho, O. (2017). Electrochemical sensor based on reduced graphene oxide/carbon black/chitosan composite for the simultaneous determination of dopamine and paracetamol concentrations in urine samples. *Journal of Electroanalytical Chemistry*, *799*, 436-443.

[18] World Health Organization. (2007). Assessment of iodine deficiency disorders and monitoring their elimination: a guide for programme managers, 3rd ed. World Health Organization.

[19] Pearce, E. N., Lazarus, J. H., Moreno-Reyes, R., & Zimmermann, M. B. (2016). Consequences of iodine deficiency and excess in pregnant women: an overview of current knowns and unknowns. *The American Journal of Clinical Nutrition*, *104*(suppl_3), 918S-923S.

[20] Elizabeth, S. (2007) WHO Report; Million have neurological disorder worldwide, Neurology Today 7, 25.

[21] Jackowska, K., & Krysinski, P. (2013). New trends in the electrochemical sensing of dopamine. *Analytical and Bioanalytical Chemistry*, *405*(11), 3753-3771.

[22] Raj, C. R., Okajima, T., & Ohsaka, T. (2003). Gold nanoparticle arrays for the voltammetric sensing of dopamine. *Journal of Electroanalytical Chemistry*, *543*(2), 127-133.

[23] Jain, R., Tiwari, D. C., & Shrivastava, S. (2014). Polyaniline–bismuth oxide nanocomposite sensor for quantification of anti-parkinson drug pramipexole in solubilized system. *Materials Science and Engineering: B*, *185*, 53-59.

[24] Khan, A., Khan, A. A. P., Rahman, M. M., Asiri, A. M., & Al-Youbi, A. O. (2015). Toward designing efficient rice-shaped polyaniline@ bismuth oxide nanocomposites for sensor application. *Journal of Sol-Gel Science and Technology*, *76*(3), 519-528.

[25] Nandapure, B., Kondawar, S., Salunkhe, M., & Nandapure, A. (2013). Nanostructure cobalt oxide reinforced conductive and magnetic polyaniline nanocomposites. *Journal of Composite Materials*, *47*(5), 559-567.

[26] Ahmad, S., Ali Khan, M. M., & Mohammad, F. (2018). Graphene/nickel oxide-based nanocomposite of polyaniline with special reference to ammonia sensing. *ACS Omega*, *3*(8), 9378-9387.

[27] Azharudeen, A. M., Karthiga, R., Rajarajan, M., & Suganthi, A. (2020). Fabrication, characterization of polyaniline intercalated NiO nanocomposites and application in the development of non-enzymatic glucose biosensor. *Arabian Journal of Chemistry*, *13*(2), 4053-4064.

CHAPTER 2
LITERATURE REVIEW

2.1 Introduction

This chapter describes a general literature review of the various concepts relevant to this study. A brief overview of biologically active molecules and their examples as well as the high and low concentration problems associated with some selected biologically active molecules in human beings. A general overview of sensors with emphasis on electrochemical sensors and their transducing methods. Furthermore, an overview of transition metal complexes as sensors and a brief review of the transition metal complexes-based electrochemical sensors for sensing biologically active molecules was also presented.

2.2 Analytes

An analyte is a substance or chemical constituent that is being identified and measured. Analytes are at times referred to as a component of blood or another body fluid. For this project, analytes are biologically active molecules.

2.3 Biologically active molecules

To define a biologically active molecule, we need first to introduce what a biomolecule is. A biomolecule, otherwise known as a biological molecule, is a commonly used term for molecules found in organisms central to one or more usual biological functions, including cell division, morphogenesis, or development [1].

Biologically active molecules exert a direct physiological effect on living organisms. Examples of these biologically active molecules are alanine, cysteine, tyrosine, and glycine, but to mention a few. These physiological impacts may be positive or negative, contingent upon the molecule, the dosage, or the bioavailability [2].

Some important classes of biomolecules includes carbohydrates, enzymes, nucleic acids, amino acids, and vitamins. We focused on some of the essential biomolecules in this project: amino acids such as dopamine and cysteine. The amino acids are important biomolecules containing both amine (NH_2) and carboxyl (-COOH) functional groups. In biological systems, these amino acids are the building blocks of proteins. Some amino acids are biosynthetic precursors for neurotransmitters. For instance, the aromatic amino acids

(tryptophan, tyrosine, phenylalanine) are the biosynthetic precursors for the neurotransmitter's serotonin, dopamine, and norepinephrine.

Other molecules that exert a physiological effect on humans looked upon in this project are iodine and uric acid. Hence, we categorize them as biologically active molecules. Iodine is a fundamental component for the thyroid gland being the vital constituent of the thyroid hormones thyroxine (T4) and triiodothyronine (T3), which control a variety of physiological processes, including protein synthesis and enzymatic activity, and are significant indicators of metabolic activity [3]. The other bioactive molecule, uric acid, has strong antioxidant properties that can neutralize considerable numbers of free radicals. As a matter of fact, over half the antioxidant capacity of blood plasma in human being comes from uric acid [4,5]. Dopamine and iodine are further discussed in the next sections.

2.4 Dopamine – definition and function

Dopamine (DA) is a biogenic monoamine that belongs to the catecholamine family of neurotransmitters and very significant to humans [6]. It can be found or produced in the brain, adrenal glands, as well as central nervous system. A molecule of dopamine comprises a catechol structure (a benzene ring containing two hydroxyl side groups) with one amine group attached by an ethyl chain.

DA performs a crucial function in the renal, mammalian hormonal, cardiovascular, and central nervous systems [7,8]. It is commonly related to motivation, pleasure, movement, attention, mood, sleep, behavior, arousal, and reward within the brain [9]. Besides, it's involved in controlling cognition and emotion. It has the responsibility of sending signals between the brain and different nerve cells of the body. The imbalance or depletion of dopamine in the central nervous system may result in various neurological disorders such as senile dementia, Parkinson's disease, and schizophrenia [10,11]. The last two conditions are important to this study; hence they are discussed in the sections below.

2.4.1 Diseases linked to Dopamine

2.4.1.1 Parkinson disease

This is a disease that is best known for uncontrollable tremors. Parkinson's disease (PD) is characterized by a dramatic decrease in dopamine-secreting cells in the substantia nigra, contributing to motor impairment [12,13,14]. This disorder is usually predominant among individuals above the age of 50 as the gradual decline in dopamine cells hits a critical level

for the disease to manifest. However, juvenile cases have been reported on rare occasions [15].

Individuals suffering from PD suffer a gradual loss of memory and a subsequent increase in behavioral disturbances [16]. These occur as early symptoms, and as they become pronounced, patients may have trouble talking, walking, or completing other simple tasks. These symptoms begin to appear when the loss of nerve cells in the mid-brain approaches 80%. Cases of PD can either be acquired, genetic or idiopathic, meaning no origin is known. PD is treatable, particularly when at its early stage. The use of L-DOPA (Levodopa), the metabolic precursor of dopamine, for the treatment of PD at its early stages has proved to be effective as it provides much-improved mobility for the patients [17,18]. However, when L-DOPA is prescribed for such a long period, some unpleasant side effects might result.

2.4.1.2 Schizophrenia

Schizophrenia is a severe psychiatric illness that affects a little less than 2% of the human population worldwide [16]. It's a chronic and painful condition characterized by distortion in a person's ability to think, feel, and behave clearly. Individuals with schizophrenia require lifetime treatment and are bound to die younger than the overall population because of other underlying medical conditions such as diabetes and heart diseases [19]. Research has revealed that schizophrenia affects both men and women equally but may spring up earlier in the younger ones, mostly the male counterparts [20,21].

Possible symptoms that are associated with schizophrenia can either be classified as positive, negative, and cognitive. Individuals with positive symptoms often "lose touch" with reality. They develop symptoms such as hallucinations, thought disorders, and movement disorders, and delusions. Individuals with negative and mental symptoms, on the other hand, exhibit disruptions to normal emotions, behaviors, and thinking. These include a deficit in attention, motivation, executive, and memory functions [22,23,16]. Schizophrenia can be treated (usually lifetime) with medicines, psychosocial support, and coordinated specialty care services to reduce symptoms and improve quality of life.

2.5 Iodine and its importance

Iodine is a significant mineral needed in the human diet for the proper functioning of the thyroid hormone required for the growth of the central nervous system, metabolism, bone health, and immune response [24]. Iodine helps synthesize triiodothyronine (T3) and

thyroxine (T4) for the thyroid to function properly. It occurs more in the form of salt than element; hence, its majorly referred to as iodide.

Iodine inadequacy affects more than a billion individuals and recognized as the world's top correctable factor of brain damage worldwide [25]. Consequently, it is necessary to prevent iodine deficiencies by adding a well-controlled intake of this element in foods such as table salt [26]. Iodine is used in industrial applications for the preparation of intermediary compounds used in synthesizing various chemicals. An iodine imbalance can result in an underactive or overactive thyroid. Too little or too much iodine intake may result in symptoms of hyperthyroidism or hypothyroidism [27]. Goiter frequently accompanies these conditions. In pregnant women, iodine deficiency can cause spontaneous abortion, growth retardation in the fetus, and still-birth [28]. Iodine deficiency in infants and children can cause neurodevelopmental deficits by impairing their intelligence level as measured by IQ [27,29,30]. The efficient determination of iodine is thus important in several domains, including health and the environment.

There are several analytical methods employed for the detection of iodine such as capillary electrophoresis [31,32,33], colorimetry [34,35,36,37], ion-exchange chromatography [38,39,40], spectrophotometry [41,42,43], and electrochemistry [44,45,46]. The most commonly used method was coulometry by the Sandell–Kolthoff reaction, in which yellow cerium (IV) is reduced to cerium (III) by As^{3+} in the presence of iodide ions [47]. These techniques are nevertheless high-priced, time-consuming, outdated, and involve complicated laboratory management and instrumentation [48]. Also, some of the technique's performances have been hampered and influenced by coexisting anions [49]. Therefore, finding a suitable anion-selective sensor could resolve these challenges. The detection of iodine needs a simple and sensitive approach utilizing cost-effective probes that allow no additional sample preparation or reagents. Electrochemical techniques present the characteristics of being fast, selective, sensitive, moderately inexpensive, and easy to implement.

2.6 Sensor

It is a device, module, or system that detects and converts signal (biological, physical, or chemical) into a signal measured electrically. Sensors contain transducers that change one form of energy into another. A sensor can be likened to an architecture of the human sense organs such as the eye, ear, and nose, acting as a stimulus receptor and communicating with a transducer that eventually leads to a signal that reaches the brain. In comparison, the human

senses transforms the input variable into an electric signal in the brain is the same way a sensor transforms the input variable into an electric signal appropriate for measurement [50].

2.7 Types of Sensors

Sensors can be ordered into two classifications based on the means of detection used in the sensor.

2.7.1 Biosensor/Biological Sensor

It is an analytical device that comprises a transducer and a biological element used to detect an analyte. The biological element may be a nucleic acid, an enzyme, or an antibody that binds with the target molecule. The transducer translates the ensuing biological response into electric signals by the transducer.

2.7.2 Chemical sensor

It is an analytical tool used to recognize a chemical substance that integrates a chemical constituent with a physicochemical detector. The chemical constituent usually contains a compound or group of compounds acting as the receptor. The receptors (synthetic) have in their structure, functional groups that can selectively interact with an analyte of interest, changing its physical properties so that the detector can gain an electric signal.

The synthetic receptors are more stable than biological ones used for biosensors. They also have a molecular weight that is moderately small and can bind more strongly to the analyte. Their primary downside is their comparatively poor biocompatibility. Chemical sensors are useful in various areas, including medicine, environmental pollution, home safety, and several others.

2.7.2.1 Types of Chemical sensors

Chemical sensors can be categorized according to the transducer operating principle:

1. Electrochemical sensor: Amperometric, Potentiometric, and Conductimetric/Impendence,

2. Optical sensor: fluorescence, absorbance, luminescence, reflectance, refractive index, optho-thermal, light scattering,

3. Electrical sensor: metal oxide, an organic semiconductor, electrolytic conductivity sensors, electric permittivity,

4. Mass sensitive sensor,

5. Thermometric sensor,

6. Magnetic sensor.

Electrochemical sensors are the most promising sensor due to their user-friendly advantages, low detection limits, low cost, a wide linear response range, and good stability and reproducibility [51].

2.8 Electrochemical sensors

According to IUPAC, electrochemical sensors are associated with a group of chemical sensors wherein the device's receptor part is connected to an electrochemical transducer [52]. Thus, it provides an effective way to analyze a sample by directly converting a reactant to a product with the generation of electric signals.

The electrochemical sensor principle can be explained by the chemical reaction occurring between an analyte and the conductive material (as a working electrode), which is monitored electrochemically. After that, the transducer transforms the result of the analyte and electrode's electrochemical interaction into a suitable electric signal in the form of an oxidation/reduction peak of the analyte at a specific potential value. This signal confirms the presence of an analyte of interest (Figure 2.1).

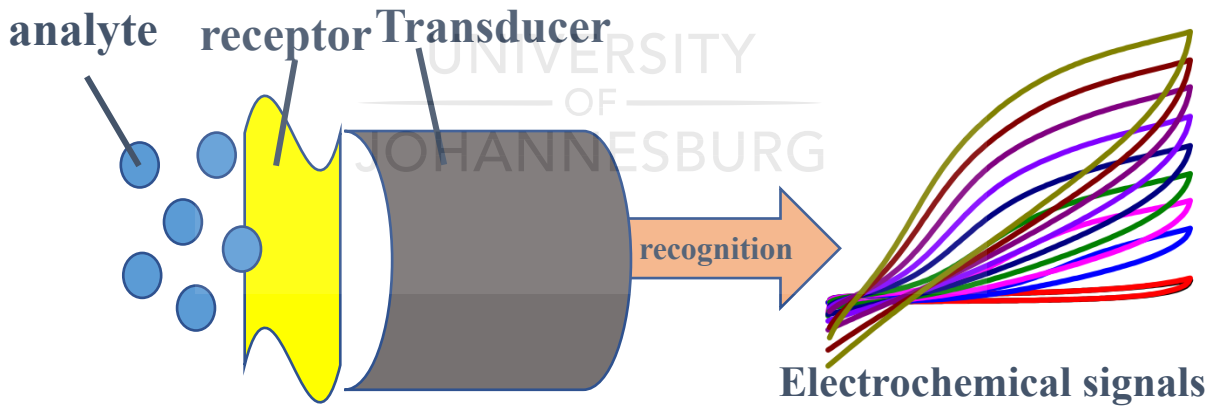

Figure 2.1: Working principle of an electrochemical sensor

Electrochemical sensors are an essential part of our daily lives, making up the most significant proportion of all chemical sensors. Electrochemical sensors may employ a two or three-electrode arrangement, and a potentiostat distinguishes the sensing performance. There is a working and a reference electrode in a two-electrode system, while the three-cell system

has a working, counter, and reference electrode. A transducer element (electrode) covered by a recognition element (chemical/molecular) forms the working electrode. A reference electrode may be Ag/AgCl electrode, Hg/HgCl electrode, while the counter electrodes are typically made up of inert material such as Pt, Au, and graphite. The counter electrode applies a current to the working electrode by conducting electricity from the signal source. It is used in an electrochemical cell to complete the current circuit and is not involved in the electrochemical reaction. The reference electrode's steady and constant potential could also be used to measure the working electrode's potential. Electrochemical reactions take place at the working electrode caused by the analyte of interest.

It is important to note that transduction/transformation of a biological or chemical signal into electric signals can be achieved by electrochemical transducers/devices that employ different techniques/mechanisms. Examples of these transducers are: voltammetric/amperometric, potentiometric, and conductometric/impedimetric. These electrochemical transducers are used in the development of electrochemical sensors. We will explore these electrochemical transducers in the next section.

2.8.1 Types of Electrochemical Sensors

2.8.1.1 Voltammetric/Amperometric Sensors:

Voltammetric sensors reveal information (reduction potential and electrochemical activity) about an analyte by measuring the current in an electrochemical cell as a function of the varying or constant potential applied [53]. Probing a chemical system with a voltammetric transducer will demand a three-electrode system: the reference, counter, and the working electrode, connected with a voltage source (potentiostat) that allows precise application of potential functions and measurement of the resultant current. The resulting curve/graph formed when the analyte's current is plotted against the working electrode's potential is called a Voltammagram [54]. Voltammetric methods can be utilized for various objectives, including determining the oxidation/reduction potential of the analyte of interest, its electrochemical activity, and kinetics of electron transfer processes. The voltammetric experiment requires a small amount of analyte with a concentration ranging between 1-10 mmol/L and a volume of 1-10 ml. Hence it can be said to be non-destructive. Some of the major types of voltammetry include square wave voltammetry, cyclic voltammetry, differential pulse voltammetry, linear sweep voltammetry, and Amperometry [55]. These are the main techniques used in the detection of various analytes reported in the literature. For

example, Cho *et al.* reported the voltmmetric determination of iodine using mechanically treated carbon nanofibers [56]. They employed the use of differential pulse voltmmetry to determine the limit of detection that produced 0.59 μM and a linear range of 5-700 μM. Shen Ming *et al.* developed an iodate sensor made up of a hybrid containing ruthenium oxide and silicon molybdate [57].

A cyclic voltammetric detection technique was used in that report, which produced a detection limit of 50 μM. The aniline complexes sensor developed in this project was designed to improve the sensitivities and detection limit of some iodine sensors reported in the literature. In addition, a sensor with a wide linear range was also developed to address other iodine illnesses that might emerge when iodine levels are too high. According to research, excess iodine, defined as concentrations larger than 4.73 μM, has been linked to health problems such as hyperthyroidism and autoimmune thyroid disease [58]. Balamurugan and his colleagues conducted a study and employed a nanostructured polymer electrode to detect iodine [59]. They adopted the amperometric technique for the detection process and achieved a linear range of 0.1-0.4 μM. A report of dopamine and uric acid detection by Cai *et al.* is not an exception [60]. They used graphene fibers enhanced with $NiCo_2O_4$ for the simultaneous detection of UA, DA, and AA using the DPV technique. A very narrow linear range of 1-13 μM and 10-26 μM for DA and UA respectively was produced by their sensor. These restricted linear ranges will pose a challenge in detecting DA and UA on patients with high concentrations. Therefore, there is a need to improve the linear range of biomolecules sensors and that we were able to achieve in the current research.

In a report documented by Majd *et al.* [61], the modified electrode could detect cysteine at high potentials of 0.8 V from the cyclic voltammogram. However, overpotential can reduce the electrochemical response of analytes on modified electrodes. Therefore, the study was aimed at developing sensors that will detect biomolecules at lower potentials. One outstanding advantage of the current research was to develop sensors that are simpler and less costly.

2.8.1.2 Conductometric Sensors

Conductometric sensors measure conductivity changes ascribable to charge transfer between the probe and analyte. They can detect a change in the conductive properties of the sample during a reaction [62,63]. The method used by these types of sensors is non-selective [64]. These sensors are simple, attractive, offer low cost, and do not require reference electrodes

[65]. According to the conductivity measurement, improvement of conductivity sensors' instrumentation has brought about analytes' fast and straightforward determination [66]. More so, conductometric devices are applicable in investigating enzymatic reactions that give rise to concentration changes of charged species in a solution [67]. It has been reported that some analytes such as creatinine acetaminophen, glucose, urea, and phosphate have been determined using conductometric biosensors [68].

2.8.1.3 Potentiometric Sensors

Several decades ago, these sensors had the most common practical applicability due to their cost, simplicity, and familiarity. A solution's potential is measured in potentiometry by measuring a working/ indicator electrode's potential against a selected reference electrode at zero current. The potential difference between the two electrodes assesses the composition of the sample [69,70,71]. Alternatively, potentiometry supplies information regarding the ion activity in an electrochemical reaction. Potentiometric devices can be divided into three types, namely ion-selective electrodes (IES), Coated Wire Electrodes (CWES), and Field Effect Transistors (FETS). Potentiometry usually uses an indicator electrode (ion-selective electrode) to measure an ion of interest activity selectively. The measurement's sensitivity will be affected when it takes the electrode to establish equilibrium with the solution. Potentiometric sensors are suitable for measuring tiny sample volumes containing low concentrations since they preferably offer the advantage of not chemically influencing a sample.

2.9 Challenges of conventional methods of sensing biologically active molecules

Several methods have been investigated to detect biologically active molecules and other analytes within the physiological system. These methods are high-pressure liquid chromatography (HPLC), brain micro-dialysis, mass spectroscopy (MS), and capillary electrophoresis (CE) [72]. These techniques were eventually substituted with imaging techniques, to cite an example; proton nuclear magnetic resonance, electroencephalography (EEG), and magnetic resonance imaging (MRI) [72]. Studies were conducted using integrated HPLC and electrochemical (EC), coupled electrochemical and fluorescence, and capillary electrophoresis laser-induced fluorescence-based analytical technique for the detection of DA, Serotonin (5HT), and acetylcholine [73,74]. Iodine was being monitored spectrometrically by Sandell–Kolthoff reaction and inductively coupled mass spectrometry

(ICP-MS) methods [75,76]. However, these methods experienced some limitations, including time consumption, expensiveness, additional sample treatment, low temporal resolution, and inability to use as point care devices (bulkiness). Hence, new techniques such as single voxel MEGA-edited PRESS magnetic resonance spectroscopy and Surface-Enhanced Raman Scattering came into the limelight [77]. Integrated analytical and imaging techniques have also been developed for the recognition of biologically active molecules. Examples of such imaging techniques include chromatography, chemiluminescence, fluorimetry, mass spectroscopy, and capillary electrophoresis. In some cases, these methods require additional time for sample preparation, skilled human resources, expensive, low sensitivity, and specificity [78,79]. Hence, the demand for a new analytical technique that can overcome these drawbacks became a necessity.

2.10 Improved Sensing Techniques

Some improved sensing techniques have been discovered as good and promising approach for sensing purposes and are now widely utilized in sensing neurotransmitters in blood plasma and urine. These techniques can be categorized into two parts, namely the electrochemical and optical methods. The electrochemical sensor mainly involves the immobilization of the working electrode with cells, antibodies, enzymes, oligonucleotides, biomimetic polymers, or catalytic nanomaterials, thereby producing conductivity or resistivity effects [80]. On the contrary, optical sensors work based on optical physics to result in either fluorescence or luminescence or endpoints. In this work, electrochemical techniques were explored in detail. The working mechanism of the electrochemical sensor has earlier been summarized in Figure 2.1.

2.11 Electrode materials

An electrode is a conductive material through which an electric current enters or leaves an electrolyte, and the electrode also determines the input and output of the process [81]. Electrodes serve as a vital components of the electrochemical cell and the location in which the equilibrium between the sensing material and the analyte in the solution is formed for oxidation-reduction [82].

Examples of materials used as electrodes are metals such as gold, silver, platinum, mercury, semiconductors such as metal oxides, and different carbonaceous materials [83]. The characteristics of the electrodes used in electrochemical sensors can have a significant influence on their quality. For an electrode to be suitable for electrochemical oxidation of

biologically active molecules, it should be made of a material with high electrical conductivity, good mechanical property, good catalytic activity and reproducibility, and low toxicity and low cost. Also, it must be physically and chemically stable and resistant to corrosion.

The working electrode, often regarded as the indicator electrode, is indisputably the most significant electrochemical cell component. It is where the electrically driven chemical reaction and electron transfer transpires. Thus, it's useful in revealing an analyte's properties. Some of the working electrodes used in electrochemical sensors are described below.

2.12 Materials used as working electrodes for electrochemical sensing

2.12.1 Metal electrodes

The most commonly employed metal electrodes in electrochemical sensing include silver, gold, aluminum, and platinum. These noble metals can be collected with high purity, quickly processed, and developed in a wide range of configurations such as rods, wires, flat sheets, and woven gauzes. In this process, the likes of platinum, aluminum, and gold electrodes were modified and used.

These metals possess a wide range of anodic potential and favorable electron kinetics. Nevertheless, their cathodic potential window range is limited due to their low hydrogen evolution overpotential. More so, their tendency to form surface oxides could result in the production of high background current, which could inevitably affect the electrode reaction kinetics of the electrodes [83,84]. The silver electrode has been described as good and utilized to produce chemically modified electrodes in electrochemical processes. Platinum and gold are easily manufactured and chemically stable. More examples of metals used as electrode materials are copper and nickel, which have been reported to be utilized for the electrochemical sensing of amino acids and carbohydrates [83,85,86]. Additionally, platinum–ruthenium and nickel-titanium electrodes possess bifunctional catalytic mechanisms and have been used in fuel cell preparations [83].

Ganjali *et al.* used gold UMEs (ultra-micro electrodes) to detect methyl morphine in human urine and plasma. They showed that the analyte could oxidize at the bare electrode, but the chemically modified electrodes produced a higher current response with a lower potential [87]. El-Said *et al.* also reported that gold electrodes were highly sensitive, especially when modified to detect epinephrine using cyclic voltammetry, produced a wide linear range of 50

µM to 1000 µM. A recent report also identified electrodes' development with gold film and their suitability for DA recognition and a cell-based chip [88,89].

2.12.2 Carbon electrodes

Carbon-based electrodes have been broadly used in electrochemical processes involving aqueous and non-aqueous solutions. They are superior to solid metal electrodes due to their excellent properties, such as chemical inertness, low resistivity, low background current, low cost, good thermal conductivity, wide anodic potential range, extraordinary mechanical properties, electrical conductivity, and high ratio. These features have been of immense usefulness in electroanalytical chemistry, mostly in the sensor tool. Examples of carbon electrodes used include glassy carbon electrode, screen printed electrode, doped diamond electrode, carbon paste electrode, carbon-ceramic electrode, graphite paste electrode, pencil graphite electrode. They possess the sp^2 bonding and the six-member aromatic ring in their structure [90]. However, these electrodes differ in their electrochemical properties due to the relative densities of their edge and basal planes [90]. In this work, the emphasis was laid on a glassy carbon electrode.

2.12.3 Glassy carbon electrode

These electrodes are the most extensively studied by being relatively cheap, have a wide potential anodic window, chemical inertness, and impermeability to gases [91,92,93]. In addition, it is a convenient inert electrode consisting of a carbon substrate that combines glassy and graphite ceramic.

Usually, the electrode is pre-treated for reproducibility by scanning over a wide range of potential windows using the cyclic voltammetry technique. Mechanical treatment is also being applied by gently polishing the surface with a figure 8 motion on a micro-fabric cloth with ~1 micron, having an alumina slurry, and then sonicated in a solvent to remove any glued alumina paste. The electrochemical properties can be modified by adjusting the surface with different materials, thereby increasing its applicability or efficiency regarding sensitivity and selectivity. It is used in different electrochemical processes such as sensing, energy, environmental remediation, and biomedical applications when modified with additional materials such as metal nanoparticles, semiconductors, and conducting polymers, to mention a few. Carbon electrodes enable scanning with increased negative potentials than gold or platinum but possess the disadvantage of being expensive, hard, and difficult to shape. The

recognition of neurotransmitters using GCE was also undertaken by different researchers [94,95]. Modifications of the GCE by various researchers gave rise to subsequent improvement in the detection.

2.13 Influence of modification of electrodes

It is often observed that the redox reaction of an analyte on a bare electrode surface using voltammetric methods including cyclic voltammetry or square wave voltammetry produces an oxidation or reduction potential that is slightly higher than the thermodynamic potential. Therefore, to improve the analyte signal's transduction in electrochemical sensing, the working electrode surface may be modified with a material that offers desirable properties, for example, electrical conductivity. The surface improvement is significant in achieving an extraordinary result with regards to sensitivity and selectivity. The working electrode may be modified with materials such as nanoparticles and semiconductors. It should be of note that the present scenario of sensors in science results from the emergence of those materials and their consequential developments in the field of material science. Unlike the solid or bare electrodes where only single overlapped signals are obtained, the modified electrode enables the resolution of each analyte's signals. In this project, the working electrodes were modified with transition metal complexes of aniline. An overview of this material and how it improved the sensing properties of the electrochemical system would be highlighted in subsequent sections.

2.14 Transition metal complexes and their importance as sensors

Transition metal complexes are anionic, cationic, or neutral species in which ligands coordinate a transition metal. [96] The transition metal complex comprises a transition metal ion that is often referred to as the central atom (or ion) that binds several ions or molecules called ligands. The bonding of the ligand with the metal usually requires the formal donation of at least one of the ligand's electron pairs.

Some ligands bind to the central metal through two or more different ligand atoms, forming part of a heterocyclic ring (mostly five and six-member) where the metal is one of the members. Such a metal complex is called “metal chelate.” On some occasions, some other ligands' stereochemistry does not allow all the binding sites to be concurrently bonded to the same metal [97,98]. This scenario implies that a potentially tridentate ligand could operate as a bidentate ligand.

Transition metal ions possess rich chemistry owing to their close-lying energy bands, which are comprised of partially filled d-orbitals. The transition metals hence operate as unique agents in various biological mechanisms. The transition metals likewise show various states of oxidation and can interact with a variety of molecules that are negatively charged.

Transition metal complexes have found importance in materials synthesis, catalysis, photochemistry, and biological systems. They exhibit different chemical, optical and magnetic properties and are promising materials for electrochemical sensor development because of their electrochemical properties, electrical properties, and stability [99]. The reactivity of these transition metal complexes is reliant on the metal's nature and the attached ligand.

The metal ions in complexes have a characteristic of a lewis acid coupled with high electron affinity, making them strong receptors for donor Lewis bases, including large numbers of the analytes we are keen on detecting. Furthermore, the transition metal complexes go through metal-ligand exchange reactions with different analytes, facilitating processes of detection via a displacement approach. In addition, the incompletely filled d orbitals of the transition metals give metal complexes desirable electronic and magnetic properties, rendering them favorable chromophores or paramagnetic centers as sensor building blocks. Therefore, in light of these highlights, metal coordination can be utilized in numerous areas of sensor fabrication.

2.14.1 Aniline-Transition Metal Complexes

The ability of aniline to form stable transition metal complexes is one of the bases of their usefulness as an analytical reagent for sensitive qualitative and quantitative determinations. Aniline is an aromatic compound consisting of an amine attached to a benzene ring (Scheme 2.1). The phenyl group has alternating double bonds, while the amino group contains nitrogen with two hydrogen atoms attached to it. The nitrogen atom on the amine ring of aniline contains a lone pair of electrons. This lone pair of an electron is donated to some highly charged metals such as Ni^{2+}, Co^{2+}, Cu^{2+}, to form a complex.

Metal complexes coordinated to appropriate ligands are chemically more effective and distinct than metal ions [100]. The preparation of transition metal complexes using aniline ligands has significantly increased ligands and complexes' pharmacological properties [101]. It is believed that the amine group from the aniline can improve the charge transfer in the aniline transition metal complexes, thus enhancing sensing performance [102]. The resonance

effect on aniline also contributes to its conductivity when complexed with metal ions. Conjugated systems having resonance structures have delocalized electrons, i.e., electrons move around the system, thus bringing more stability to them. Scheme 2.2 presents the resonance structure of aniline. The participation of lone pairs of electrons on nitrogen causes the resonance structures of aniline.

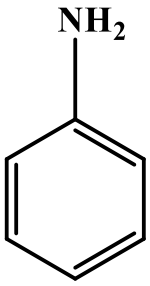

Scheme 2.1: Structure of aniline

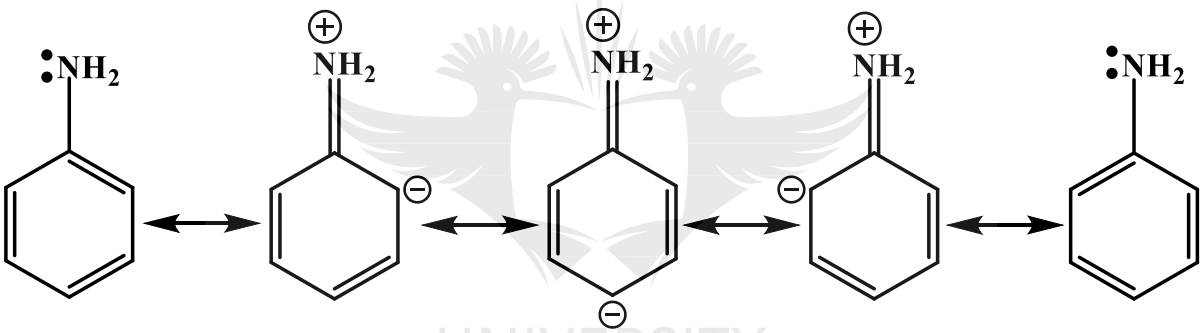

Scheme 2.2: Resonance structure of aniline

2.14.2 Transition metal complexes for the electrochemical detection of biologically active molecules

Electrochemical sensors play a significant role in different fields, including biomedical analysis [103], bioelectronics [104], cell [105], microbe analysis [106], molecule determination [107], industrial processes [108], monitoring different species in the atmosphere [109], and food quality control [110] [111,112].

They utilize the sensitivity and selectivity of chemical receptors toward their corresponding analytes in conjunction with the electrochemical transducers to convert complex chemical signals into simple, easy-to-use signals. Transition metal complexes as chemical receptors can improve the sensitivity and catalytic response of fabricated electrochemical sensors. Transition metal complex materials have gained ground in medicine, environmental sciences,

and basic studies. In electrochemical sensing of biologically active molecules, transition metal complexes containing Schiff base ligands have mostly been explored. Pazalja and his co-workers reported cysteine recognition with an electrochemical sensor based on Ru(III) Schiff base complex and a carbon nanotube. The observations showed that combining multi-walled carbon nanotubes with the complex material used to modify the electrodes produced an enhancement of the oxidation current signal for cysteine detection [113]. Hassanzadeh and his colleagues reported ascorbic acid and dopamine sensing using a cobalt Schiff base complex and a surfactant as a modifier for a carbon paste electrode. The findings revealed that the modified electrode improved the electrochemical recognition of ascorbic acid and dopamine [114].

Zare-Mehrjardi and Hamid [115] reported a dopamine and ascorbic acid electrochemical sensor based on a Schiff base complex of molybdenum and toluidine to modify a carbon paste electrode. The results revealed that surface regeneration, easy design of the modified electrode, good peak resolution, and sub-micromolar detection limits categorize the prepared electrode for simultaneous voltammetric determination of dopamine and ascorbic acid. Amiri *et al.* [116] reported uric and ascorbic acid detection performed simultaneously through a carbon electrode modified with Schiff base composite containing cobalt. The effect of certain parameters, such as scan rates and pH, were investigated. Experimental results showed that with a rise in pH, the current responses for ascorbic and uric acid oxidation changed towards negative potential, showing that protons have participated in their processes of electrode reaction.

In some other works, Xu and his co-workers developed a Macrocyclic nickel(II) complex and hydrophilic polyurethane film electrodes for the electrocatalytic oxidation and selective detection of norepinephrine [117]. They observed that the Ni(II) complex-modified electrode negatively shifted oxidation potential and increased current in phosphate buffer at pH 7.4. Furthermore, the Ni(II) complex-modified electrode, when coated with polyurethane film, increased the selectivity for norepinephrine over ascorbic acid and uric acid. Zheng and Song developed Nickel(II)–baicalein complex modified multiwall carbon nanotube paste electrode for the electrocatalytic oxidation of glycine [118]. The cheap and effective electrochemical sensor reveals enhanced reversibility and improved current response towards the oxidation of glycine.

Majdi and his colleagues described the electrochemical recognition of biomolecules such as alanine, l-arginine, l-phenylalanine, l-lysine, and glycine on a glassy carbon electrode

modified nickel curcumin complex [119]. The results indicate that the amino acids were oxidized through an electrocatalytic mechanism on the redox mediator, which was immobilized on the electrode surface. Also, Leonardi *et al.* developed a novel manganese (III) complex for the electrochemical sensing of ascorbic acid [120]. The sensor demonstrated high sensitivity to ascorbic acid in the presence of some interfering molecules.

In another attractive report by Maree and Nyokong, ring-substituted cobalt phthalocyanine complexes were synthesized and applied for cysteine's electrocatalytic oxidation [121]. The results showed that the catalytic currents and cysteine oxidation potential are solely reliant on the pH of the solution. As the pH increases, the potential becomes more negative, and with a rise in pH, the catalytic currents decrease. Ni *et al.* demonstrated the amperometric determination of epinephrine with an osmium complex and Nafion double-layer membrane modified electrode [122]. The modified electrode displayed excellent electrocatalytic activity for epinephrine oxidation. Flavia *et al.* developed a Cobalt Salophen complex to detect iodide using amperometric and potentiometric techniques [123]. They found out that the amperometric technique produced a lower detection limit than the potentiometric method.

The above literature shows that metal complexes of aniline have not been explored for sensing applications. Hence, this research explores the aniline metal complexes of Bi, Ni, and Co for the electrochemical sensing of some biologically active molecules. As a result, a more straightforward method to synthesize these complexes was adopted, which proved to be an advantage over what has been reported in the literature.

2.15 References

[1] Bunge, M. (1979). Treatise on Basic Philosophy, Volumes 3-4: Ontology.

[2] Chalmers (2020, July 23). Bioactive compounds, Food Bioactives Centre, *University of Gothenburg*. http://www.chalmers.se/chem/fbac-en2012.

[3] Li, Y. J., Tseng, Y. T., Unnikrishnan, B., & Huang, C. C. (2013). Gold-nanoparticles-modified cellulose membrane coupled with laser desorption/ionization mass spectrometry for detection of iodide in urine. *ACS Applied Materials & Interfaces*, *5*(18), 9161-9166.

[4] Ames, B. N., Cathcart, R., Schwiers, E., & Hochstein, P. (1981). Uric acid provides an antioxidant defense in humans against oxidant-and radical-caused aging and cancer: a hypothesis. *Proceedings of the National Academy of Sciences*, *78*(11), 6858-6862.

[5] Becker, B. F. (1993). Towards the physiological function of uric acid. *Free Radical Biology and Medicine*, *14*(6), 615-631.

[6] Sun, W., Wang, X., Wang, Y., Ju, X., Xu, L., Li, G., & Sun, Z. (2013). Application of graphene–SnO_2 nanocomposite modified electrode for the sensitive electrochemical detection of dopamine. *Electrochimica Acta*, *87*, 317-322.

[7] Wightman, R. M., May, L. J., & Michael, A. C. (1988). Detection of dopamine dynamics in the brain. *Analytical Chemistry*, *60*(13), 769A-793A.

[8] Heien, M. L., Khan, A. S., Ariansen, J. L., Cheer, J. F., Phillips, P. E., Wassum, K. M., & Wightman, R. M. (2005). Real-time measurement of dopamine fluctuations after cocaine in the brain of behaving rats. *Proceedings of the National Academy of Sciences*, *102*(29), 10023-10028.

[9] Choudhary, M., Shukla, S. K., Islam, R. U., Witcomb, M. J., Holzapfel, C. W., & Mallick, K. (2013). Polymerization assisted reduction reaction: a sequential electron–proton transfer reaction catalyzed by gold nanoparticle. *The Journal of Physical Chemistry C*, *117*(44), 23009-23016.

[10] Ali, S. R., Ma, Y., Parajuli, R. R., Balogun, Y., Lai, W. Y. C., & He, H. (2007). A nonoxidative sensor based on a self-doped polyaniline/carbon nanotube composite for sensitive and selective detection of the neurotransmitter dopamine. *Analytical Chemistry*, *79*(6), 2583-2587.

[11] Caudle, W. M., Colebrooke, R. E., Emson, P. C., & Miller, G. W. (2008). Altered vesicular dopamine storage in Parkinson's disease: a premature demise. *Trends in Neurosciences*, *31*(6), 303-308.

[12] Dickson DV (2007). "Neuropathology of movement disorders". In Tolosa E, Jankovic JJ (eds.). Parkinson's disease and movement disorders. Hagerstown, MD: Lippincott Williams & Wilkins. 271–283.

[13] Divino da Rocha, M., Pereira Dias Viegas, F., Cristina Campos, H., Carolina Nicastro, P., Calve Fossaluzza, P., Alberto Manssour Fraga, C., J Barreiro, E. & Viegas, C. (2011). The role of natural products in the discovery of new drug candidates for the treatment of neurodegenerative disorders II: Alzheimer's disease. *CNS & Neurological Disorders-Drug Targets (Formerly Current Drug Targets-CNS & Neurological Disorders)*, *10*(2), 251-270.

[14] Santos, V. L. (2015). *Perfil epidemiológico da Doença de Parkinson no Brasil.*

[15] Valenzuela, C. F., Puglia, M. P., & Zucca, S. (2011). Focus on: neurotransmitter systems. *Alcohol Research & Health*, *34*(1), 106.

[16] Ellenbroek, B. A., & Cesura, A. M. (2014). Antipsychotics and the dopamine–serotonin connection. In *Small Molecule Therapeutics for Schizophrenia* (pp. 1-49). Springer, Cham.

[17] National Collaborating Centre for Chronic Conditions. (2006). Symptomatic pharmacological therapy in Parkinson's disease. *Parkinson's Disease. London: Royal College of Physicians*, 59-100.

[18] Sonnenschein, S. F., & Grace, A. A. (2020). Insights on current and novel antipsychotic mechanisms from the MAM model of schizophrenia. *Neuropharmacology*, *163*, 107632.

[19] Laursen, T. M., Nordentoft, M., & Mortensen, P. B. (2014). Excess early mortality in schizophrenia. *Annual Review of Clinical Psychology*, *10*, 425-448.

[20] Szymańska, K., Kuśmierska, K., & Demkow, U. (2014). Inherited disorders of brain neurotransmitters: pathogenesis and diagnostic approach. In *Neurotransmitter Interactions and Cognitive Function* (pp. 1-8). Springer, Cham.

[21] Raine, A. (2018). Antisocial personality as a neurodevelopmental disorder. *Annual Review of Clinical Psychology*, *14*, 259-289.

[22] Grace, A. A., & Gomes, F. V. (2019). The circuitry of dopamine system regulation and its disruption in schizophrenia: insights into treatment and prevention. *Schizophrenia Bulletin*, *45*(1), 148-157.

[23] Sonnenschein, S. F., & Grace, A. A. (2020). Insights on current and novel antipsychotic mechanisms from the MAM model of schizophrenia. *Neuropharmacology*, *163*, 107632.

[24] Zimmermann, M. B., Jooste, P. L., & Pandav, C. S. (2008). Iodine-deficiency disorders. *The Lancet*, *372*(9645), 1251-1262.

[25] Vanderpas, J. B., & Moreno-Reyes, R. (2017). Historical aspects of iodine deficiency control. *Minerva Medica*, *108*(2), 124-135.

[26] Chailapakul, O., Amatatongchai, M., Wilairat, P., Grudpan, K., & Nacapricha, D. (2004). Flow-injection determination of iodide ion in nuclear emergency tablets, using boron-doped diamond thin film electrode. *Talanta*, *64*(5), 1253-1258.

[27] National Research Council. (2005). *Health implications of perchlorate ingestion*. National Academies Press.

[28] Zimmermann, M. B. (2009). Iodine deficiency. *Endocrine Reviews*, *30*(4), 376-408.

[29] Santiago-Fernandez, P., Torres-Barahona, R., Muela-Martinez, J. A., Rojo-Martinez, G., Garcia-Fuentes, E., Garriga, M. J., Leon, A.G., & Soriguer, F. (2004). Intelligence quotient and iodine intake: a cross-sectional study in children. *The Journal of Clinical Endocrinology & Metabolism*, *89*(8), 3851-3857.

[30] Levie, D., Korevaar, T. I., Bath, S. C., Murcia, M., Dineva, M., Llop, S., Espada, M., Van Herwaarden, A.E., De Rijke, Y.B., Ibarluzea, J.M. & Sunyer, J. (2019). Association of maternal iodine status with child IQ: a meta-analysis of individual participant data. *The Journal of Clinical Endocrinology & Metabolism*, *104*(12), 5957-5967.

[31] De Macedo, A. N., Macri, J., Hudecki, P. L., Saoi, M., McQueen, M. J., & Britz-McKibbin, P. (2017). Validation of a capillary electrophoresis assay for monitoring iodine nutrition in populations for prevention of iodine deficiency: an interlaboratory method comparison. *The Journal of Applied Laboratory Medicine*, *1*(6), 649-660.

[32] Ito, K., Ichihara, T., Zhuo, H., Kumamoto, K., Timerbaev, A. R., & Hirokawa, T. (2003). Determination of trace iodide in seawater by capillary electrophoresis following transient isotachophoretic preconcentration: comparison with ion chromatography. *Analytica Chimica Acta*, *497*(1-2), 67-74.

[33] Vitali, L., Horst, B. L., Heller, M., Fávere, V. T., & Micke, G. A. (2011). Using multiple short-end injections to develop fast electrophoretic separations—applications in iodide analysis. *Journal of Chromatography A*, *1218*(28), 4586-4591.

[34] Zhou, R., Huang, X., An, Q., Xu, W., Liu, Y., Xu, D., Lin, Q., Wang, S. & Zhang, J. (2021). A convenient and sensitive colorimetric iodide assay based on directly inducing morphological transformation of gold nanostars. *Journal of Food & Drug Analysis*, *29*(1).

[35] Hou, X., Chen, S., Tang, J., Xiong, Y., & Long, Y. (2014). Silver nanoplates-based colorimetric iodide recognition and sensing using sodium thiosulfate as a sensitizer. *Analytica Chimica Acta*, *825*, 57-62.

[36] Sandell, E. I., & Kolthoff, I. M. (1934). Chronometric catalytic method for the determination of micro quantities of iodine. *Journal of the American Chemical Society*, *56*(6), 1426-1426.

[37] Jopke, P., Bahadir, M., Fleckenstein, J., & Schnug, E. (1996). Iodine determination in plant materials. *Communications in Soil Science and Plant Analysis*, *27*(3-4), 741-751.

[38] Yu, L., ZhaNg, X., JiN, J., Che, S., & Yu, L. (2011). Simultaneous determination of chloride, bromide and iodide in foodstuffs by low pressure ion-exchange chromatography with visible light detection. *Czech Journal of Food Sciences*, *29*(6), 634-640.

[39] Hou, X., Dahlgaard, H., Rietz, B., Jacobsen, U., & Nielsen, S. P. (2000). Pre-Separation Neutron Activation Analysis of Sewater, Urine and Milk for Iodide and Iodate. *Journal of Radioanalytical and Nuclear Chemistry*, *244*(1), 87-91.

[40] Ito, K. (1997). Determination of iodide in seawater by ion chromatography. *Analytical Chemistry*, *69*(17), 3628-3632.

[41] Shishehbore, M. R., Sheibani, A., & Jokar, R. (2010). Kinetic spectrophotometric determination of trace amounts of iodide in food samples. *Analytical Sciences*, *26*(4), 497-501.

[42] Edmonds, J. S., & Morita, M. (1998). The determination of iodine species in environmental and biological samples (Technical report). *Pure and Applied Chemistry*, *70*(8), 1567-1584.

[43] Xie, Z., & Zhao, J. (2004). Reverse flow injection spectrophotometric determination of iodate and iodide in table salt. *Talanta*, *63*(2), 339-343.

[44] Khunseeraksa, V., Kongkaew, S., Thavarungkul, P., Kanatharana, P., & Limbut, W. (2020). Electrochemical sensor for the quantification of iodide in urine of pregnant women. *Microchimica Acta*, *187*(11), 1-11.

[45] Pereira, F. C., Fogg, A. G., Ugo, P., Bergamo, E. P., Stradiotto, N. R., & Zanoni, M. V. B. (2005). Determination of Iodide and Idoxuridine at a Glutaraldehyde-Cross-Linked Poly-l-Lysine Modified Glassy Carbon Electrode. *Electroanalysis: An International Journal Devoted to Fundamental and Practical Aspects of Electroanalysis*, *17*(14), 1309-1316.

[46] Tian, L., Liu, L., Chen, L., Lu, N., & Xu, H. (2005). Electrochemical determination of iodide on a vanadium oxide–polypropylene carbonate coated glassy carbon electrode. *Talanta*, *66*(1), 130-135.

[47] Wang, W., Xu, G., Cui, X. T., Sheng, G., & Luo, X. (2014). Enhanced catalytic and dopamine sensing properties of electrochemically reduced conducting polymer nanocomposite doped with pure graphene oxide. *Biosensors and Bioelectronics*, *58*, 153-156.

[48] Li, Y. J., Tseng, Y. T., Unnikrishnan, B., & Huang, C. C. (2013). Gold-nanoparticles-modified cellulose membrane coupled with laser desorption/ionization mass spectrometry for detection of iodide in urine. *ACS applied Materials & Interfaces*, *5*(18), 9161-9166.

[49] Pienpinijtham, P., Han, X. X., Ekgasit, S., & Ozaki, Y. (2011). Highly sensitive and selective determination of iodide and thiocyanate concentrations using surface-enhanced Raman scattering of starch-reduced gold nanoparticles. *Analytical Chemistry*, *83*(10), 3655-3662.

[50] Hulanicki, A., Glab, S., & Ingman, F. O. L. K. E. (1991). Chemical sensors: definitions and classification. *Pure and Applied Chemistry*, *63*(9), 1247-1250.

[51] Widrig, C. A., Porter, M. D., Ryan, M. D., Strein, T. G., & Ewing, A. G. (1990). Dynamic electrochemistry: methodology and application. *Analytical Chemistry*, *62*(12), 1-20.

[52] Hulanicki, A., Glab, S., & Ingman, F. O. L. K. E. (1991). Chemical sensors: definitions and classification. *Pure and Applied Chemistry*, *63*(9), 1247-1250.

[53] Kissinger, P., & Heineman, W. R. (Eds.). (2018). *Laboratory Techniques in Electroanalytical Chemistry, Revised and Expanded*. CRC press.

[54] Harris, Daniel C. (2010). Quantitative Chemical Analysis, Macmillan, Ninth Edition (9 ed.). W.H. Freeman and Company.

[55] Labib, M., Sargent, E. H., & Kelley, S. O. (2016). Electrochemical methods for the analysis of clinically relevant biomolecules. *Chemical Reviews*, *116*(16), 9001-9090.

[56] Cho, E., Perebikovsky, A., Benice, O., Holmberg, S., Madou, M., & Ghazinejad, M. (2018). Rapid iodine sensing on mechanically treated carbon nanofibers. *Sensors*, *18*(5), 1486.

[57] Chen, S. M., Song, J. L., & Thangamuthu, R. (2007). Electrocatalytic Behavior of Mixed-Valent RuO⁄Ru$(CN)_6^{4-}$⁄ $SiMo_{12}O_{40}^{4-}$ Hybrid Film Modified Electrodes Toward Oxidation of Neurotransmitters and Iodate Reduction. *Journal of The Electrochemical Society*, *154*(10), E153.

[58] World Health Organization. (2013). *Urinary iodine concentrations for determining iodine status in populations* (No. WHO/NMH/NHD/EPG/13.1). World Health Organizations.

[59] Balamurugan, A., Lin, C. Y., Nien, P. C., & Ho, K. C. (2012). Electrochemical Preparation of a Nanostructured Poly (amino naphthalene sulfonic acid) Electrode Using

CTAB as a Soft Template and Its Electrocatalytic Application for the Reduction of Iodate. *Electroanalysis*, *24*(2), 325-331.

[60] Cai, W., Lai, J., Lai, T., Xie, H., & Ye, J. (2016). Controlled functionalization of flexible graphene fibers for the simultaneous determination of ascorbic acid, dopamine, and uric acid. *Sensors and Actuators B: Chemical*, *224*, 225-232.

[61] Majd, S. M., Teymourian, H., & Salimi, A. (2013). Fabrication of an Electrochemical L-Cysteine Sensor Based on Graphene Nanosheets Decorated Manganese Oxide Nanocomposite Modified Glassy Carbon Electrode. *Electroanalysis*, *25*(9), 2201-2210.

[62] Grieshaber, D., MacKenzie, R., Vörös, J., & Reimhult, E. (2008). Electrochemical biosensors-sensor principles and architectures. *Sensors*, *8*(3), 1400-1458.

[63] Ronkainen, N. J., Halsall, H. B., & Heineman, W. R. (2010). Electrochemical biosensors. *Chemical Society Reviews*, *39*(5), 1747-1763.

[64] Kriz, D., Kempe, M., & Mosbach, K. (1996). Introduction of molecularly imprinted polymers as recognition elements in conductometric chemical sensors. *Sensors and Actuators B: Chemical, 33*(1), 178–181.

[65] Svetlicic, V., Schmidt, A. J., & Miller, L. L. (1998). Conductometric sensors based on the hypersensitive response of plasticized polyaniline films to organic vapors. *Chemistry of Materials, 10*(11), 3305–3307.

[66] Lesho, M. J., & Sheppard, N. F. (1996). Adhesion of polymer films to oxidized silicon and its effect on performance of a conductometric pH sensor. *Sensors and Actuators B: Chemical, 37*(1), 61–66.

[67] D'Orazio, P. (2003). Biosensors in clinical chemistry. *Clinica Chimica Acta*, *334*(1-2), 41-69.

[68] Razavi, H., & Janfaza, S. (2015). Medical nanobiosensors: A tutorial review. *Nanomedicine Journal*, *2*(2), 74-87.

[69] Eggins, B. R. (2008). *Chemical Sensors and Biosensors* (Vol. 28). John Wiley & Sons.

[70] Chaubey, A., & Malhotra, B. (2002). Mediated biosensors. *Biosensors and Bioelectronics*, *17*(6-7), 441-456.

[71] D'Orazio, P. (2003). Biosensors in clinical chemistry. *Clinica Chimica Acta*, *334*(1-2), 41-69.

[72] Hugo Cifuentes Castro, V., Lucia Lopez Valenzuela, C., Carlos Salazar Sanchez, J., Pardo Pena, K., J Lopez Perez, S., Ortega Ibarra, J., & Morales Villagran, A. (2014). An

update of the classical and novel methods used for measuring fast neurotransmitters during normal and brain altered function. *Current Neuropharmacology*, *12*(6), 490-508.

[73] Hubbard, K. E., Wells, A., Owens, T. S., Tagen, M., Fraga, C. H., & Stewart, C. F. (2010). Determination of dopamine, serotonin, and their metabolites in pediatric cerebrospinal fluid by isocratic high-performance liquid chromatography coupled with electrochemical detection. *Biomedical Chromatography*, *24*(6), 626-631.

[74] Zapata, A., Chefer, V. I., Parrot, S., & Denoroy, L. (2013). Detection and quantification of neurotransmitters in dialysates. *Current Protocols in Neuroscience*, *63*(1), 7-4.

[75] Sandell, E. B., & Kolthoff, I. M. (1937). Micro determination of iodine by a catalytic method. *Microchimica Acta*, *1*(1), 9-25.

[76] Caldwell, K. L., Maxwell, C. B., Makhmudov, A., Pino, S., Braverman, L. E., Jones, R. L., & Hollowell, J. G. (2003). Use of inductively coupled plasma mass spectrometry to measure urinary iodine in NHANES 2000: comparison with previous method. *Clinical Chemistry*, *49*(6), 1019-1021.

[77] O'Gorman, R. L., Michels, L., Edden, R. A., Murdoch, J. B., & Martin, E. (2011). In vivo detection of GABA and glutamate with MEGA-PRESS: reproducibility and gender effects. *Journal of Magnetic Resonance Imaging*, *33*(5), 1262-1267.

[78] Polo, E., & Kruss, S. (2016). Nanosensors for neurotransmitters. *Analytical and Bioanalytical Chemistry*, *408*(11), 2727-2741.

[79] Moon, J. M., Thapliyal, N., Hussain, K. K., Goyal, R. N., & Shim, Y. B. (2018). Conducting polymer-based electrochemical biosensors for neurotransmitters: A review. *Biosensors and Bioelectronics*, *102*, 540-552.

[80] Chauhan, N., Jain, U., & Soni, S. (2019). Sensors for Food Quality Monitoring. In *Nanoscience for Sustainable Agriculture* (pp. 601-626). Springer, Cham.

[81] Allmand, A. J., & Ellingham, H. J. T. (1924). *The Principles of Applied Electrochemistry*. Longmans, Green.

[82] Harper, A., & Anderson, M. R. (2010). Electrochemical glucose sensors—developments using electrostatic assembly and carbon nanotubes for biosensor construction. *Sensors*, *10*(9), 8248-8274.

[83] Li, G., & Miao, P. (2013). Theoretical background of electrochemical analysis. In *Electrochemical Analysis of Proteins and Cells* (pp. 5-18). Springer, Berlin, Heidelberg.

[84] Johnson, D. C., & LaCourse, W. R. (1990). Liquid chromatography with pulsed electrochemical detection at gold and platinum electrodes. *Analytical Chemistry*, *62*(10), 589A-597A.

[85] Fan, C., Li, G., Zhuang, Y., Zhu, J., & Zhu, D. (2000). Iodide modified silver electrode and its application to the electroanalysis of hemoglobin. *Electroanalysis: An International Journal Devoted to Fundamental and Practical Aspects of Electroanalysis*, *12*(3), 205-208.

[86] Gutes, A., Carraro, C., & Maboudian, R. (2011). Nonenzymatic glucose sensing based on deposited palladium nanoparticles on epoxy-silver electrodes. *Electrochimica Acta*, *56*(17), 5855-5859.

[87] Ganjali, M. R., Norouzi, P., Dinarvand, R., Farrokhi, R., & Moosavi-Movahedi, A. A. (2008). Development of fast Fourier transformations with continuous cyclic voltammetry at an Au microelectrode and its application for the sub nano-molar monitoring of methyl morphine trace amounts. *Materials Science and Engineering: C*, *28*(8), 1311-1318.

[88] El-Said, W. A., Kim, T. H., Kim, H., & Choi, J. W. (2010). Three-dimensional mesoporous gold film to enhance the sensitivity of electrochemical detection. *Nanotechnology*, *21*(45), 455501.

[89] El-Said, W. A., Lee, J. H., Oh, B. K., & Choi, J. W. (2010). 3-D nanoporous gold thin film for the simultaneous electrochemical determination of dopamine and ascorbic acid. *Electrochemistry Communications*, *12*(12), 1756-1759.

[90] Li, G., & Miao, P. (2013). Theoretical background of electrochemical analysis. In *Electrochemical Analysis of Proteins and Cells* (pp. 5-18). Springer, Berlin, Heidelberg.

[91] Dekanski, A., Stevanović, J., Stevanović, R., Nikolić, B. Ž., & Jovanović, V. M. (2001). Glassy carbon electrodes: I. Characterization and electrochemical activation. *Carbon*, *39*(8), 1195-1205.

[92] Uslu, B., & Ozkan, S. A. (2007). Electroanalytical application of carbon-based electrodes to the pharmaceuticals. *Analytical Letters*, *40*(5), 817-853.

[93] Vedhi, C., Selvanathan, G., Arumugam, P., & Manisankar, P. (2009). Electrochemical sensors of heavy metals using novel polymer-modified glassy carbon electrodes. *Ionics*, *15*(3), 377.

[94] Zhao, H., Zhang, Y., & Yuan, Z. (2002). Determination of dopamine in the presence of ascorbic acid using poly (hippuric acid) modified glassy carbon electrode. *Electroanalysis: An International Journal Devoted to Fundamental and Practical Aspects of Electroanalysis*, *14*(14), 1031-1034.

[95] Oztekin, Y., Tok, M., Bilici, E., Mikoliunaite, L., Yazicigil, Z., Ramanaviciene, A., & Ramanavicius, A. (2012). Copper nanoparticle modified carbon electrode for determination of dopamine. *Electrochimica Acta*, *76*, 201-207.

[96] Cox, T. (2004). *BIOS Instant Notes in Inorganic Chemistry*. Garland Science.

[97] Gilreath, E. S. (1958). *Fundamental Concepts of Inorganic Chemistry*. McGraw-Hill.

[98] Houghton, R. P. H. (1979). *Metal Complexes-Organic Chemistry*. CUP Archive.

[99] Santos, L. S., Landers, R., & Gushikem, Y. (2011). Application of manganese (II) phthalocyanine synthesized in situ in the SiO_2/SnO_2 mixed oxide matrix for determination of dissolved oxygen by electrochemical techniques. *Talanta*, *85*(2), 1213-1216.

[100] Al-Amiery, A. A., Saif, A., Rawa, M., & Maysaa, A. (2010). Synthesis, characterization, and antibacterial study of metal complexes derived from bis (5-benzyl-1, 3, 4-thiadiazol-2-yl) methane. *Journal of Chemical and Pharmaceutical Research*, *2*(3), 120-126.

[101] Muthusamy, S., & Natarajan, R. (2016). Pharmacological activity of a few transition metal complexes: A short review. *J. Chem. Bio. Ther*, *1*(2), 1-17.

[102] Mohtasebi, A., Chowdhury, T., Hsu, L. H., Biesinger, M. C., & Kruse, P. (2016). Interfacial charge transfer between phenyl-capped aniline tetramer films and iron oxide surfaces. *The Journal of Physical Chemistry C*, *120*(51), 29248-29263.

[103] Wang, Q., Liu, F., Yang, X., Wang, K., Wang, H., & Deng, X. (2015). Sensitive point-of-care monitoring of cardiac biomarker myoglobin using aptamer and ubiquitous personal glucose meter. *Biosensors and Bioelectronics*, *64*, 161-164.

[104] Di Pietrantonio, F., Benetti, M., Cannatà, D., Verona, E., Palla-Papavlu, A., Fernández-Pradas, J. M., & D'Auria, S. (2015). A surface acoustic wave bio-electronic nose for detection of volatile odorant molecules. *Biosensors and Bioelectronics*, *67*, 516-523.

[105] Wang, C., Madiyar, F., Yu, C., & Li, J. (2017). Detection of extremely low concentration waterborne pathogen using a multiplexing self-referencing SERS microfluidic biosensor. *Journal of Biological Engineering*, *11*(1), 1-11.

[106] Aynalem, B., & Muleta, D. (2021). Microbial Biosensors as Pesticide Detector: An Overview. *Journal of Sensors*, *2021*.

[107] Ahmad, R., Khan, M., Tripathy, N., Khan, M. I. R., & Khosla, A. (2020). Hydrothermally synthesized nickel oxide nanosheets for non-enzymatic electrochemical glucose detection. *Journal of The Electrochemical Society*, *167*(10), 107504.

[108] Dhall, P., Kumar, A., Joshi, A., Saxsena, T. K., Manoharan, A., Makhijani, S. D., & Kumar, R. (2008). Quick and reliable estimation of BOD load of beverage industrial wastewater by developing BOD biosensor. *Sensors and actuators B: Chemical*, *133*(2), 478-483.

[109] Sekhar, P. K., Moore, Z., Aravamudhan, S., & Khosla, A. (2017). A new low-temperature electrochemical hydrocarbon and NOx sensor. *Sensors*, *17*(12), 2759.

[110] Ciriello, R., Cataldi, T. R., Crispo, F., & Guerrieri, A. (2015). Quantification of l-lysine in cheese by a novel amperometric biosensor. *Food chemistry*, *169*, 13-19.

[111] Castillo-Ortega, M. M., Del Castillo-Castro, T., Ibarra-Bracamontes, V. J., Nuno-Donlucas, S. M., Puig, J. E., & Herrera-Franco, P. J. (2007). Urea sensing film prepared by extrusion from DBSA-doped polyaniline-poly (styrene-co-potassium acrylate) in a poly (n-butyl methacrylate) matrix. *Sensors and Actuators B: Chemical*, *125*(2), 538-543.

[112] Hrapovic, S., Liu, Y., Male, K. B., & Luong, J. H. (2004). Electrochemical biosensing platforms using platinum nanoparticles and carbon nanotubes. *Analytical Chemistry*, *76*(4), 1083-1088.

[113] Pazalja, M., Kahrović, E., Zahirović, A., & Turkušić, E. (2016). Electrochemical sensor for determination of L-cysteine based on carbon electrodes modified with Ru (III) Schiff base complex, carbon nanotubes, and Nafion. *Int. J. Electrochem. Sci*, *11*, 10939-10952.

[114] Hassanzadeh, N., & Zare-Mehrjardi, H. R. (2017). Selective electrochemical sensing of dopamine and ascorbic acid using carbon paste electrode modified with cobalt Schiff Base complex and a surfactant. *Int. J. Electrochem. Sci*, *12*, 3950-3964.

[115] Zare-Mehrjardi, H. R. (2018). Preparation of Modified Electrode using Toluidine Blue O and Molybdenum Schiff Base Complex for Detection of Dopamine in the presence of Ascorbic Acid. *Anal. Bioanal Electrochem*, *10*(1), 52-63.

[116] Amiri, M., Bezaatpour, A., Pakdel, Z., & Nekoueian, K. (2012). Simultaneous voltammetric determination of uric acid and ascorbic acid using carbon paste/cobalt Schiff base composite electrode. *Journal of Solid State Electrochemistry*, *16*(6), 2187-2195.

[117] Xu, G. R., Chang, H. Y., Cho, H., Meng, W., Kang, I. K., & Bae, Z. U. (2004). Macrocyclic nickel (II) complex and hydrophilic polyurethane film electrodes for the electrocatalytic oxidation and selective detection of norepinephrine. *Electrochimica Acta*, *49*(24), 4069-4077.

[118] Zheng, L., & Song, J. F. (2009). Nickel (II)–baicalein complex modified multiwall carbon nanotube paste electrode and its electrocatalytic oxidation toward glycine. *Analytical Biochemistry*, *391*(1), 56-63.

[119] Majdi, S., Jabbari, A., Heli, H., & Moosavi-Movahedi, A. A. (2007). Electrocatalytic oxidation of some amino acids on a nickel–curcumin complex modified glassy carbon electrode. *Electrochimica Acta*, *52*(14), 4622-4629.

[120] Leonardi, S. G., Aloisio, D., Donato, N., Rathi, S., Ghosh, K., & Neri, G. (2014). Electrochemical sensing of ascorbic acid by a novel manganese (III) complex. *Materials Letters*, *133*, 232-235.

[121] Maree, S., & Nyokong, T. (2000). Electrocatalytic behavior of substituted cobalt phthalocyanines towards the oxidation of cysteine. *Journal of Electroanalytical Chemistry*, *492*(2), 120-127.

[122] Ni, J. A., Ju, H. X., Chen, H. Y., & Leech, D. (1999). Amperometric determination of epinephrine with an osmium complex and Nafion double-layer membrane modified electrode. *Analytica Chimica Acta*, *378*(1-3), 151-157.

[123] De Souza, F. C., Vegas, C. G., da Silva, D. A. I., Ribeiro, M. S., Cabral, M. F., de Melo, M. A., Mattos, R.M.T., Faria, R.B., & D'Elia, E. (2016). Amperometric and potentiometric determination of iodide using carbon electrodes modified with salophen complex. *Journal of Electroanalytical Chemistry*, *783*, 49-55.

CHAPTER 3

EXPERIMENTAL METHODOLOGY

3.1 Introduction

This chapter deals with the experimental procedures employed to attain the aim/objectives of this research work. It sequentially describes the synthesis route and techniques for the material and optical characterization of the materials utilized in this research. The whole chapter can be divided into four sections, as follows:

- Materials: Basic information on all the materials used throughout the study.
- Experimental Design: An outline of the entire sequential steps taken to resolve the problem of this research.
- Methodology: A comprehensive detail on the characterization and instrumental techniques used in developing an electrochemical sensor.

3.2 Chemicals and Materials

All the chemicals used throughout the study were of analytical grade and used as it is without additional purification. Ultra-pure Milli-Q water (from Millipore) with 18.2 MΩ at 25 ^{o}C was used to prepare all solutions. All the materials used in the whole study are listed in Table 3.1.

3.3 Experimental Design

There were some sequential steps put in place for the research to achieve its objectives. Firstly, the materials were synthesized and characterized using various techniques such as TEM, XRD, XPS, FTIR, UV-Vis. Then, upon successful synthesis and characterization of the materials, their electrochemical properties were investigated. This was done to find its potential as a biomolecule sensor with the aid of a three-electrode system and a Potentiostat. A diagrammatic description of the entire research work is shown in Figure 3.1.

Table 3.1: Chemicals and materials used in the work

Serial No	Chemicals/Materials	Source
1	Dopamine	Sigma-Aldrich
2	Potassium Iodide	Sigma-Aldrich
3	Uric acid	Sigma-Aldrich
4	Cysteine	Sigma-Aldrich
5	Sodium Sulfide	Merck
6	Bismuth Nitrate Pentahydrate	Fluka Chemica
7	Cobalt sulfate heptahydrate	Sigma-Aldrich
8	Nickel chloride hexahydrate	Sigma-Aldrich
9	Buffer components: Na_2HPO_4, KH_2PO_4, and KCl	Rochelle chemicals
10	Pt auxiliary electrode	BASi
11	Glassy carbon electrode	BASi
12	Ag/AgCl electrode	BASi
13	Alumina micro polish powder (1, 0.3, and 0.05 micron)	Buehler
14	Ultra-pure Milli Q water with 18.2 MΩ at 25 ^oC	Millipore
15	Nafion	Sigma-Aldrich
16	Ethyl Acetate	Merck
17	Ethanol	Sigma-Aldrich
18	Methanol	Sigma-Aldrich
19	Nitric acid	Rochelle
20	Sulphuric acid	Rochelle
21	Acetone	Promark Chemicals
22	Aniline	Sigma-Aldrich

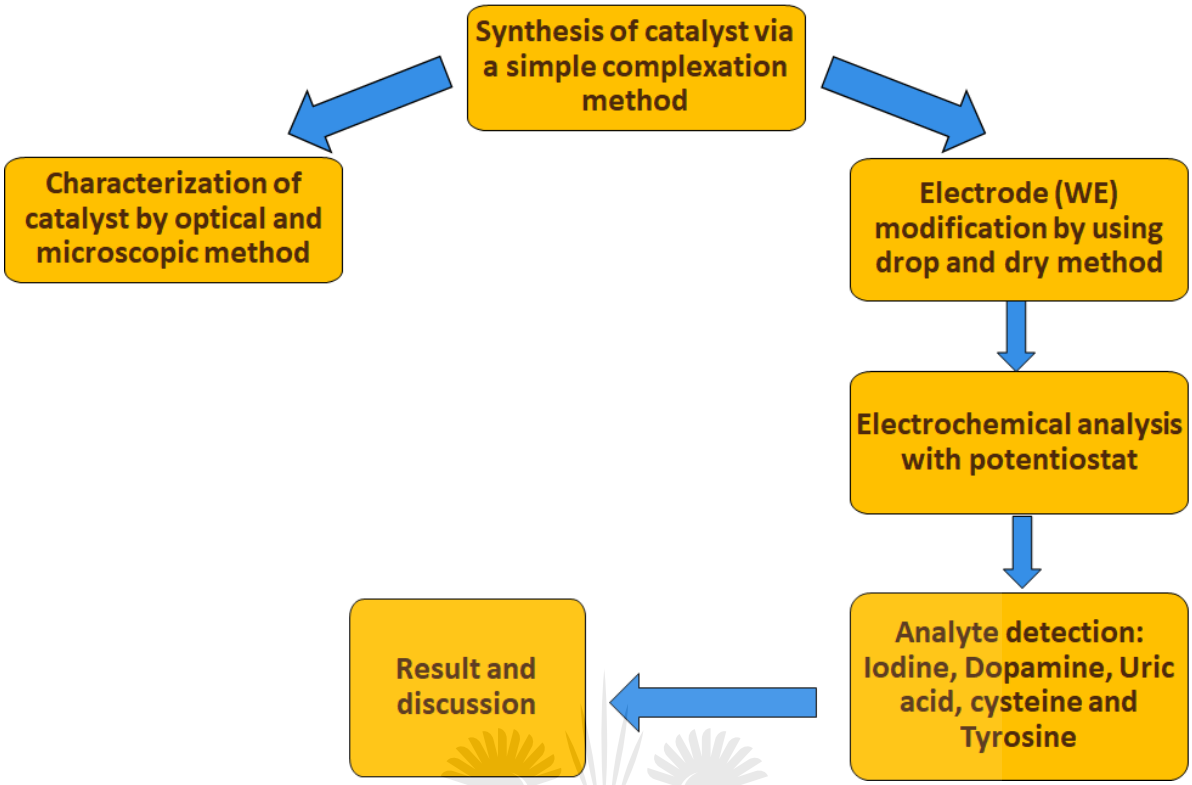

Figure 3.1: Flow chart of the entire research work

In designing the electrochemical sensor, the following successive steps were used.

1. Electrode and Buffer preparation: This involves cleaning the electrode for use and preparing the electrolyte buffer system for electrochemical analysis.

2. Standardization of the electrode: This step ensures the electrode's cleanliness by taking some electrochemical measurements. The behavior of the electrodes in the presence of blank analytes could also be ascertained.

3. Optical and Electrochemical measurements: Voltammetric and optical methods were used to characterize the complex materials to extract useful details concerning electrode modification to develop electrochemical sensors. The techniques used were: Fourier Transform Infrared Spectroscopy (FTIR), Transmission electron microscopy (TEM), Scanning electron microscopy (SEM), Elemental analysis (EA), Nuclear Magnetic Resonance (NMR) Spectrometry, X-ray diffractometry (XRD), Cyclic Voltammetry (CV), Square wave Voltammetry (SWV), and Chronoamperometry (CA).

4. Preparation of the aniline metal complex modified platform: This involves modifying the bare electrode with the synthesized material to develop an electrochemical sensor. The electrodes were modified using the 'drop and dry method.'

5. Analyte sensing: This step involves the electrochemical recognition of analytes (iodine, dopamine, uric acid, and cysteine). The electrochemical techniques used for these analytes recognition are cyclic voltammetry (for quantitative), square wave voltammetric, and chronoamperometric (for qualitative).

6. Electrochemical sensor evaluation: This involves measuring response to analytes, stability, selectivity, sensitivity, reproducibility, linearity, and detection limit.

3.3.1 Buffer preparation

The phosphate buffer saline (PBS) was used as an electrolyte solution because its pH resembles pH-controlled conditions of physiological conditions. The PBS solution was prepared by dissolving 4.34456 g of K_2HPO_4 and 3.4025 g of KH_2PO_4 in a separate 250 ml volumetric flask.

3.3.2 Preparation of Ferri/Ferrocyanide $[Fe(CN)_6]^{3-/4-}$

5 mM of $[Fe(CN)_6]^{3-/4-}$ was prepared by dissolving 0.1646 g of $K_3Fe(CN)_6$ and 0.212 g of $K_4Fe(CN)_6$ were dissolved in 100 ml (10 mM) PBS to make a concentration of 5 mM (Ferri:Ferro-cyanide = 1:1). The prepared samples were used as FCN electrolytes.

3.3.3 Electrode preparation

The electrochemical setup involved a conventional three-electrode system that consists of a reference electrode (RE) made up of Ag/AgCl type, a glassy carbon electrode (GCE) as the working electrode (WE), and a platinum wire as the counter electrode (CE), as shown in Figure 3.2. The GCE was modified with synthesized materials using the drop and dry method. The GCE was always washed at the end of each run by careful polishing with alumina slurry of various sizes (0.05. 0.03 and 1.0 μM), separately and successively ultrasonicated in distilled water and ethanol for 3 mins. The CE was always cleaned by placing it in a red flame until it becomes red hot; after that, it was rinsed with de-ionized water. Finally, the RE was stored continuously in a solution of 3 M KCl when not being used.

A final control process was always conducted before the working electrode (GCE) is modified and ready for use. This control process involves placing the electrode in a 10 mM, 7.5 pH PBS solution in an electrochemical system and running a CV scan between a potential window of -0.1 V to 0.7 V at 50 mVs^{-1} scan rate. The non-appearance of a peak within this electrochemical window confirms the working electrode's cleanliness.

Figure 3.2: The three-electrode system in an electrochemical cell configuration coupled with a potentiometer

3.3.4 Synthesis Method

The synthesis of the transition metal complexes was done at room temperature. Temperature plays a huge role in the shape and size of nanomaterials or complexes. A transition metal salt of the metal complex to be prepared was used as a metal precursor in each section. The metal complexes were formed as an aqueous solution of the metal precursors was added dropwise to an aniline solution (in methanol /ethanol). The generated complex precipitates, resulting in the creation of metal complex particles. The aniline in the solution acts as a precipitating agent. All the aniline transition metal complexes were synthesized by a similar procedure. The synthesized samples were divided into different portions for characterizations and experiments.

Equations (3.1) and (3.2) were used as models for the preparation of solutions utilized in this project.

$$Mass = \frac{molarity(M) * volume(ml) * molar\ mass(\frac{g}{mol})}{1000} \quad (3.1)$$

$$C_1V_1 = C_2V_2 \quad (3.2)$$

C_1 and C_2 are concentration in moles per liter

3.4 Methodology

3.4.1 Material Characterization

3.4.1.1 Fourier Transform Infrared Spectroscopy (FTIR)

The FTIR is a versatile, non-destructive, and non-contact analytical tool used to identify the vibration characteristics of chemical functional groups present in materials by obtaining their infrared spectrum of absorption or emission. It is built upon the absorption of light by molecules in the infrared region of the electromagnetic spectrum. The irradiation of a molecule with infrared light induces vibrations within the molecule. As an interaction occurs between the infrared light and the sample, chemical bonds will stretch/bend/contract in response to the light. Chemical compounds absorb infrared radiation with their absorption peak energy corresponding to their bonds' vibration frequency or energy [1]. Consequently, the analyzed sample's molecular fingerprints can be generated as the different functional groups absorbs characteristic frequencies of the infrared radiation irrespective of the structure of the rest of the molecule. These processes make infrared spectroscopy effective for a range of analyses. The infrared (IR) spectrum of any sample can be obtained within a few seconds without any elaborate sample preparation. A functional group in an analyzed sample is usually checked by comparing the band wavenumber position with the chemical structure. In this study, FTIR was utilized to obtain the characteristic IR peaks of the synthesized materials used to modify the glassy carbon electrodes. The infrared (FTIR) spectra were measured using a Shimadzu IRAffinity-1 in wavenumber range 500-5000 cm^{-1} with a spectral resolution of 8 cm^{-1}.

3.4.1.2 Ultraviolet-Visible spectroscopy (UV-vis)

This analytical technique is used to determine the optical properties (transmittance, absorbance, and reflectance) of liquids and solids. UV-Visible spectroscopy involves measuring the attenuation of a beam of light after it is passed through a sample at a specific wavelength in the UV or visible spectrum. The sample absorbs a fraction of the light, causing the molecules within the sample to undergo electronic transitions (excitation of the electrons from the ground state to a higher energy state). There exist various transitions between the bonding, anti-bonding, non-bonding, pi, and sigma electron orbitals. But most absorptions of UV-Visible light by molecules within a sample often occur with the excitation of non-bonding orbital or pi-bonding to the antibonding pi-molecular orbital. These transitions result in absorption bands that are characteristic features of the molecules in the sample [2]. The extent of absorption at different wavelengths is related to the number of molecules absorbing the radiations. Thus, the UV-Visible spectrum provides a plot of optical absorbance against a wavelength range. Substances identified with UV-Visible are always confirmed by comparing their spectrum with a reference/standard spectrum. However, UV-Vis spectra cannot be solely used for the complete identification of an unknown substance. The quantitative calculation of the absorbance and concentration of absorbing species is possible and guided by Beer Lambert's law according to Equation (3.3) [3].

$$A = \varepsilon c l \quad (3.3)$$

Here, A is the measured absorbance, which can be defined as log (I_o/I) in which *Io* is the intensity of incident light, and *I* is the intensity of the transmitted light.

ε is the molar absorptivity (extinction coefficient), which is constant for an organic sample.

c is the molar concentration of the sample,

L is the path length of light in the sample

The above linear relationship between the absorbance and the sample concentration (Equation 3.3) can be used to determine the concentration of an unknown material. A UV-Visible spectrophotometer was used to monitor the optical changes that occurred upon the transition metal aniline complexes' synthesis in this work. The absorption spectra of the materials were obtained using Shimadzu Spectrophotometer (UV-1800) in wavelength range 200-800 nm.

3.4.1.3 Transmission electron microscopy (TEM)

TEM is a microscopic technique that utilizes electron beams through an ultra-thin specimen in the electron microscope to illuminate the sample to form an image. The image is magnified and focused onto an imaging device, such as a fluorescent screen, a layer of photographic film, or to be detected as a sensor such as a charge-coupled device (CCD) camera. The produced images are of high resolution because the electron's wavelength is 100000 times shorter than visible light. Its operation is carried out at high voltages of about 200 kV to 400 kV. The interaction of the electron beam with the whole thickness of the sample produces a TEM image that tends to be a projection of the entire sample, including the surface and internal structure. The samples were placed in absolute ethanol and sonicated for 10 mins. After that, a drop of the sonicated solutions was placed on a copper grid coated with carbon. Samples were left to air-dry before introducing into the TEM instrument. In this study, the TEM analysis was carried out to determine the internal structure of the samples. The morphologies were captured on a JEOL-JEM-2100 transmission electron microscope (TEM), operating at a voltage of 200 kV.

3.4.1.4 Scanning electron microscopy (SEM)

SEM technique gives information on the surface morphology and composition of a material. The instrument uses high-energy electrons to interact with the surface of an electrically conductive material by producing different signals. Due to its electron usage, the material must be electrically conductive or covered with a conductive layer (carbon or gold) before SEM analysis to increase its conductivity. SEM's basic principle is that the electron beam emitted from an electron gun is finely focused with electromagnetic lenses and an objective lens on a small spot on the specimen surface [4]. These beams of electrons are deflected across a specimen at regulated speeds to produce images. The whole system, from the electron source, through the lenses, to the detector, operates under a high vacuum to prevent the loss of the emitted electrons to air. The incident electrons interact with sample atoms to produce signals. These signals are collected and processed by the detector to provide information on the sample's surface morphology and composition [5].

Three essential signal types from the electron beam's interaction with the specimen atoms are backscattered electrons, secondary electrons, and X-rays. Secondary electrons (SE) imaging mode is mostly used for imaging in SEM. Secondary electrons have low energy (less than 50 eV). Thus, they are generated from regions around the specimen surface and produce a high

lateral resolution signal. In this project, SEM was utilized for examining the surface morphology of the complex materials. The prepared samples' surface morphology was investigated using a scanning electron microscope (TESCAN VEGAS) with a high voltage of 20 kV at a working distance of approximately 19 mm.

3.4.1.5 Elemental analysis (EA)

Elemental analysis (EA) is an analytical technique that is used to analyze the elemental or isotopic composition of a material. The method could be used for qualitative (determining what elements are present) and quantitative analysis (determining how much each is present). The most common form of elemental analysis, CHNX analysis, is used to determine the mass fractions of carbon, hydrogen, nitrogen, and heteroatoms (X) (halogens, sulfur) of a sample [6]. This analysis could help determine an unknown compound's structure and determine a synthesized compound's structure and purity. The elemental analysis is also the best and cheapest way of assessing the purity of the sample. In this work, EA was utilized for CHNX analysis of one of the complex materials. Elemental analyses were performed on a Vario Elementar III microcube CHNS analyzer with a 950 ^{o}C furnace temperature and helium as a carrier gas.

3.4.1.6 Nuclear Magnetic Resonance (NMR) Spectrometry

Nuclear Magnetic Resonance (NMR) spectroscopy is a valuable analytical chemistry technique used in quality control and research to determine the content and purity of a sample and its molecular structure. For example, NMR can quantitatively analyze mixtures containing known compounds. The basis of NMR is that an atomic nucleus's magnetic dipoles interact with an external magnetic field, leading to a nuclear energy level diagram having distinct eigenvalues. These eigenvalues are associated with certain eigenstates in which an atom can exist. The spinning nucleus's magnetic dipole is aligned when in a lower energy state than the external magnetic field while in a higher state [7,8,9]. The transition between these states is stimulated with the help of a radiofrequency transmitter. The absorbed energy is further recorded by a radio frequency receiver in the form of a resonance signal. The major types of NMR include proton (H-NMR), carbon (C-NMR). These techniques are generally used to elucidate the number of protons and carbon in a compound. The two techniques could provide valuable information that can be used to deduce the structure of organic compounds. The ^{1}H NMR helps to determine the type and number of hydrogen (H)

atoms, while ^{13}C NMR determines the type and number of carbon (C) atoms in a molecule. The ^{1}H NMR is associated with a small fraction of sample concentration and a rapid spectrum response. However, because of just 1.1 percent natural ^{13}C isotope abundance, ^{13}C NMR requires a longer scan period with the concentrated sample required to obtain a nice, detailed spectrum. In this work, the NMR technique was used to validate the identity of the synthesized materials further. At room temperature, all proton nuclear magnetic resonance (1H NMR) spectra observations were performed on a Bruker 500 MHz spectrophotometer. Chemical shift d in parts per million (ppm) downfield with reference to deuterated solvent (2.50 ppm for DMSO-d_6) was reported for all 1H NMR spectra (0.00 ppm). Multiplicities were presented as s (singlet), d (doublet), and t (triplet). Coupling constants *J* values were expressed in Hz, and the number of protons was expressed as n*H*. A 101 MHz NMR spectrometer was used to obtain decoupled C NMR spectra at room temperature. With reference to deuterated solvent, spectra were reported as the chemical shift in units of parts per million (ppm) downfield (39.81 ppm for DMSO-d_6 or 77.16 ppm for $CDCl_3$).

3.4.1.7 X-ray diffractometry (XRD)

The XRD is a non-destructive analytical technique used for revealing qualitative and quantitative information about unknown crystalline materials. It is a versatile technique that can be used to gain insights into a material's molecular and atomic structure, crystal phase, and crystal orientation. X-rays are short wavelength radiation occupying the region between the gamma and the ultraviolet rays in the electromagnetic spectrum. Their wavelengths are comparable to the size of atoms. Hence, they are very suitable for investigating the arrangement of atoms in a variety of crystalline materials. In XRD analysis, a crystalline atom produces an incident beam of X-rays to diffract into several separate directions. Bragg's law is satisfied when the interactions between the atoms of the sample and the incident rays produce constructive interference (and diffracted rays). The generated X-ray patterns form a characteristic of the crystals present in the sample. The diffracted X-ray intensity is measured as the sample is scanned over a range of 2θ angles. The Braggs law provides a relationship between the wavelength of the incident X-rays, the angle of incidence, and the spacing between the atoms' crystal lattice planes. It is expressed as [10,11]:

$$n\lambda = 2d \sin \theta \quad (3.4)$$

where n is a positive integer known as the order of diffraction and is often equal to unity, λ is the incident X-ray beam's wavelength, and θ is the incident Bragg's angle.

In this study, XRD analysis was used to investigate the crystal planes and crystal size of the electrodes' fabrication materials. Before the analysis, the samples were placed onto the sample 40 K and 25 mA using Cu Ky radiation with a wavelength of 1.5406 A. Data was collected with step intervals of 0.05^o over 2θ in the range of $10\text{-}90^o$ for each sample with an acquisition time of 2 secs. Powder X-ray diffraction (pXRD) studies were carried out on a PAN analytical X'Pert PRO X-ray powder diffractometer operating with Cu Ka radiation (λ = 1.5406 Å) at room temperature. The wide-angle (2θ = 10-80°) diffraction pattern at a step rate of $0.1°\cdot min^{-1}$ was measured.

3.4.1.8 X-ray Photoelectron Spectroscopy (XPS)

XPS is a commonly used spectroscopic technique for measuring the surface elemental composition, empirical formulas, chemical states, and the electronic state of the elements within a material [12,13]. The specimens are illuminated with a monochromatic X-ray source (photons), resulting in the emission of core-shell photoelectrons. The ejected electrons are at characteristic binding energy values unique to the element and particular atomic orbits. A detector analyzes the energy of those ejected electrons. A plot of these binding energies versus the relative number of electrons is used to identify the elements present and their quality (except hydrogen and helium). The characteristic XPS peaks, corresponding to the electrons' electronic configuration within the atoms, e.g., 1s, 2s, 2p, 3s, etc., are used to identify the number of elements within the area irradiated directly. The XPS must be performed under Ultra-High Vacuum (UHV) conditions [14,15,16].

In this study, XPS measurements were performed using a VG MultiLab 2000 system with a monochromatic X-ray source, Mg Ka (1253.6 eV). The analysis was accomplished to validate elements present in the synthesized material and the binding energies.

3.4.2 Electrochemical Characterization

To evaluate the performance of the synthesized materials as sensing material, all electrochemical techniques in this study were employed using a Potentiostat Biologic SP-300 (500 mA to 10 A) as earlier shown in Figure 3.2. The Potentiostat is coupled with EC lab software using a computer, allows us to evaluate electrochemical performance of materials using various techniques available in EC lab from which we used Cyclic Voltammetry, Electrochemical Impedance Spectroscopy, square wave voltammetry, and

Chronoamperometry using an electrochemical cell. The electrochemical cell used consist of a glassy carbon electrode (GCE) serving as the working electrode, a silver/silver chloride electrode (Ag/AgCl) as a reference electrode, a platinum wire as a counter electrode, and a neutral electrolyte (10 mM PBS used for the whole study).

3.4.2.1 Cyclic Voltammetry (CV)

Cyclic voltammetry (CV) is the most extensively used electrochemical technique for qualitative and quantitative electrochemical reactions. The technique is commonly employed for the study of mechanism, kinetics, and thermodynamic of chemical reactions, analysis of coupled electrochemical reactions or adsorption processes [17,18]. This technique can also study the reversibility, formal oxidation, and reduction potentials of a system [19-23]. A typical CV experiment is usually carried out using a three-electrode system consisting of a reference, working, and counter electrodes. The reference electrode is one in which the potential is known, and it allows the measurement of the potential at the working electrode. The working electrode is one in which oxidation and reduction occur, while the counter/auxiliary electrode serves to close the circuit in an electrochemical cell. The electrochemical cell (Figure 3.2) consists of an electrolytic solution with three different electrodes inside it and connected to a potentiostat. The electrolytic solution provides ions to the electrodes in the course of oxidation and reduction. The electrodes are left stationary in the electrolytic solution, which remains undisturbed.

In CV studies, the potential is endlessly changed as a function of time [24]. The working electrode's potential is usually scanned from an initial potential (E_i) to the final potential (E_f) and consequently returns to the initial potential (E_i). The initial potential is determined such that the chemical species of interest are not initially oxidized or reduced. The upper limit potential is also chosen so that the oxidation/reduction of the species under investigation occurs within the potential interval, $E_f - E_i$. The rate at which the potential changes is termed scan rate. The potential at which the scanning takes reverse back is referred to as the switching potential. The point where the voltage applied is sufficient to have caused oxidation or reduction of an analyte. The current obtained during the potential scan is measured and plotted against the voltage (potential). The graph of current against voltage is referred to as a cyclic voltammogram (Figure 3.3). The magnitude of oxidation and reduction currents and the voltammogram formed often depends on the selected initial and final

potential, scan rate, analyte concentration, the formal redox potential, standard rate constant, and the diffusion coefficient of the redox couple [24].

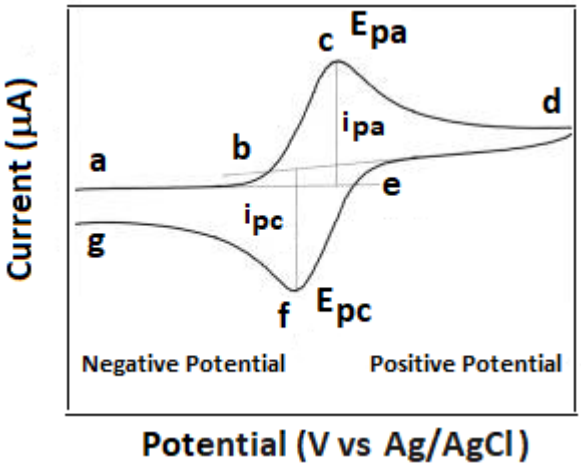

Figure 3.3: Schematic illustration of typical cyclic voltammogram showing the important peak parameters.

The curve in Figure 3.3 represents a typical cyclic voltammogram. The voltammogram comprises the system's current response from an applied voltage, which explains the forward and backward scan representing the oxidation and reduction reactions, respectively. The oxidation process occurs from the initial potential (a) to the switching potential (d). In this region, the potential is scanned positively to cause oxidation. The resulting current is called anodic current (I_{pa}). The corresponding peak potential occurs at (c), called the anodic peak potential (E_{pa}). The Epa is reached when all of the substrates at the surface of the electrode have been oxidized. After the switching potential has been reached (d), the potential scans negatively from (d) to (g). This process results in cathodic current (I_{pc}) and a reduction to occur. The peak potential at (f) is called the cathodic peak potential (E_{pc}) and is reached when all of the substrates at the surface of the electrode have been reduced. The potential is applied between the reference and working electrodes, while the current flow is measured between the working and counter electrodes. According to the literature, many researchers have used the cyclic voltammetry technique to analyze redox status, electrode behavior and for the limit of detection in different research settings, especially for sensing purposes. Vareesh *et al.* synthesized a cobalt Phthalocyanine complex for dopamine recognition and made use of cyclic voltammetry to calculate the detection limit [25]. Gopinath *et al.* also employed cyclic voltammetry to detect uric acid using a novel Schiff base complex as a modifier [26].

3.4.2.2 Electrochemical impedance spectroscopy (EIS)

Electrochemical impedance spectroscopy is a useful technique that applies a sinusoidal potential excitation to an electrochemical cell producing an alternating current signal which is measured and analyzed. Generally, an electrode's surface is probed by scanning an AC signal over a range of frequencies to generate an impedance spectrum. The generated spectrum is usually recorded in two phases: the in-phase-current response that determines the impedance's real (resistive) component, while the out of phase component determines the capacitive component [27]. When a sinusoidal potential is applied to an electrode surface, the current produced will have the same frequency as the applied sinusoidal potential but may experience a phase shift. The phase shift is determined by the electrochemical system's relative resistive and capacitive characteristics. EIS is an effective technique for characterizing materials based on how they obstruct current flow, and it is measured in resistance. The technique gives a more accurate way of measuring the resistance of a material to the flow of electricity because it also accounts for mechanisms such as capacitance and induction.

In the EIS technique, electron transfer takes place at a high frequency, while mass transfer takes place at a low frequency. Impedance results are generated at the end of each frequency. These results are commonly simulated to the equivalent circuit of resistors and capacitors representing physical processes occurring in the electrochemical system being studied. Moreso, a plot known as the Nyquist plot, shown in Figure 3.4, can represent EIS data. In this plot, an imaginary impedance that shows the inductive and capacitive character of the cell is plotted against the actual impedance of the cell [28].

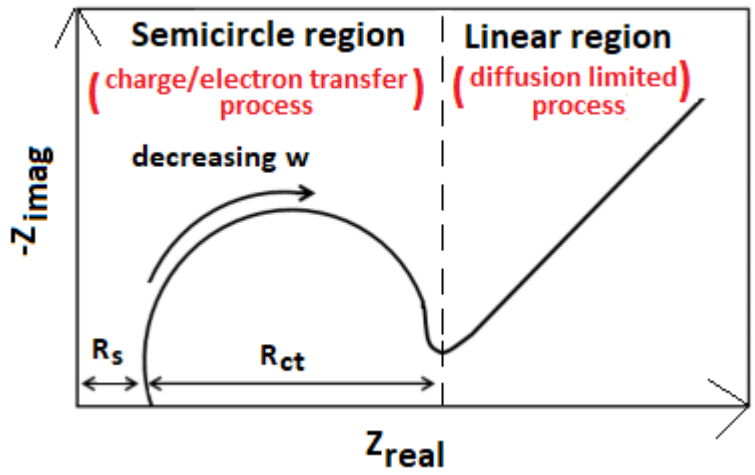

Figure 3.4: A typical Nyquist plot for an electrochemical system.

For electrochemical sensors, data retrieved from the Nyquist plot includes the charge-transfer resistance and the diffuse lay resistance. Both the electron transfer-limited process and the diffusion-limiting phase of the electrochemical process can be defined by two regions in the impedance spectrum [29,30]. The charge transfer process (electron transfer limited process) is represented by the semicircle portion of the EIS plot, whose diameter is equal to the material's charge transfer resistance (Rct). This area of the EIS plot is usually found at higher frequencies. The diameter is proportional to the material's resistivity and, by extension, inversely proportional to the material's conductivity. The linear portion of the EIS plot usually found at lower frequencies represents the diffusion-limited process at the electrode interface [29,30]. This reveals the diffusion-limiting step of the electrochemical process solution-phase resistance. From Figure 3.4, the charge transfer resistance (Rct) is inversely proportional to the rate of electron transfer, whereas mass-transfer constraints cause the Warburg impedance (Zw). Rs, known as solution-phase resistance, is derived primarily from electrolyte resistance and is primarily used in conductivity sensors for analytical purposes [31].

Electrochemical impedance spectroscopy helps determine the qualities of a metal-enriched material. A material possessing a larger surface area and a lower electrochemical impedance will exhibit excellent electrocatalytic properties [30]. The EIS technique has been used in different research applications to probe the electrochemical behavior at the surface of the electrode. Atacan employed EIS to investigate the interfacial changes of his modified electrodes for cysteine detection [32]. Qin *et al.* also used EIS to investigate the interfacial changes of their monodispersed gold nanoparticles for DA detection [33].

3.4.2.3 Square wave Voltammetry (SWV)

Square wave voltammetry (SWV) is a pulse voltammetric technique that uses a combined square wave and staircase potential applied to a stationary electrode [34]. A square wave voltammetry is also a differential technique in which a potential waveform composed of symmetrical waves of constant amplitude is superimposed on a base staircase potential with the squarewave's forward pulse coinciding with the staircase step [35,36]. It involves applying a potential waveform to the working electrode and measuring a resulting current for each wave period [37]. A plot of the net current measured against each waveform cycle's applied potential gives a squarewave voltammogram. The square wave consists of a pulse height/squarewave amplitude, the staircase/peak height, the pulse time, and the cycle period

[24]. The peak height of an SWV is directly proportional to the concentration of the electroactive species in the solution. The SWV has the advantage of excellent peak separation and high sensitivity over cyclic voltammetry. Moreso, SWV is often preferred to other pulse voltammetric techniques such as differential pulse voltammetry and normal pulse voltammetry because it offers more rapid analysis [38]. SWV has been applied in different nanomaterial applications, most importantly sensing. Umapathi *et al.* used SWV to determine the efficiency of their CuSe material for dopamine detection [39]. Beitollahi constructed a cysteine and tyrosine sensor with graphene nanosheets and ethyl 2-(4-ferrocenyl[1,2,3]triazol-1-yl). They used SWV to determine the analytical performance of the sensor [40]. In this study, SWV was employed to confirm our analyte detection results from the cyclic voltammetry experiments.

3.4.2.4 Chronoamperometry (CA)

Amperometry is a technique whereby a pulsed potential is applied to the working electrode and the current, which results from the faradaic process at the electrode due to the potential step being monitored with respect to time. During Chronoamperometric measurements, the working electrode is stepped from a potential, E_1, where there is no current flow, where the oxidation or reduction of the electrochemically active species does not take place to a potential, E_2 where the current is attributed to the electrode reaction. The resulting current–time transient is then recorded. The current-time dependence can be monitored (Figure 3.5b) using the Cottrell equation [41].

$$i(t) = \frac{nFAcD^{\frac{1}{2}}}{\pi^{-\frac{1}{2}}t^{-\frac{1}{2}}} = kt^{-\frac{1}{2}} \quad (3.5)$$

In the above equation, n corresponds to the number of electrons, F is a constant (Faraday); A represents the electrode's surface area, c is the solution concentration, D is taken as diffusion coefficient of the solution, t is time, and k is the rate constant.

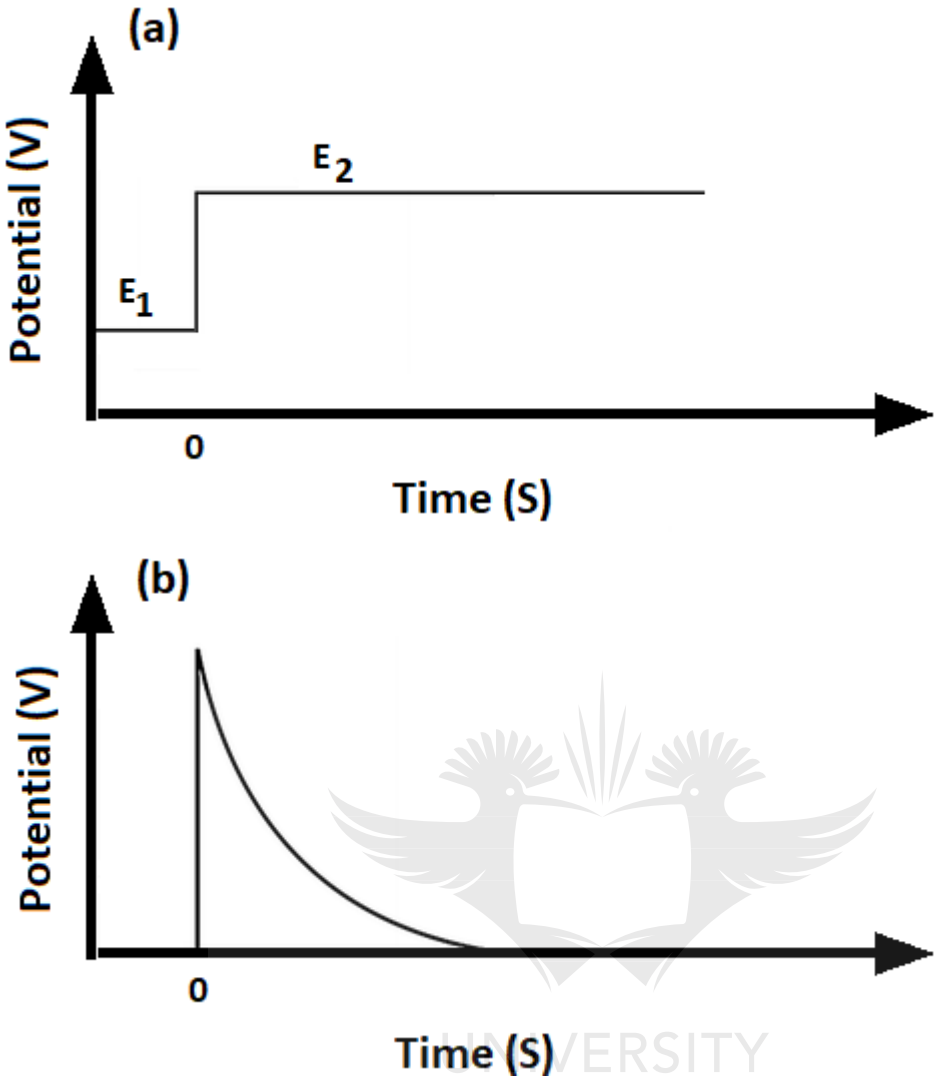

Figure 3.5: Typical chronoamperometric (a) potential-time waveform (b) resultant current-time response.

The current-time response is a representation of the change in gradient concentration at the vicinity of the surface. It is a slow expansion of the diffusion layer linked with the reduction of the reactant as time increases. Chronoamperometry contrasts to all pulsed techniques and develops high charging currents that decay exponentially like any resistor-capacitor (RC) circuit with time. The process provides a good signal-to-noise ratio because the current is integrated over a prolonged duration. The Chronoamperometry technique can measure the diffusion coefficient of electroactive species or the working electrode's surface area. It can also measure a material's selectivity against some interferents that could coexist with the target analytes. In this study, chronoamperometry was mainly employed to evaluate the synthesized materials' selectivity to the analytes of interest. The amperometric technique is

used by researchers primarily for calculating detection limits. Vareesh *et al.* employed chronoamperometry to calculate the limit of detection for their dopamine sensor fabricated with a cobalt phthalocyanine complex [42]. Also, Feng Wang *et al.* used the amperometric technique to calculate the analytical sensitivity of their glucose sensor made with a nickel (II) metal-organic framework/carbon nanotubes composite [43].

3.5 Parameters to determine the performance of an Electrochemical sensor

Some parameters have been evaluated from the above-mentioned EC Lab techniques to study the synthesized materials' sensing performance. Sensitivity, the limit of detection, defines the potential of the material for electrochemical sensor application. In this project, all parameters are calculated dependent on the active material's mass on the glassy carbon electrode's glassy surface.

3.5.1 Sensitivity

Sensitivity refers to the ratio of the output change Δy to the input change Δx under steady-state operation. It is the slope of the output-input characteristic curve, otherwise known as the calibration curve. The sensitivity of our electrochemical sensors with a geometrical surface area was calculated as the slope of the calibration curve divided by the active surface area of the electrode, as shown in Equation (3.6) [3].

$$Sensitivity = \frac{Slope\ of\ calibration\ plot, m\ (\mu A \mu M^{-1})}{Active\ surface\ area\ of\ electrode, A(cm^2)} \quad (3.6)$$

The electrode's area was calculated to be 0.070695 cm^2 using $\pi(d/2)^2$, where d is the diameter of the geometrical active sensing area of the electrode taken as 0.3 cm^2 and $\pi = 3.142$.

3.5.2 Limit of Detection (LOD)

The detection limit of a biosensor refers to the lowest amount of known concentration of an analyte that can be detected but not necessarily quantitated as an exact value. There are many ways of evaluating the detection limit. In this study, the limit of detection was calculated using a calibration curve. Equation (3.7) expresses the formula to calculate LOD [3].

$$LOD = \frac{t\ x\ standard\ deviation\ of\ the\ response}{slope\ of\ the\ calibration\ curve} \quad (3.7)$$

Where t is the signal to noise ratio. The signal-to-noise ratio is usually calculated by comparing the measured signals from samples with known low analyte concentrations with those from blank samples and determining the minimum concentration at which the analyte

can be sensed. To estimate the detection limit, a signal-to-noise ratio of 3 or 2 to 1 is usually considered appropriate.

The standard deviation of the response can be estimated using either y-residuals or y-intercepts of regression lines.

3.6 Sub conclusion

The experimental design and characterization tools adopted for the project have been presented in this chapter. The material is subjected to various structural, compositional, and morphological techniques for the investigation. The characterization of the synthesized materials confirms their successful synthesis and recommendation for sensing application. A detailed study of the electrochemical techniques carried out to evaluate the synthesized material's performance as a sensor has been presented in this chapter.

3.7 References

[1] Stuart, B., George, B., & McIntyre, P. (1996). Modern infrared spectroscopy applied to soil humic substances chemistry. *Science of the Total Environment*, *117*(118), 41-52.

[2] Field, L.D., Sternhell, S., Kalman, J.R. (2012). *Organic structures from spectra*. John Wiley & Sons.

[3] Skoog, D.A., West D.M., & Holler F.J., Crouch, S.R. (2014) *Fundamentals of Analytical Chemistry.* (Ed.9th). Singapore: Cengage Learning.

[4] Chatti, S., Laperrière, L., Reinhart, G., & Tolio, T. (Eds.). (2019). *Scanning Tunneling Microscopy BT - CIRP Encyclopedia of Production Engineering*. Springer Berlin Heidelberg.

[5] Bhushan, B. (Ed.). (2012). *Encyclopedia of Nanotechnology* (No. 544.1). Dordrecht, Netherlands: Springer.

[6] Sahu, R. C., Patel, R., & Ray, B. C. (2011). Removal of hydrogen sulfide using red mud at ambient conditions. *Fuel Processing Technology*, *92*(8), 1587-1592.

[7] Bai S. (2006) Nuclear magnetic resonance instrumentation. *Encyclopedia of Analytical Chemistry*. John Wiley & Sons, Ltd.

[8] Darbeau RW. (2006). Nuclear Magnetic Resonance (NMR) spectroscopy: a review and a look at its use as a probative tool in deamination chemistry. Appl Spectrosc Rev; 41:401-25.

[9] Gerothanassis IP, Troganis A, Exarchou V, Barbarossou K. (2002). Nuclear magnetic resonance (NMR) spectroscopy: basic principles and phenomena, and their applications to chemistry, biology and medicine. Chem Educ Res Pract; 3:229-252.

[10] Moseley, H. G. J. (1913). XCIII. The high-frequency spectra of the elements. *The London, Edinburgh, and Dublin Philosophical Magazine and Journal of Science*, *26*(156), 1024-1034.

[11] Moseley, H. G. J., & Darwin, C. G. (1913). XIV. The reflexion of the X-rays. *The London, Edinburgh, and Dublin Philosophical Magazine and Journal of Science*, *26*(151), 210-232.

[12] Steinhardt, R.G. and Serfass, E.J. (1953). *Surface Analysis with the X-Ray Photoelectron Spectrometer*. Analytical Chemistry, 25(5): 697-700.

[13] Vickerman, J.C. and Gilmore, I.S. (2009). *Surface Analysis : The Principal Techniques*. 2nd ed. Chichester, U.K.: Wiley. xix, 666.

[14] Buschow, K.H.J. (2001). *Encyclopedia of Materials: Science and Technology*. Amsterdam ; New York: Elsevier.

[15] Martin, P. M. (2009). *Handbook of deposition technologies for films and coatings: science, applications and technology*. William Andrew.

[16] Hüfner, S. (2013). *Photoelectron spectroscopy: principles and applications*. Springer Science & Business Media. 15,662

[17] Brownson, D. A., & Banks, C. E. (2014). The handbook of Graphene Electrochemistry. *The handbook of Graphene Electrochemistry.*

[18] Marken, F., Neudeck, A., Bond, A. M., & Scholz, F. (2010). *Electroanalytical Methods: Guide to Experiments and Applications.* Scholz, F., ed.

[19] Allen, J. B., & Larry, R. F. (2001). Electrochemical methods: fundamentals and applications. John Wiley & Sons, Inc. *Department of Chemistry and Biochemistry, University of Texas at Austin.*

[20] Brown, M. J., Raymond, J., Homa, D., Kennedy, C., & Sinks, T. (2011). Association between children's blood lead levels, lead service lines, and water disinfection, Washington, DC, 1998–2006. *Environmental Research*, *111*(1), 67-74.

[21] Hibbert, D. B. (1993). Introduction to electrochemistry. In *Introduction to Electrochemistry* (pp. 1-10). Palgrave, London.

[22] Kaifer, A. E., & Gómez-Kaifer, M. (2008). *Supramolecular Electrochemistry*. John Wiley & Sons.

[23] Randles, J. E. (1948). A cathode ray polarograph. Part II.-The current-voltage curves. *Transactions of the Faraday Society*, *44*, 327-338.

[24] Compton, R. G., & Banks, C. E. (2018). *Understanding voltammetry*. World Scientific.

[25] Sajjan, V. A., Mohammed, I., Nemakal, M., Aralekallu, S., Kumar, K. H., Swamy, S., & Sannegowda, L. K. (2019). Synthesis and electropolymerization of cobalt tetraaminebenzamidephthalocyanine macrocycle for the amperometric sensing of dopamine. *Journal of Electroanalytical Chemistry*, *838*, 33-40.

[26] Gopinath, S. K., Pari, M., Rudrannagari, A., Kattebasaveshwara, I. B., & Halappa, S. K. (2020). Synthesis, Characterization and Electrochemical Sensor Based Upon Novel Schiff Base Metal Complexes Derived from the Non-Steroidal Anti-inflammatory Drug, Flufenamic Acid for the Determination of Uric acid and their Biological Applications.

[27] Wellstead, P., & Cloutier, M. (2012). Modelling and simulation of brain energy metabolism: Energy and Parkinson's disease. In *Systems biology of Parkinson's disease* (pp. 19-38). Springer, New York, NY.

[28] Barsoukov, E., & Macdonald, J. R. (Eds.). (2018). *Impedance Spectroscopy: Theory, Experiment, and Applications*. John Wiley & Sons.

[29] Fabregat, G., Cordova-Mateo, E., Armelin, E., Bertran, O., & Aleman, C. (2011). Ultrathin films of polypyrrole derivatives for dopamine detection. *The Journal of Physical Chemistry C*, *115*(30), 14933-14941.

[30] Lavanya, N., & Sekar, C. (2017). Electrochemical sensor for simultaneous determination of epinephrine and norepinephrine based on cetyltrimethylammonium bromide assisted SnO2 nanoparticles. *Journal of Electroanalytical Chemistry*, *801*, 503-510.

[31] Webster, R. (Ed.). (2001). *Neurotransmitters, drugs and brain function*. John Wiley & Sons.

[32] Atacan, K. (2019). CuFe2O4/reduced graphene oxide nanocomposite decorated with gold nanoparticles as a new electrochemical sensor material for L-cysteine detection. *Journal of Alloys and Compounds*, *791*, 391-401.

[33] Qin, X., Zhang, J., Shao, W., Liu, X., Zhang, X., Chen, F., Qin, X., Wang, L., Luo, D. & Qiao, X. (2021). Modification of electrodes with self-assembled, close-packed AuNPs for improved signal reproducibility toward electrochemical detection of dopamine. *Electrochemistry Communications*, *133*, 107161.

[34] Ramaley, L., & Krause, M. S. (1969). Theory of square wave voltammetry. *Analytical Chemistry*, *41*(11), 1362-1365.

[35] Kounaves, S. P. (1997). Voltammetric techniques. *Handbook of Instrumental Techniques for Analytical Chemistry*, 709-726.

[36] Wang, J. (1995). Electroanalysis and biosensors. *Analytical Chemistry*, *67*(12), 487-492.

[37] Monk, P. M. (2008). *Fundamentals of Electroanalytical Chemistry* (Vol. 29). John Wiley & Sons.

[38] Dogan-Topal, B., Ozkan, S. A., & Uslu, B. (2010). The analytical applications of square wave voltammetry on pharmaceutical analysis. *The Open Chemical and Biomedical Methods Journal*, *3*(1).

[39] Umapathi, S., Masud, J., Coleman, H., & Nath, M. (2020). Electrochemical sensor based on CuSe for determination of dopamine. *Microchimica Acta*, *187*(8), 1-13.

[40] Beitollahi, H., Ganjali, M. R., Norouzi, P., Movlaee, K., Hosseinzadeh, R., & Tajik, S. (2020). A novel electrochemical sensor based on graphene nanosheets and ethyl 2-(4-ferrocenyl-[1, 2, 3] triazol-1-yl) acetate for electrocatalytic oxidation of cysteine and tyrosine. *Measurement*, *152*, 107302.

[41] Girault, H. H. (2004). *Analytical and Physical Electrochemistry*. CRC Press.

[42] Sajjan, V. A., Mohammed, I., Nemakal, M., Aralekallu, S., Kumar, K. H., Swamy, S., & Sannegowda, L. K. (2019). Synthesis and electropolymerization of cobalt tetraaminebenzamidephthalocyanine macrocycle for the amperometric sensing of dopamine. *Journal of Electroanalytical Chemistry*, *838*, 33-40.

[43] Wang, F., Chen, X., Chen, L., Yang, J., & Wang, Q. (2019). High-performance non-enzymatic glucose sensor by hierarchical flower-like nickel (II)-based MOF/carbon nanotubes composite. *Materials Science and Engineering: C*, *96*, 41-50.

CHAPTER 4
ELECTROCHEMICAL RESPONSE OF BISMUTH-ANILINE COMPLEX UNDER THE EXPOSURE OF ORGANIC AND INORGANIC ENVIRONMENT

4.1 Introduction

Compounds containing bismuth have drawn immense interest from scientists owing to their multifunctional properties. In several domains, including organic synthesis [1], harvesting [2], energy storage [3], and electronics applications, pure and investigative research concerning bismuth-based materials has been initiated [4]. In addition, researchers have been encouraged to experiment on drugs synthesized from bismuth due to bismuth's low toxicity, especially those showing activity against a tumor, bacterial, and microbial infections [5].

Bismuth-based compounds have been reported to display promising results for rapid and simple sensing of biomolecules [6]. For example, bismuth oxide in the nano range has played a substantial role in the hybridization of DNA [7], glucose [8], and hydrogen peroxide sensing [9]. In biological samples, bismuth-based oxide nanoparticles (Bi_2WO_6) have also been documented for rapid electrochemical sensing of oxidative stress [10].

Iodine and dopamine are indispensable biologically active molecules that play significant functions in living organisms. Iodine has functions related to the neurological system, cell growth, and brain development [11,12]. For people with low iodine dietary intake, it may also be used as a nutritional supplement.

On the other hand, dopamine is a chemical messenger between brain neurons associated with the human body's most important functions, such as motivation, reward, memory, body movements, attention, and cognitive functions [13-16]. The imbalance of iodine and dopamine could result in mental retardation, goiter, and hypothyroidism in the case of iodine [17], and Parkinson's disease (PD) in dopamine [18]. Hence, their effective and efficient determination is necessary.

This work has been published in ***Springer Nature Applied. Science.*** **2, 2043 (2020).** https://doi.org/10.1007/s42452-020-03802-y

In this report, we have prepared a hybrid system of bismuth aniline through a simple complexation strategy. The synthesis of the organic-inorganic complex material was verified by the Infra-red spectroscopic technique to obtain the system's optical properties. Transmission electron microscopy was applied to visualize the microscopic property, and X-ray photoelectron spectroscopy technique calculated the structural property. Finally, the hybrid material was employed as an electrode modifier for iodide-ion and dopamine electrochemical recognition.

4.2 Experimental

4.2.1 Materials

As an analytical grade, dopamine, $Bi(NO_3)_3$.$5H_2O$, KI, and aniline were obtained and made use of without any additional purification. All additional reagents were used as acquired in this research.

4.2.2 Sample preparation and methods of characterization

The bismuth (III) aniline complex (BAC) was prepared under stirring conditions by applying 5 ml of prepared 0.1 M Bi (NO_3). $5H_2O$ solution to 0.48g of aniline dissolved in 10 mL of CH_3OH). A white precipitate emerged, leaving the reaction for an hour. For TEM analysis, a small fraction of the product was taken, and TEM images were captured with an instrument, JEOL-JEM-2100, operating at a voltage of 200 kV. The remainder of the substance was cleansed. For further characterization, the residue mass was collected, vacuum dried, and analyzed with X-ray diffractometer (Shimadzu XD-3A) using Cu-Kα radiation, NMR spectra with a Bruker 500 MHz NMR spectrometer, FTIR, Shimadzu IRAffinity-1, UV-vis 1800 Shimadzu UV spectrophotometer, and X-ray photoelectron spectra with 560 ECSA/SAM instrument. The leftover part of the dried mass was utilized for iodide-ion and dopamine recognition as an electrode material. Cyclic voltammetry (CV), square wave voltammetry (SWV), and chronoamperometry (CA), electrochemical impedance spectroscopy (EIS) methods were used for electrochemical measurements through a potentiostat (Bio-logic, SP-200 model). A three-electrode electrochemical cell was utilized to assess the synthesized material's electrocatalytic activity, with a glassy carbon electrode (GCE) serving as the working electrode. A silver/silver chloride electrode (Ag/AgCl) and a platinum wire were used as the reference and counter electrodes, separately.

4.3. Results and discussion

4.3.1 Morphological studies

Spectral properties of different transition metal and aniline-related complexes (and aniline derivatives) are well known in the literature [19]. Conversely, there is no research on the chemistry of complexation involving bismuth and aniline. The TEM image as presented in Figure 4.1A and B shows the as-synthesized BAC, with differing magnifications. Figure 4.1B is the magnified image from Figure 4.1A of the region chosen (within the box). The figures show a uniform matrix of the complex was clear, confirming that BAC has a homogeneous material phase. The SEM micrograph of the BAC can be shown in Figure 4.1C. The micrograph demonstrates an inhomogeneous matrix with a crushed ice-like appearance.

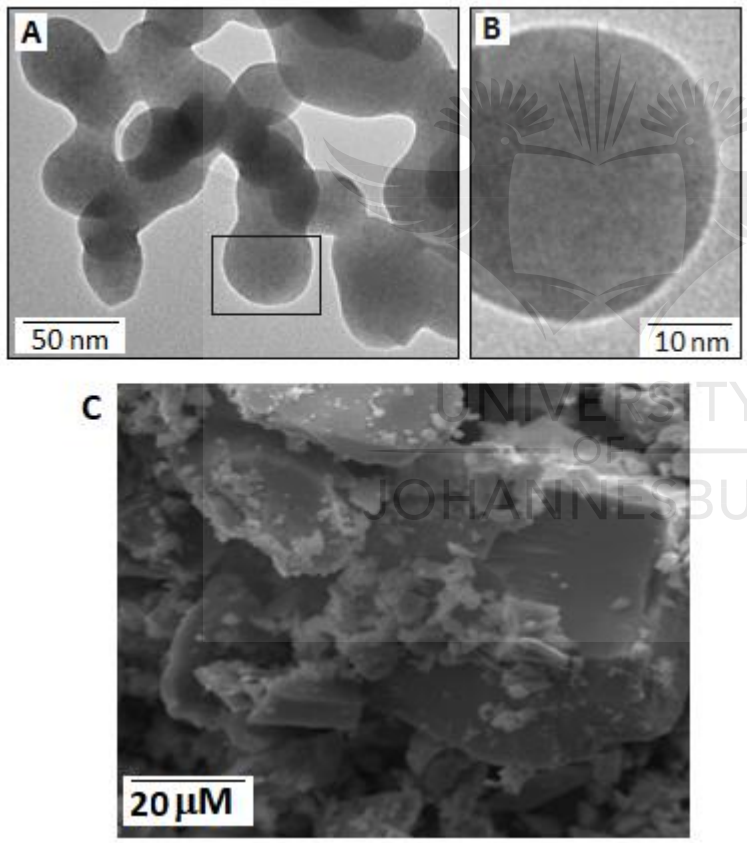

Figure 4.1: High magnification TEM pictures of the BAC (A and B), and (C) is the SEM image of Bi (III)-aniline complex.

4.3.2 FTIR analysis

The FTIR spectrum of aniline and the complex material (Bi (III) aniline) is displayed in Figure 4.2 (A and B). Aniline shows a bending vibration of N-H at 1630 cm^{-1} in the IR spectrum (a), and the benzenoid ring shows a C=C stretching vibration at 1494 cm^{-1}. A C-N stretching for aromatic amine is identified at 1269 cm^{-1}, while N-H wag vibration occurred at peaks 754 and 690 cm^{-1}, respectively. Bands vibrating at 1050 and 1087 cm^{-1} are due to aromatic C-H in-plane bending vibration. At 2975 and 2890 cm^{-1}, asymmetric C-H stretching vibration was noticed. At 3407 cm^{-1}, the spectra (a) exhibit a wideband related to the N-H stretching mode. This band shifted to a lower frequency (3397 cm^{-1}) upon complexation as indicated by the BAC spectrum. This indicates the linkage between the metal ion and the nitrogen group of the aniline [20,21]. The absence of most peaks and a broad signal production demonstrates Bi metal's coordination with the aniline's nitrogen group as shown in the spectrum (b). Moreso, due to bismuth addition, the different vibrational modes of aniline have been limited, resulting in the bismuth-aniline complex (BAC) seen in spectrum B.

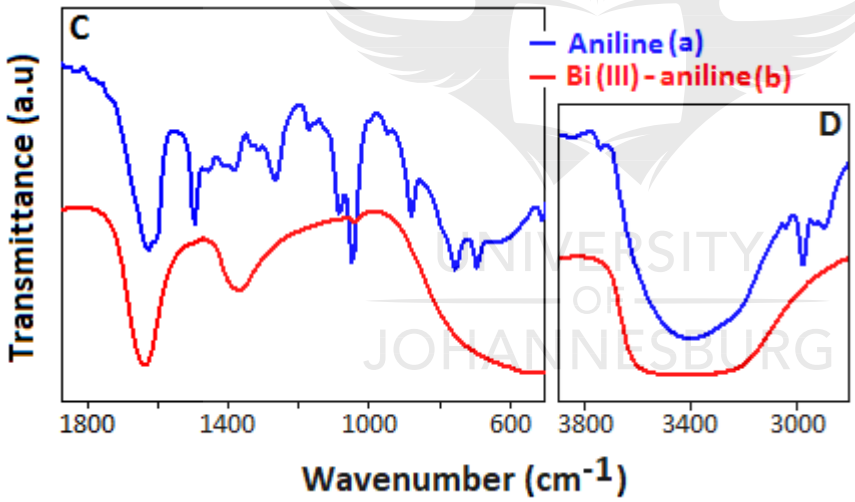

Figure 4.2: FTIR spectrum of (a) aniline (b) BAC, with several stretching and bending vibration modes.

4.3.3 X-ray Photoelectron Spectroscopy (XPS)

An X-ray Photoelectron Spectroscopy (XPS) technique was also used to study the surface composition of the organic-inorganic hybrid complex. The occurrence of bismuth, nitrogen, and carbon in the sample was established by the survey spectrum (Figure 4.3A). Within the range of 156-168 eV, the high-resolution XPS spectrum revealed two significant peaks at

159.3 and 164.4 eV. These peaks can be attributed to Bi 4f7/2 and Bi 4f5/2, accordingly for Bi (III) [22] as shown in Figure 4.3B. The observed peaks with a separation of 5.1 eV confirm that the bismuth's oxidation state in the complex was +3 and agrees with previous reports [23,24,25,26]. The deconvolution in the complex of C1 spectra consisting of peaks around 284.7 eV and 286.9 eV validates the existence of C-C, C-H, and C-N bonds in the complex Figure 4.3C [27]. After deconvolution, the prominent N1s asymmetric peak indicates the existence of structures of the benzenoid (-NH-) and anilinium ion (N+) forms at 400.2 and 402.2 eV, respectively, as shown in Figure 4.3D [27].

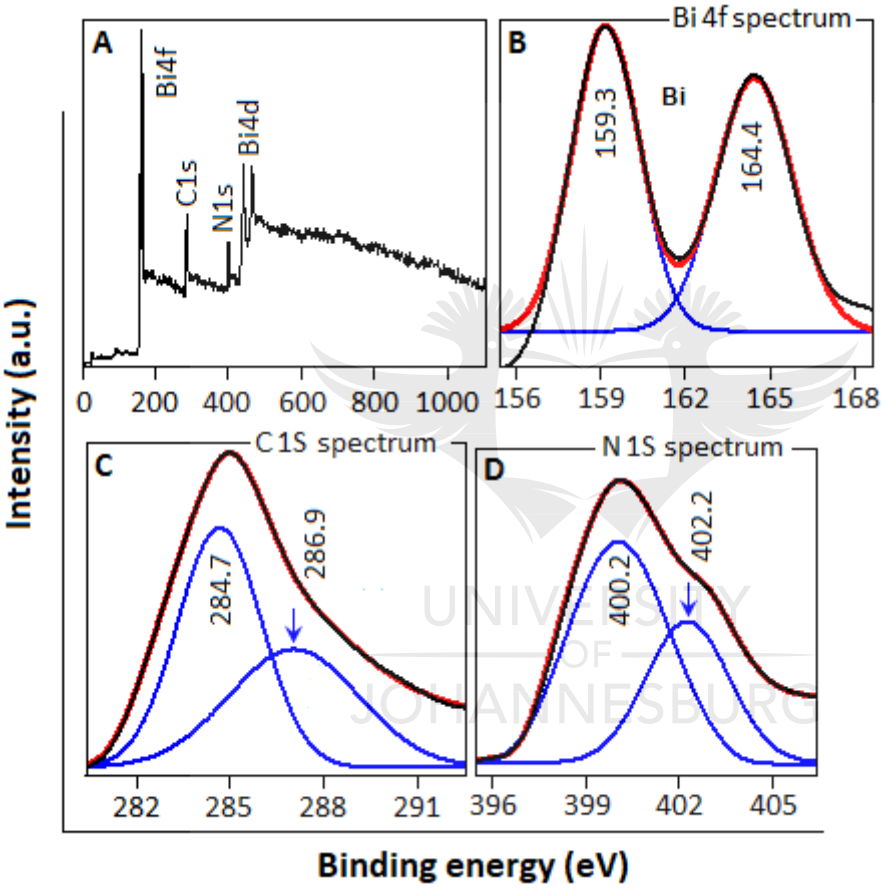

Figure 4.3: (A) The BAC's XPS spectrum. (B-D) The deconvoluted Bi 4f, C 1S, and N 1S high-resolution XPS spectra, respectively.

4.3.4 NMR Spectra

To further confirm the synthesis of the BAC, ^{1}H NMR analysis was run using DMSO as a solvent. The NMR shifts for the proton of the aniline and the bismuth metal complex are as shown in Table S4.1. The free ligand's 1H NMR spectrum (Figure S4.1) revealed triplet

peaks in the range of 7.05–7.08 ppm, duplet peaks in the range of 6.38–6.65 ppm, and triplet peaks in the range of 6.55–6.57 ppm.

The aromatic protons are responsible for these peaks, respectively [28]. The broad singlet peak noticed at 4.97 ppm can be attributed to the amine (NH_2) protons. These peaks were shifted to 7.01–7.04 ppm as triplets, duplet peaks in the region of 6.58-6.60 ppm, and triplet peaks in the region of 6.50-6.53 ppm in the BAC spectrum (Figure S4.2). The amine (NH_2) protons, on the other hand, moved downfield at 5.07 ppm in relation to the 4.97 ppm on the aniline spectrum. This important shift in the aromatic and amine groups verified Bi (III) ion coordination through the nitrogen atom of the amine group [29]. These findings back up the complex's IR spectra.

4.3.5 Electronic spectra

The electronic spectra of the aniline and the bismuth aniline complex in DMSO were recorded at room temperature and can be shown in Figure 4.4. The spectra of the aniline consist of a single energy band around 290 nm originating from benzene's ring π – π* transition and the excitation of the quinoid ring [30]. This transition could also be found in the UV-vis spectrum of the BAC but shifted toward lower wavelengths (blue shift) at 270 nm, confirming the coordination of the aniline moiety with the bismuth metal. The blue shift could result from a decrease in the conjugation of the system after complexation [31]. The drop in intensity results from a different concentration of the BAC that is best for absorbance.

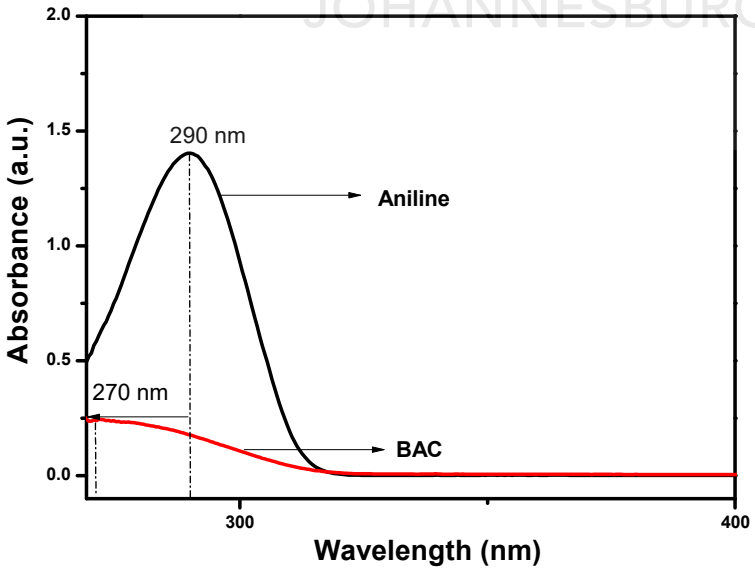

Figure 4.4: Electronic spectra of aniline and bismuth aniline complex (BAC).

4.3.6 Electrochemical characterization

The modified electrode was characterized with electrochemical impedance spectroscopy (EIS) to probe its electrochemical behavior. EIS studies typically provide useful information on the kinetics of electron transfer at the electrode's surface. A semicircle section of Nyquist plots from EIS measurements is generally directly related to charge transfer resistance and inversely proportional to the material's conductivity. The linear part reveals the diffusion limiting step of the electrochemical process. From Figure 4.5A and B, a straight line was observed at lower frequencies for both BAC and bare electrodes, indicating a diffusion limiting process at the electrode's surfaces. Moreso, a smaller semicircle was observed for the BAC, indicating lesser resistance and higher conductivity than the bare electrode. The conductivity of the BAC could be attributed to the charge hopping mechanism through the metal, which mediates the effective charge migration through the aniline moiety [32]. The inclusion of the bismuth ion in the π-electron delocalization of the aniline also contributes to the complex conductivity [33].

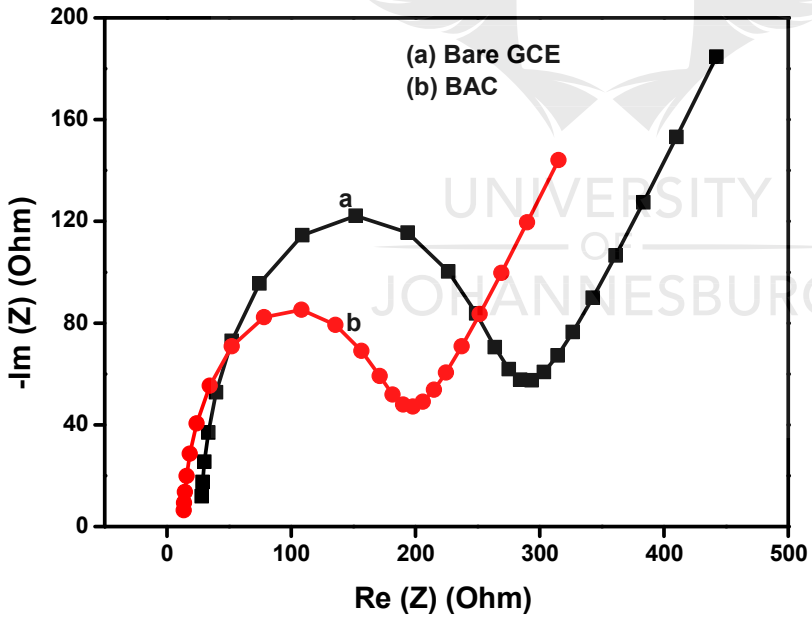

Figure 4.5: Electrochemical impedance spectra of (A) bare electrode (B) BAC modified GCE within the frequency range from 1 KHz to 7 MHz, in 5 mM hexacyanoferrate (III) with 0.1 M KCl.

4.3.7 Electrochemical behavior of iodine on GCE and BAC modified electrode

The electrocatalytic activity of BAC/GCE for iodine oxidation was studied using cyclic voltammetry (CV). Figure 4.6A illustrates the CV responses in the absence (inset) and presence (main) of KI (120 μM) on the bare GCE and the BAC/GCE in an electrolyte solution of phosphate buffer scanning at a rate of 50 mVs^{-1}. There was no redox peak at GCE and BAC/GCE without KI, but BAC/GCE had a higher background current than GCE. This may be because BAC has a large specific area. In the presence of KI, peaks emerged at both electrodes with the BAC/GCE current higher than that of the GCE. The results show that the modified electrode can promote the oxidation of iodine.

To obtain useful information on kinetic parameters for iodine oxidation, CV's of the BAC/GCE electrode in phosphate buffer (pH 7.4) were run at varied scan rates in the presence of 80 μM KI (Figure 4.6B). As the scan rates were increased, the peak currents increased with the oxidation potential shifting towards a more positive area [34]. Figure 4.6C shows a linear relationship between peak current (I_{pa}) and scan rate (v), and Figure 4.6D shows a linear relationship between peak current (I_{pa}) and the square root of scan rate ($v^{1/2}$). Linearity with regression coefficients of 1 and 0.9867, respectively, suggested that the electrode transfer reaction was an adsorption process. Similar behavior has been reported in some previous literature [35].

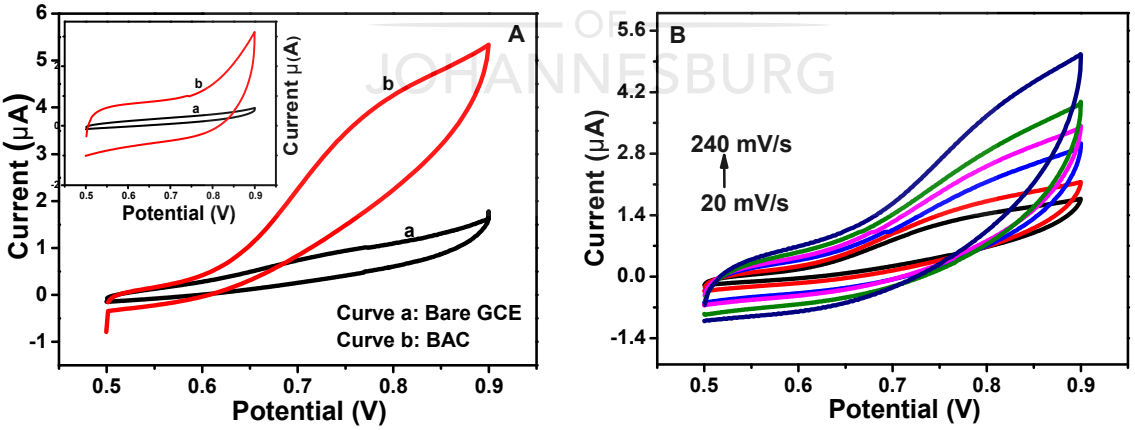

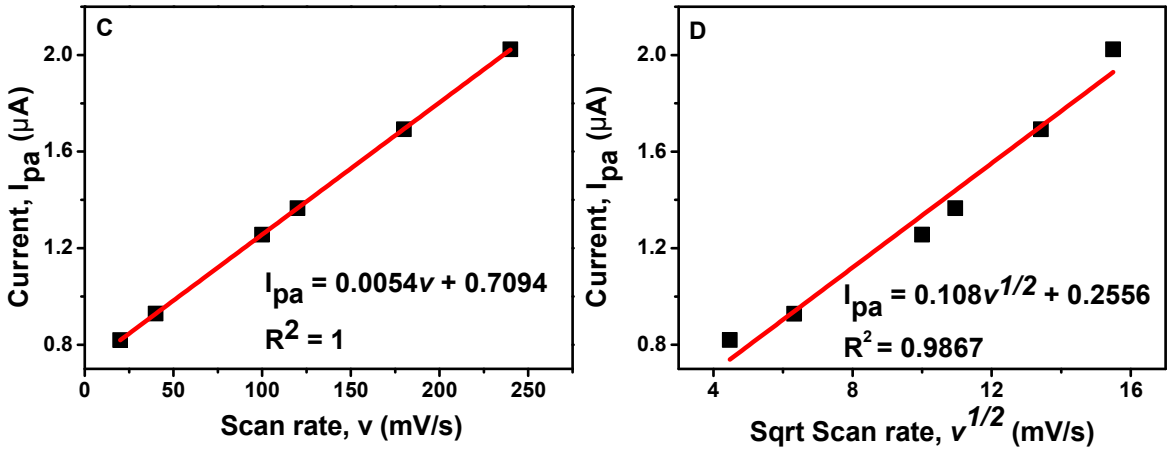

Figure 4.6: (A) CV's of (a) Bare GCE (b) BAC/GCE in the absence and presence of 120 μM KI **(B)** CV's of 80 μM KI at BAC/GCE containing 0.01 M PBS electrolyte (pH 7.4) at varied scan rates (20-240 mV/s). Plots of **(C)** peak current I_{pa} vs. scan rate, *V* **(D)** peak current I_{pa} vs. square root of scan rate, $V^{1/2}$.

4.3.8 Iodide detection at BAC modified electrode

The iodide ions sensing using the aniline-bismuth complex is documented in this report using an electrochemical technique. With the aid of a drop and dry modification procedure, the BAC material was placed on the polished glass carbon electrode in a nitrogen atmosphere. With an electrolyte solution of phosphate buffer of 10 mM concentration, the cyclic voltammogram signal was recorded under varying KI solution concentrations scanning at 50 mVs^{-1}. Oxidation of iodide ions with the modified electrode and observing the scenario by the cyclic voltammetric procedure is the principle behind this present method. Considering that I^- ion is a moderate reducing agent, I_2 is formed by the oxidation of I^- in the presence of a catalyst [36] and, then again, by the reducing Bi (III) to form Bi (0). The cyclic voltammetric curve indicates that the anodic current value was increased with an increase in KI concentration, Figure 4.7A. The current value was observed at 1.05 μA in the absence of KI. No noticeable enhancement of the anodic current value was detected when the added concentration of KI got to 40 μM. A substantial increase in the current response (3.78 μA) was noticed upon increasing the KI concentration to 100 μM. A maximum current of 11.6 μA was attained after the addition of 350 μM KI. The result produced a sensitivity of 1.05 $A/M/cm^2$ and a detection limit value of 23.6 μM. The BAC modified electrode's electrocatalytic potential for iodate anion detection was additionally affirmed by the square wave voltammetry method (Figure 4.7B). With an increase in anion (I^-) concentration, a

steady rise in current values has been seen. A peak current response of 26.2 µA was attained when KI's concentration reached 250 µM. There was a drift in oxidation peaks towards the negative potential, demonstrating that iodide ion oxidation with an increasing KI concentration is simple and efficient. The squarewave voltammetry approach yielded sensitivity and detection limit values of 2.6 A/M/cm^2 and 23.17 µM, respectively.

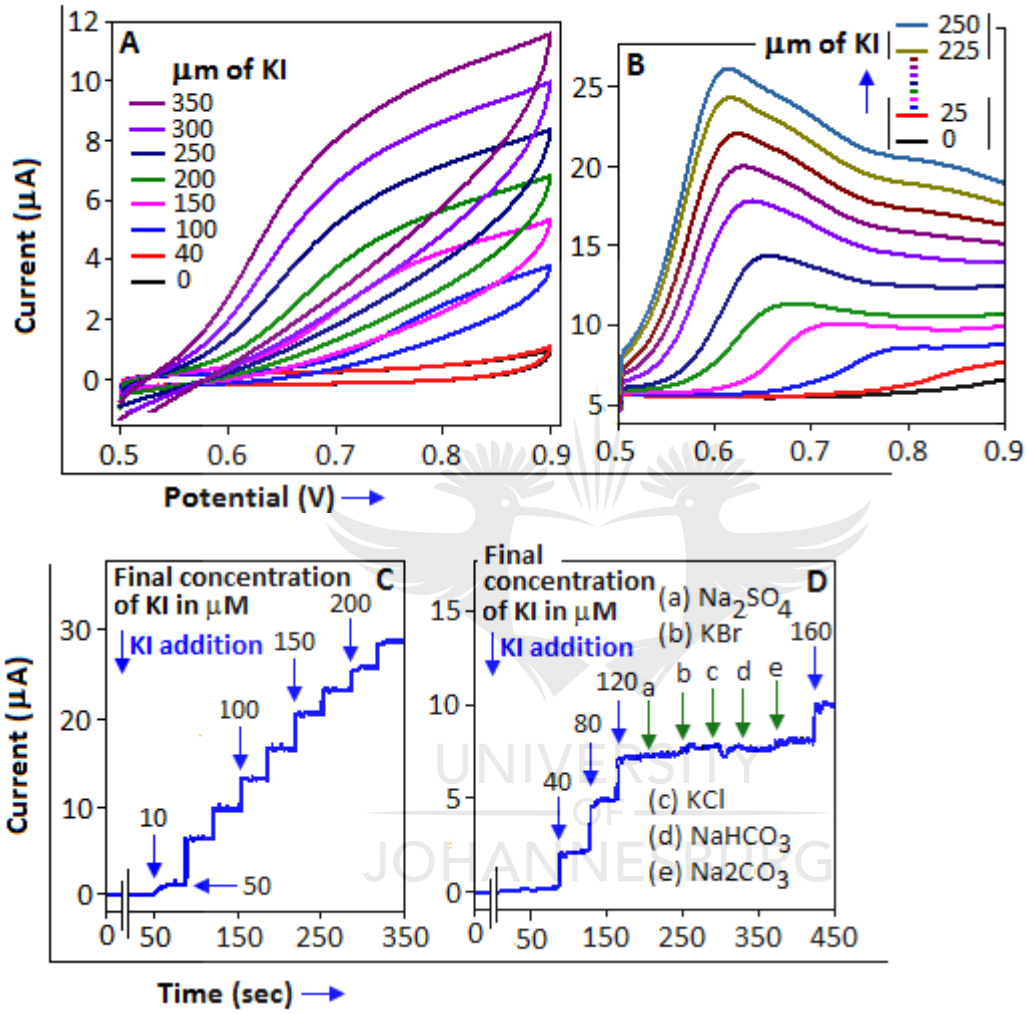

Figure 4.7: (A) The CV's and (B) SWV's of electrodes modified with BAC (C) BAC chronoamperometric response (D) Chronomperometric response at BAC modified electrodes).

MATLAB programming was used to calculate the sensitivity and the detection limit values (Figure S4.3). Iodide ions added in succession (at potential difference of 0.70 V) produced an amperometric current response that increased linearly producing a sensitivity of 3.7 A.M/cm^2 and LOD estimate of 16.21 µM (Figure 4.7C). The detection limit is much lower than some other iodine sensors [37,38], whose detection limit is above 30 µM. Although, its detection

limit is higher than some sensors developed by Kosminsky [39] and Zou [40]. This proposed sensor has the advantage of being simpler and less costly to develop. It also offers a wide linear range than most sensors reported in the literature [41,42,43]. Furthermore, it displayed good selectivity in the presence of 50 µM solution of each Na_2SO_4, KBr, KCl, $NaHCO_3$, and Na_2CO_3 (Figure S4.3D).

4.3.9 Electrochemical behavior of dopamine at the modified electrode

The electrochemical behavior of dopamine was studied at GCE and BAC/GCE electrodes both in the absence and presence of DA (70 µM) and their CV responses are indicated as shown in Figure 4.8A. The curves show that in the absence of DA (inset), BAC/GCE had a higher background current than the GCE while in the presence of DA (main), both electrodes produced a peak, but the peak current of the BAC/GCE was more enhanced. This indicates dopamine can be oxidized effectively at the BAC modified electrode.

To study the kinetic characteristics of the modified electrode on DA oxidation, CV's of the BAC/GCE electrode was run by varying the scan rates upon the addition of DA (Figure 4.8B). An increase in peak current was observed as the scan rates were increased. To verify the process occurring at the electrode, a graph of Ipa (anodic peak current) vs. scan rate was plotted as shown in Figure 4.8C, which produced a linear relationship for DA oxidation with a regression coefficient of 0.98434. A plot Ipa against the square root of scan rate (Figure 4.8D) also gave a linear relationship with correlation regression of 0.99263. This result suggests that the electron transfer reaction was an adsorption process. To further confirm the electrode process, log Ipa vs. log v was plotted (Figure 4.8E). The plot produced a linear relationship with a slope of 0.66, suggesting the electrode process was adsorption controlled [44]. This result is supported by previously reported literature [35,45].

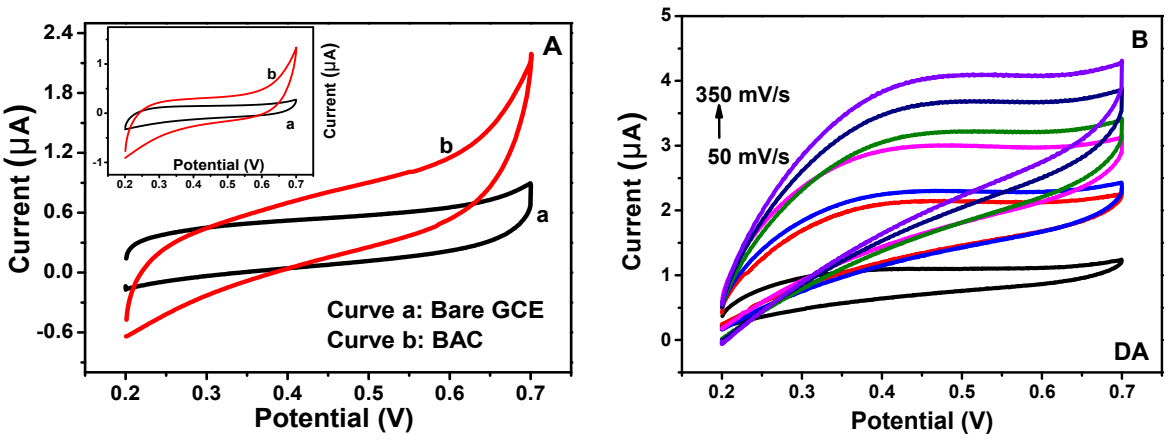

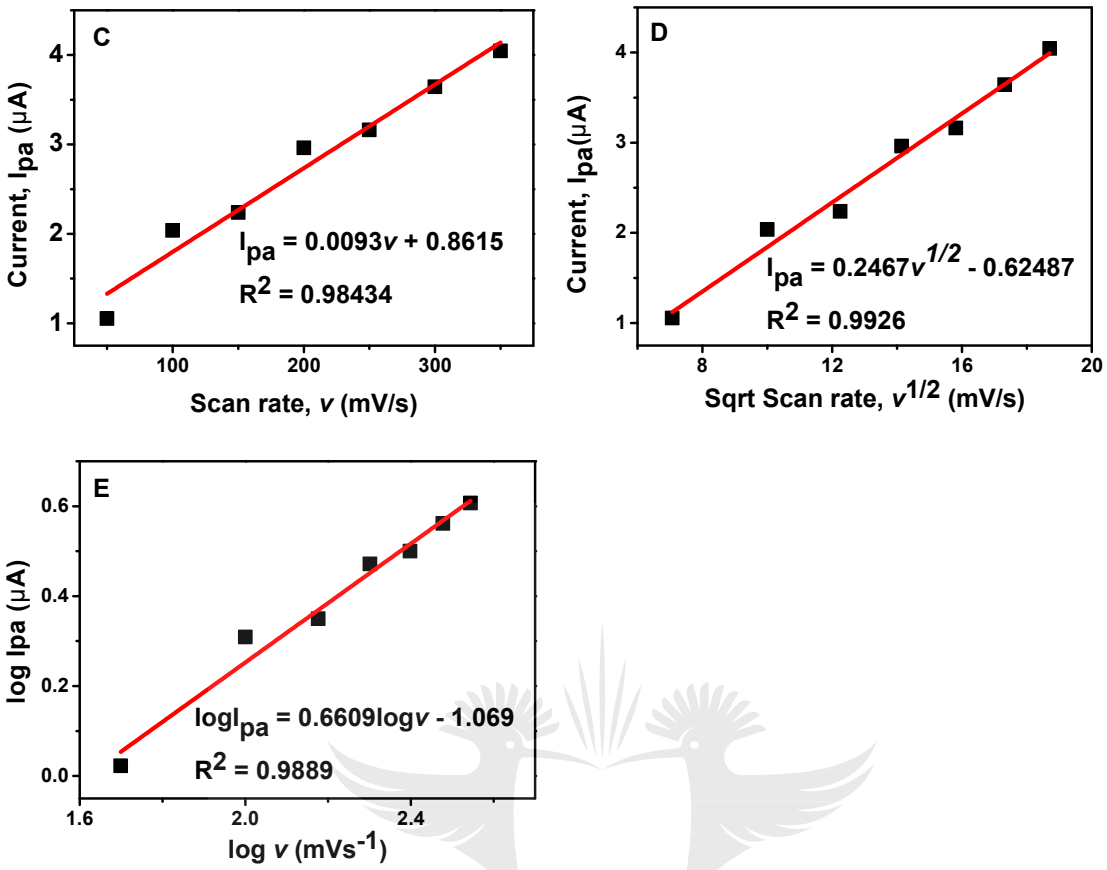

Figure 4.8: (A) CV's of (a) Bare GCE (b) BAC/GCE in the absence and presence of 120 µM DA **(B)** CV's of 80 µM DA at BAC/GCE in 0.01 M PBS electrolyte at varying scan rates (50-350 mV/s). Plots of **(C)** I_{pa} vs. V **(D)** I_{pa} vs., $V^{1/2}$ **(E)** log I_{pa} vs. V.

4.3.10 Dopamine detection at BAC modified electrode

Dopamine is a neuromodulator containing monoamine, and the deficiency of dopamine in the physiological system may cause several neurological problems [46,47]. Dopamine influences many facets of brain functionality and synaptic plasticity as a neuromodulator [48,49]. The cardiovascular and renal systems are affected by dopamine secretion irregularities [50,51], and reduced levels of dopamine release could be linked to a variety of neurological disorders [52]. Various methods for detecting dopamine have been developed by researchers, which may help the early detection of many disorders due to elevated levels of dopamine in the physiological system. In terms of operational and instrumentation simplicity, colorimetric recognition of dopamine has an advantage. The use of ligand-modified silver nanoparticles for sensitive and selective colorimetric DA detection has been published, allowing for identifying high-sensitivity dopamine species [53]. Another report highlighted the recognition

of DA colorimetrically using gold nanoparticles. The addition of DA brought about the aggregation of the nanoparticles and a color change in the solution. [54]. Dopamine detection based on fluorescence properties is also well known in literature [55]. An electrochemiluminescent DA sensor made with poly-(luminol-benzidine sulfate) has also been documented for its high specificity and detection in the nano-molar region [56]. Kim *et al*. also reported on DA detection utilizing cylindrical modified gold electrodes [57].

The modified glassy carbon electrode also recognizes dopamine efficiently through an electrochemical sensing process. Cyclic voltammogram signals of varying dopamine concentrations in the 10 mM phosphate buffer solution were shown in Figure 4.9A at a 50 mVs^{-1} scan rate. The potential applied was 0.2 to 0.7 V, and the sensitivity and detection limit measured was 0.22 $A.M^{-1}.cm^{-2}$ and 39.0 µM, correspondingly. Under the optimized experimental setting, the BAC-modified electrode's amperometric response to consecutive increment in dopamine concentration was examined. The amperometric current response of dopamine at time intervals is shown in Figure 4.9B at 0.45 V within the 20 to 180 µM concentration range. Sensitivity and detection limit estimates of 0.12 $A/M/cm^2$ and 12.3 µM, were obtained respectively. The detection limit was relatively higher than some reported sensors in the literature [58,59], but it exhibits a wider linear range than them. The catalyst's selectivity for identifying dopamine was studied by introducing to the electrolyte some possible interfering species such as uric acid, serotonin tryptophan, ascorbic acid histamine, and glucose (50 µM each). These interferents were irresponsive to the current response from the amperometric curve (Figure 4.9C).

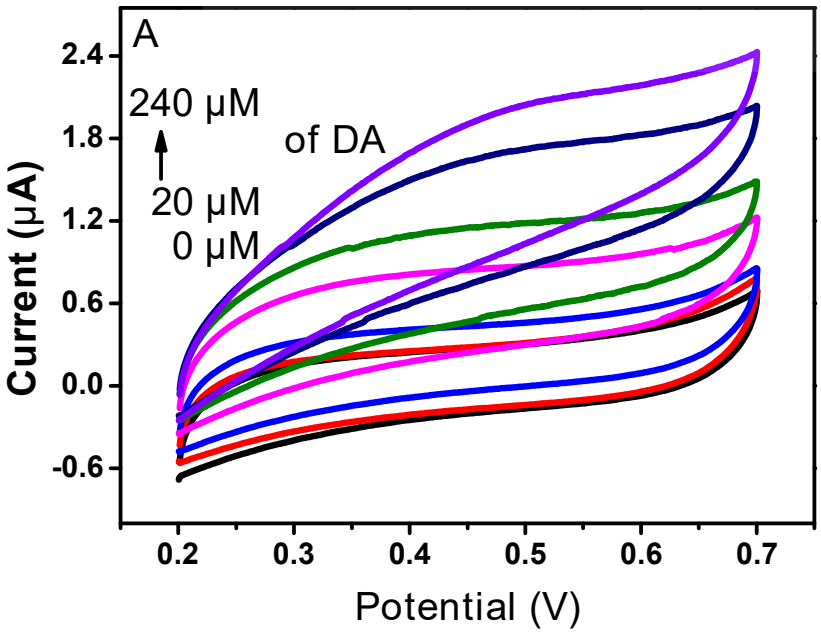

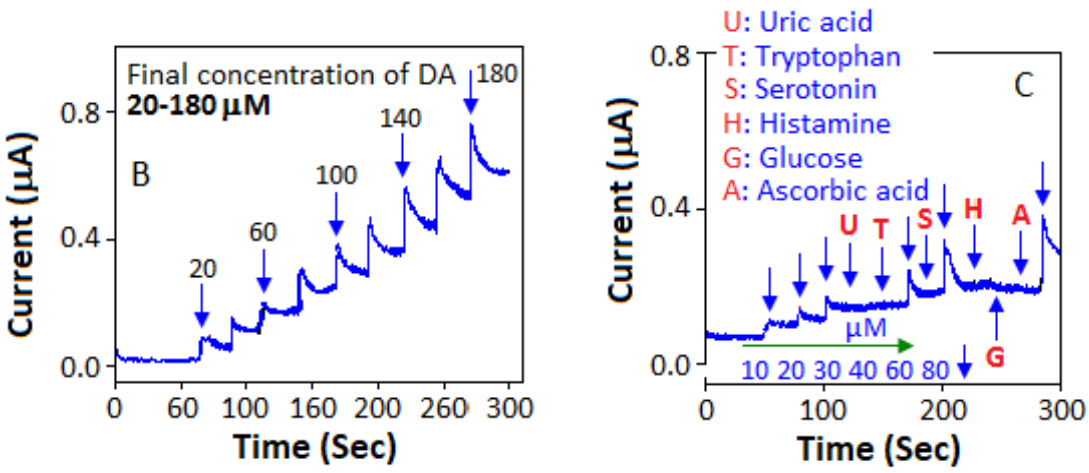

Figure 4.9: (A) Cyclic voltammetric response of BAC-modified electrode in 10 mM PBS with increasing DA concentration in 0.01 M PBS electrolyte at 50 mV/s scan rate. (b) The chronoamperometric response of BAC's upon successive addition of dopamine concentration between 20 to 180 µM, and a potential of 0.45 V, (C) The effects of high concentration (50 µM) of interfering species on DA detection. (Dopamine concentration increases in the direction of the arrow shown).

4.4 Sub-conclusion

A simple approach to developing a hybrid system built upon an organic-inorganic complex material has been documented in this report. The development of a complex system containing bismuth-aniline, which has been used as an electroactive material for identifying iodine, has been verified by various characterization techniques. The sensitivity and the detection limit values of 2.6 A/M/cm^2 and 23.17 µM were established for iodide ions detection with the help of a square wave voltammetric technique. As exemplified by cyclic voltammogram signals, the material also demonstrated its efficacy for electrochemical dopamine determination, with the sensitivity and detection limits estimate being 0.12 A/M/cm^2 and 12.3 µM, correspondingly. In the presence of interfering species, the amperometric technique also showed the catalyst's selectivity for dopamine alone.

4.5 References

[1] Bothwell, J. M., Krabbe, S. W., & Mohan, R. S. (2011). Applications of bismuth (III) compounds in organic synthesis. *Chemical Society Reviews*, *40*(9), 4649-4707.

[2] Tang, M. C., Barrit, D., Munir, R., Li, R., Barbé, J. M., Smilgies, D.M., Del Gobbo, S., Anthopoulos, T.D. & Amassian, A. (2019). Bismuth-Based Perovskite-Inspired Solar Cells: In Situ Diagnostics Reveal Similarities and Differences in the Film Formation of Bismuth- and Lead-Based Films. *Solar RRL*, *3*(7), 1800305.

[3] Ghosh, S. K., Perla, V. K., Kumar, P., & Mallick, K. (2019). The dielectric and electrical properties of bismuth oxide nanoparticles within organic network: the effect of temperature and the role of polarons. *Materials Research Express*, *6*(5), 055022.

[4] Perla, V. K., Ghosh, S. K., & Mallick, K. (2019). Nonvolatile switchable resistive behaviour via organic–inorganic hybrid interactions. *Journal of Materials Science*, *54*(3), 2324-2332.

[5] Keogan, D. M., & Griffith, D. M. (2014). Current and potential applications of bismuth-based drugs. *Molecules*, *19*(9), 15258-15297.

[6] Shahbazi, M. A., Faghfouri, L., Ferreira, M. P., Figueiredo, P., Maleki, H., Sefat, F., Hirvonen, J. & Santos, H. A. (2020). The versatile biomedical applications of bismuth-based nanoparticles and composites: therapeutic, diagnostic, biosensing, and regenerative properties. *Chemical Society Reviews*, *49*(4), 1253-1321.

[7] Taufik, S., Yusof, N. A., Tee, T. W., & Ramli, I. (2011). Bismuth oxide nanoparticles/chitosan/modified electrode as biosensor for DNA hybridization. *Int. J. Electrochem. Sci*, *6*, 1880-1891.

[8] Ding, S. N., Shan, D., Xue, H. G., & Cosnier, S. (2010). A promising biosensing-platform based on bismuth oxide polycrystalline-modified electrode: characterization and its application in development of amperometric glucose sensor. *Bioelectrochemistry*, *79*(2), 218-222.

[9] Periasamy, A. P., Yang, S., & Chen, S. M. (2011). Preparation and characterization of bismuth oxide nanoparticles-multiwalled carbon nanotube composite for the development of horseradish peroxidase based H_2O_2 biosensor. *Talanta*, *87*, 15-23.

[10] Muthumariyappan, A., Rajaji, U., Chen, S. M., Chen, T. W., Li, Y. L., & Ramalingam, R. J. (2019). One-pot sonochemical synthesis of Bi_2WO_6 nanospheres with multilayer reduced graphene nanosheets modified electrode as rapid electrochemical sensing platform

for high sensitive detection of oxidative stress biomarker in biological sample. *Ultrasonics Sonochemistry*, *57*, 233-241.

[11] Çiftçi, H., & Tamer, U. (2011). Electrochemical determination of iodide by poly (3-aminophenylboronic acid) film electrode at moderately low pH ranges. *Analytica Chimica Acta*, *687*(2), 137-140.

[12] Delange, F., de Benoist, B., Pretell, E., & Dunn, J. T. (2001). Iodine deficiency in the world: where do we stand at the turn of the century? *Thyroid*, *11*(5), 437-447.

[13] Paus, T. (2001). Primate anterior cingulate cortex: where motor control, drive and cognition interface. *Nature Reviews Neuroscience*, *2*(6), 417-424.

[14] Volkow, N. D., Wang, G. J., Fowler, J. S., Tomasi, D., & Telang, F. (2011). Addiction: beyond dopamine reward circuitry. *Proceedings of the National Academy of Sciences*, *108*(37), 15037-15042.

[15] Wise, R. A. (2004). Dopamine, learning and motivation. *Nature Reviews Neuroscience*, *5*(6), 483-494.

[16] Cools, R. (2008). Role of dopamine in the motivational and cognitive control of behavior. *The Neuroscientist*, *14*(4), 381-395.

[17] Stanbury, J. B., Ermans, A. E., Bourdoux, P., Todd, C., Oken, E., Tonglet, R., Vidor, G., Braverman, L.E. & Medeiros-Neto, G. (1998). Iodine-induced hyperthyroidism: occurrence and epidemiology. *Thyroid*, *8*(1), 83-100.

[18] Galvan, A., & Wichmann, T. (2008). Pathophysiology of parkinsonism. *Clinical Neurophysiology*, *119*(7), 1459-1474.

[19] Ahuja, I. S., Brown, D. H., Nuttall, R. H., & Sharp, D. W. A. (1966). The preparation and properties of some aniline complexes of metal (II) sulphates and nitrates. *Journal of the Chemical Society A: Inorganic, Physical, Theoretical*, 938-941.

[20] Lee-Thorp, J. A., Rüede, J. E., & Thornton, D. A. (1978). The infrared spectra (3500—150 cm-1) of aniline complexes of cobalt (II), nickel (II), copper (II) and zinc (II) halides. *Journal of Molecular Structure*, *50*(1), 65-71.

[21] Fuson, N., Josien, M. L., Powell, R. L., & Utterback, E. (1952). The NH Stretching Vibration and NH–N Hydrogen Bonding in Several Aromatic Compounds. *The Journal of Chemical Physics*, *20*(1), 145-152.

[22] Reddy, K. H., Martha, S., & Parida, K. M. (2012). Facile fabrication of Bi_2O_3/Bi–$NaTaO_3$ photocatalysts for hydrogen generation under visible light irradiation. *RSC Advances*, *2*(25), 9423-9436.

[23] Kumar, P., Singh, J., & Pandey, A. C. (2013). Rational low temperature synthesis and structural investigations of ultrathin bismuth nanosheets. *RSC Advances*, *3*(7), 2313-2317.

[24] Devi, N., Ghosh, S. K., Perla, V. K., & Mallick, K. (2020). Organic-inorganic Complexation Chemistry-Mediated Synthesis of Bismuth–Manganese Bimetallic Oxide for Energy Storage Application. *ACS omega*, *5*(30), 18693-18699.

[25] Cheng, H., Huang, B., Lu, J., Wang, Z., Xu, B., Qin, X., Zhang, X. & Dai, Y. (2010). Synergistic effect of crystal and electronic structures on the visible-light-driven photocatalytic performances of Bi_2O_3 polymorphs. *Physical Chemistry Chemical Physics*, *12*(47), 15468-15475.

[26] Han, S., Li, J., Yang, K., & Lin, J. (2015). Fabrication of a β-Bi_2O_3/BiOI heterojunction and its efficient photocatalysis for organic dye removal. *Chinese Journal of Catalysis*, *36*(12), 2119-2126.

[27] Patil, S. H., Gaikwad, A. P., Sathaye, S. D., & Patil, K. R. (2018). To form layer by layer composite film in view of its application as supercapacitor electrode by exploiting the techniques of thin films formation just around the corner. *Electrochimica Acta*, *265*, 556-568.

[28] Devi, T. P., & Singh, R. H. (2010). Complexes of nickel (II) with the schiff bases derived from condensation of salicylaldehyde and Bis-Ni (AMUH) $2Cl_2$. *Rasayan J. Chem*, *3*, 14.

[29] Skauge, T., Turel, I., & Sletten, E. (2002). Interaction between ciprofloxacin and DNA mediated by Mg^{2+} -ions. *Inorganica Chimica Acta*, *339*, 239-247.

[30] Li, X. H., Wu, B., Huang, J. E., Zhang, J., & Liu, Z. F. (2003). Fabrication and characterization of well-dispersed single-walled carbon nanotube/polyaniline composites. *Carbon (New York, NY)*, *41*(8), 1670-1673.

[31] Friedel, R. A., & Orchin, M. (1958). *Ultraviolet Spectra of Aromatic Compounds Chemistry*. John Wiley, New York.

[32] Fischer, P., & Seanor, D. A. (1982). Dielectric breakdown phenomena in polymers. In *Electrical Properties of Polymers* (pp. 320-327). New York: Academic Press.

[33] Zaki, Z. M. (2000). Spectral, thermal and electrical properties of some new azo complexes. *Spectrochimica Acta Part A: Molecular and Biomolecular Spectroscopy*, *56*(10), 1917-1923.

[34] Zhao, Y., Bai, J., Wang, L., XuHong, E., Huang, P., Wang, H., & Zhang, L. (2006). Simultaneous electrochemical determination of uric acid and ascorbic acid using L-cysteine self-assembled gold electrode. *Int. J. Electrochem. Sci*, *1*, 363-371.

[35] Ganesh, P. S., & Swamy, B. K. (2015). Sodium dodecyl sulphate/poly (brilliant blue)/multi-walled carbon nanotube modified carbon paste electrode for the voltammetric resolution of dopamine in the presence of ascorbic acid and uric acid. *Journal of Analytical & Bioanalytical Techniques*, *6*(6), 1.

[36] Lagorce, J. F., Thomes, J. C., Catanzano, G., Buxeraud, J., Raby, M., & Raby, C. (1991). Formation of molecular iodine during oxidation of iodide by the peroxidase/H2O2 system: Implications for antithyroid therapy. *Biochemical Pharmacology*, *42*, S89-S92.

[37] Chen, S. M., Song, J. L., & Thangamuthu, R. (2007). Electrocatalytic Behavior of Mixed-Valent RuO⁄Ru $(CN)_6$ $^{4-}$⁄ $SiMo_{12}O_{40}$ $^{4-}$ Hybrid Film Modified Electrodes Toward Oxidation of Neurotransmitters and Iodate Reduction. *Journal of The Electrochemical Society*, *154*(10), E153.

[38] Haghighi, B., Hamidi, H., & Gorton, L. (2010). Formation of a robust and stable film comprising ionic liquid and polyoxometalate on glassy carbon electrode modified with multiwalled carbon nanotubes: Toward sensitive and fast detection of hydrogen peroxide and iodate. *Electrochimica Acta*, *55*(16), 4750-4757.

[39] Kosminsky, L., & Bertotti, M. (1999). Determination of iodate in salt samples with amperometric detection at a molybdenum oxide modified electrode. *Electroanalysis: An International Journal Devoted to Fundamental and Practical Aspects of Electroanalysis*, *11*(9), 623-626.

[40] Zou, B. X., Liu, X. X., Diamond, D., & Lau, K. T. (2010). Electrochemical synthesis of WO_3/PANI composite for electrocatalytic reduction of iodate. *Electrochimica Acta*, *55*(12), 3915-3920.

[41] Li, T. J., Lin, C. Y., Balamurugan, A., Kung, C. W., Wang, J. Y., Hu, C. W., Wang, C.C., Chen, P.Y., Vittal, R. and Ho, K.C., (2012). Modification of glassy carbon electrode with a polymer/mediator composite and its application for the electrochemical detection of iodate. *Analytica Chimica Acta*, *737*, 55-63.

[42] Balamurugan, A., Lin, C. Y., Nien, P. C., & Ho, K. C. (2012). Electrochemical Preparation of a Nanostructured Poly (amino napthalene sulfonic acid) Electrode Using CTAB as a Soft Template and Its Electrocatalytic Application for the Reduction of Iodate. *Electroanalysis*, *24*(2), 325-331.

[43] Walcarius, A., Lefevre, G., Rapin, J. P., Renaudin, G., & Francois, M. (2001). Voltammetric Detection of Iodide after Accumulationby Friedel's Salt. *Electroanalysis: An*

International Journal Devoted to Fundamental and Practical Aspects of Electroanalysis, *13*(4), 313-320.

[44] Gosser, D. K. (1993). *Cyclic voltammetry: simulation and analysis of reaction mechanisms* (Vol. 43). New York: VCH.

[45] Gilbert, O., Swamy, B. K., Chandra, U., & Sherigara, B. S. (2009). Electrocatalytic oxidation of dopamine and ascorbic acid at poly (Eriochrome Black-T) modified carbon paste electrode. *International Journal of Electrochemical Science*, *4*(4), 582-591.

[46] Buddhala, C., Loftin, S. K., Kuley, B. M., Cairns, N. J., Campbell, M. C., Perlmutter, J. S., & Kotzbauer, P. T. (2015). Dopaminergic, serotonergic, and noradrenergic deficits in Parkinson disease. *Annals of Clinical and Translational Neurology*, *2*(10), 949-959.

[47] Howes, O. D., McCutcheon, R., Owen, M. J., & Murray, R. M. (2017). The role of genes, stress, and dopamine in the development of schizophrenia. *Biological Psychiatry*, *81*(1), 9-20.

[48] Hefco, V., Yamada, K., Hefco, A., Hritcu, L., Tiron, A., & Nabeshima, T. (2003). Role of the mesotelencephalic dopamine system in learning and memory processes in the rat. *European Journal of Pharmacology*, *475*(1-3), 55-60.

[49] Swamy, B. K., & Venton, B. J. (2007). Carbon nanotube-modified microelectrodes for simultaneous detection of dopamine and serotonin in vivo. *Analyst*, *132*(9), 876-884.

[50] Lupu, S., Lete, C., Marin, M., Totir, N., & Balaure, P. C. (2009). Electrochemical sensors based on platinum electrodes modified with hybrid inorganic–organic coatings for determination of 4-nitrophenol and dopamine. *Electrochimica Acta*, *54*(7), 1932-1938.

[51] Zhao, Y., Gao, Y., Zhan, D., Liu, H., Zhao, Q., Kou, Y., Shao, Y., Li, M., Zhuang, Q. & Zhu, Z. (2005). Selective detection of dopamine in the presence of ascorbic acid and uric acid by a carbon nanotubes-ionic liquid gel modified electrode. *Talanta*, *66*(1), 51-57.

[52] Dalley, J. W., & Roiser, J. P. (2012). Dopamine, serotonin and impulsivity. *Neuroscience*, *215*, 42-58.

[53] Palanisamy, S., Zhang, X., & He, T. (2016). Simple colorimetric detection of dopamine using modified silver nanoparticles. *Science China Chemistry*, *59*(4), 387-393.

[54] Leng, Y., Xie, K., Ye, L., Li, G., Lu, Z., & He, J. (2015). Gold-nanoparticle-based colorimetric array for detection of dopamine in urine and serum. *Talanta*, *139*, 89-95.

[55] Chen, X., Chen, S., & Ma, Q. (2017). Fluorescence detection of dopamine based on nitrogen-doped graphene quantum dots and visible paper-based test strips. *Analytical Methods*, *9*(15), 2246-2251.

[56] Wang, Y., Hamid, S., Zhang, X., Akhtar, N., Zhang, X., & He, T. (2017). An electrochemiluminescent biosensor for dopamine detection using a poly (luminol–benzidine sulfate) electrode modified by tyramine oxidase. *New Journal of Chemistry*, *41*(4), 1591-1597.

[57] Kim, D. S., Kang, E. S., Baek, S., Choo, S. S., Chung, Y. H., Lee, D., ... & Kim, T. H. (2018). Electrochemical detection of dopamine using periodic cylindrical gold nanoelectrode arrays. *Scientific Reports*, *8*(1), 1-10.

[58] Wei, Y., Liu, Y., Xu, Z., Wang, S., Chen, B., Zhang, D., & Fang, Y. (2020). Simultaneous Detection of Ascorbic Acid, Dopamine, and Uric Acid Using a Novel Electrochemical Sensor Based on Palladium Nanoparticles/Reduced Graphene Oxide Nanocomposite. *International Journal of Analytical Chemistry*, *2020.*

[59] Zhu, Q., Bao, J., Huo, D., Yang, M., Hou, C., Guo, J., Chen, M., Fa, H., Luo, X. & Ma, Y. (2017). 3D graphene hydrogel–gold nanoparticles nanocomposite modified glassy carbon electrode for the simultaneous determination of ascorbic acid, dopamine and uric acid. *Sensors and Actuators B: Chemical*, *238*, 1316-132.

CHAPTER 5
AN ELECTROCHEMICAL SENSOR BASED ON NICKEL ANILINE COMPLEX FOR DETECTION OF CYSTEINE

5.1 Introduction

Cysteine (Cys) is a non-essential amino acid that serves as a key precursor to the antioxidant glutathione. Cysteine contributes to cellular antioxidant protection and metabolism [1,2]. It also contains a sulphydryl group with high nucleophilicity, which significantly functions in biological processes. Cysteine deficiency could cause retarded growth, liver damage, and hair depigmentation [3]. Hence, the need to determine cysteine levels in the serum to prevent these diseases. The sensitive and selective detection of cysteine is crucial in developing efficient nanomaterials/nanocomplexes and methods for cysteine recognition. More than a few analytical approaches have been established for cysteine sensing. These techniques include flow injection [4], liquid chromatography (HPLC) [5], gas chromatography coupled with mass spectrometry [6], chemiluminescence [7], and fluorimetry [8]; just to mention a few. Compared to the methods listed, electrochemical determination has been considered a viable method that offers many potential advantages in forming a point-of-care sensor system since they are fast, cheap, highly sensitive, and easy to use. But one of the drawbacks often encountered with the electrochemical techniques of cysteine analysis is the bare electrode materials that come with high over-potential oxidation and slow electrochemical responses [9]. Hence, the need to modify the bare electrodes is essential. Several electrodes modified chemically have been reported for the electrocatalytic recognition of cysteine in recent years. Liu *et al.* have used a platinum nanoparticles/poly(*o*-aminophenol) film modified GCE to determine cysteine concentration [10]. Lee *et al.* investigated cysteine voltammetric behavior on a cyclotricatechylene modified carbon electrode [11]. Pei and co-workers have also studied the combined use of polyaniline and $CuGeO_3$ nanowire to improve the efficacy of carbon electrodes for cysteine detection [12].

Our recent report successfully synthesized a bismuth aniline complex to detect dopamine and iodine [13]. Combining aniline with some transition metals gives rise to a complex with a novel catalytic and luminescent property. A recent report opined that complexes containing nickel as a central atom could be used as appropriate material to analyze important pharmaceutical and biological constituents [14]. Ni-based nanomaterials are recognized for demonstrating tremendous electrocatalytic behavior in the field of biosensing. This

remarkable catalytic activity originates from the formation of the Ni(II)/Ni(III) redox pair on an electrode surface [15].

In this study, a facile complexation route was used to prepare the nickel-aniline complex (NAC). The hybrid material was used as a modifier to improve the electrocatalytic detection capability of cysteine. The selectivity and reproducibility of the electrode were also studied using chronoamperometry and cyclic voltammetry methods.

5.2 Experimental

5.2.1 Materials.

Nickel chloride, aniline, and cysteine were received as analytical grades and made use of without any additional purification. As required, Merck provided the ethanol and Mili Q water with specific resistivity 17 MΩ was used in the study. All received chemicals and solvents that were used are of analytical grade.

5.2.2 Preparation of nickel (II) aniline complex

In a standard experiment, 3 ml of ethanol was used to dissolve 0.0098 g of nickel chloride. The dissolved nickel chloride solution was gently added to aniline solution dissolved in ethanol (0.48g of aniline in 10 mL of ethanol) under stirring conditions. A precipitate bluish in color was observed due to the complexation between nickel and aniline, and the reaction was left overnight. The material was filtered, washed, and dried under vacuum and subjected to different characterization techniques to verify the complex's successful formation and establish its surface and optical properties. The complex material, nickel (II) aniline complex was also used as an electrocatalyst for the successful detection of cysteine molecules.

5.2.3 Material characterization

Elemental analyses were performed on a VarioElementar III microbe CHN analyzer. The NMR spectra were measured on a Bruker 500 MHz spectrophotometer to justify the formation of a complex. The chemical shifts are measured in parts per million (ppm) in comparison to tetramethylsilane (TMS) as internal standards in DMSO (Dimethylsulfoxide). The complex material's morphology was investigated using a scanning electron microscope (TESCsAM VEGAS). The X-ray diffraction pattern for the NAC was collected on a PAN analytical X'Pert PRO X-ray powder diffractometer. The instrument had a Cu Ka1 X-ray source and a minimum step size of 0.001^{o}. Functional groups in the material were identified

using FTIR (Shimadzu IRAffinity-1). Optical measurements were done with a UV-VIS spectrophotometer (Shimadzu U-1800) within a wavelength of 200 - 800 nm. All electrochemical studies were performed using a Bio-logic SP-200 electrochemical workstation. Electrochemical experiments were conducted with an electrochemical cell comprising of a bare GCE as working electrode, silver/silver chloride electrode (saturated KCl) used as the reference electrode, and platinum wire (0.5 mm) as the counter electrode. An aqueous phosphate buffer solution (10 mM) was used as an electrolyte.

5.2.4 Preparation and fabrication of the nickel (II) aniline complex modified GCE

The working electrode's surface, the glassy carbon electrode, had first been polished with a paste of silica-alumina on a polishing surface before being ultrasonicated for 3 mins in deionized water. Next, the electrode was cleaned with deionized water after ultrasonication and dried in the air. Next, the synthesized material was deposited on the GCE using a 'drop and dry' method. At the end of each session, the electrode was cleansed to remove loosely bonded material. Finally, an equal amount of the catalyst was used for electrode modification for further electrochemical measurements.

5.3 Results and Discussions

5.3.1 Infrared spectral studies

The establishment of the complex material was validated by FTIR spectroscopy as illustrated in Figure 5.1. A peak showing at 3248 cm^{-1} is a characteristic peak to OH groups' stretching vibration and bending vibration from the coordinated water molecules in the complex. The hydrogen-bonded *v*(N-H---N) band, which appears in the spectrum of aniline at 3429 cm^{-1} [16,17], is changed into a *v*(N-H---Cl) band in the complexes, which has a lower wavenumber (3313 cm^{-1}) than the free ligand. The band implies coordination between the nitrogen group of the amine and the nickel-metal [18,19]. In the NAC spectra, aniline's 1259 cm^{-1} *v*(C-N) band appears near 1232 cm^{-1}, whereas the aryl ring stretching frequency at 1600 cm^{-1} is unaffected by coordination. The peaks found at 752 and 693 cm^{-1} in both spectrums are ascribed to N–H's wag vibration, while the C=C stretching vibration for the benzenoid ring is visible at 1495 cm^{-1}. Vibration bands appearing at 1045 cm^{-1} of aniline and 1032 cm^{-1} of the complex are assigned for aromatic C–H in-plane bending vibration.

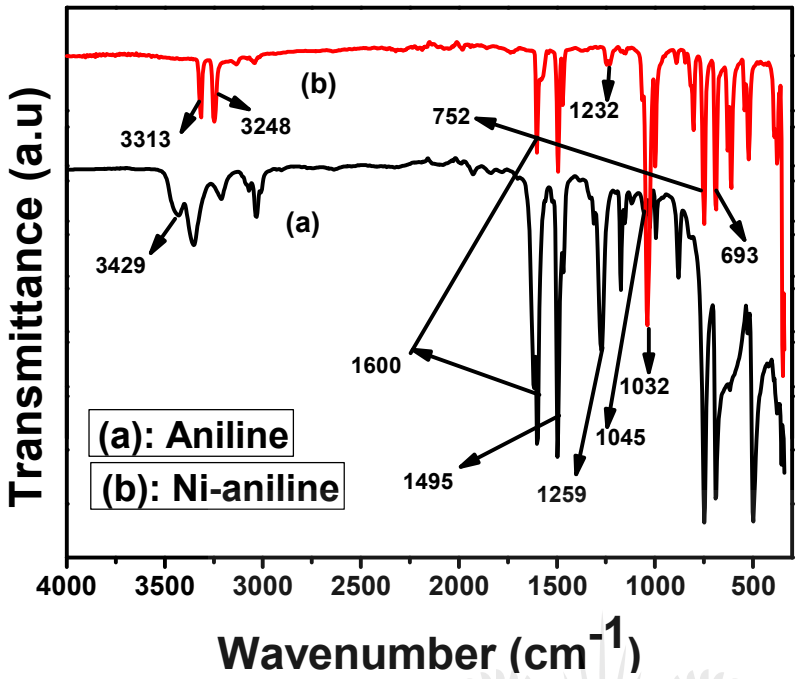

Figure 5.1: FTIR spectra of (a) aniline and (b) Ni (II) aniline complex.

5.3.2 NMR Spectral Analysis

To further verify NAC synthesis, ^{1}H and ^{13}C NMR analysis were conducted. ^{1}H and ^{13}C NMR is known for providing diagnostic methods for proton and carbon positional elucidation. In this analysis, the signal assignments are dependent on chemical shifts and patterns of intensity. The ^{1}H and ^{13}C NMR spectral information of aniline and its Ni (II) complex in DMSO-d_6 are presented in Table S5.1, and the spectra are given in Figure S5.1–S5.4. The ^{1}H NMR spectrum of the free ligand (Figure S5.1) displayed triplet peaks in the region of 7.05– 7.08 ppm, duplet at 6.38–6.65 ppm, and triplet at 6.55–6.57 ppm. These peaks are attributed to the aromatic protons, respectively [19].

Furthermore, the amine (NH_2) protons appeared as a broad peak at 4.97 ppm. These peaks were shifted to 7.12 ppm as singlet and 5.21–5.41 ppm as duplets in the NAC spectrum (Figure S5.2). These peaks are attributed to two and three sets of aromatic protons, respectively. However, the amine (NH_2) protons shifted to the upfield at 3.19 ppm as broad. This significant shift in the aromatic and the amine due to vibration confirmed Ni (II) ion coordination through the amine group's nitrogen atom [20]. The broadening of the peaks is due to the paramagnetic nature of nickel. That also confirms the formation of the nickel (II) aniline complex. These results corroborate the IR spectra of the complex.

Similarly, the free ligand's ^{13}C NMR spectrum (Figure S5.3) showed peaks at 148.45, 128.80, 115.87, and 114. 01 ppm and this accounts for all the carbons. These peaks were shifted upon complexation (Figure S5.4) to 139.93, 129.50, 129.21, and 119.41 ppm. Interestingly, the carbon atom directly attached to the amine group on the aromatic ring in the ligand undergoes a significant shift to 139.93 ppm from 148.45 ppm due to the coordination of the nickel-metal through the amine nitrogen. This shift is a consequence of the nitrogen atom's increased electron density.

5.3.3 Elemental Analysis

To further confirm the stoichiometry and structure of the synthesized NAC, the elemental analysis, consisting of carbon, hydrogen, nitrogen, and nickel contents of the complex were analyzed. The data obtained are presented in Table 5.1. The result showed that the aniline was coordinated to the Ni (II) ion in a 1:2 mole ratio of nickel to aniline, giving rise to tetrahedral geometry. The complex contained two water molecules as part of the coordination sphere and chloride as counter ions. Based on this analysis and other spectroscopic analyses conducted on the complex, the complex's proposed structure is presented in Figure 5.2.

Table 5.1: Elemental analysis data of the Ni (II)–aniline complex

Compound	**Molecular formula (molar mass)**	**Microanalysis: found (calculate) %**			
		C	**H**	**N**	**Ni**
[Ni-aniline] Cl_2	$C_{12}H_8Cl_2N_2NiO_2$ (351.8829)	40.60 (40.96)	5.07 (5.16)	7.41 (7.96)	16.23 (16.68)

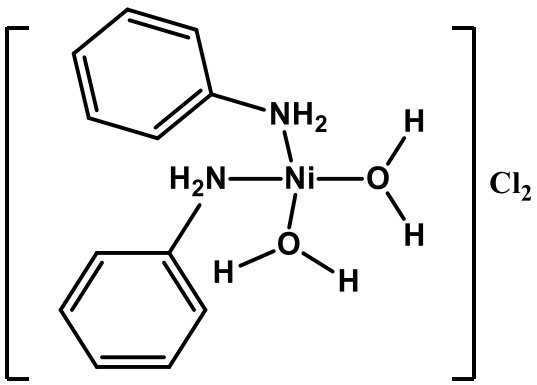

Figure 5.2: Proposed structure of the Ni (II) aniline complex.

5.3.4 UV Spectra

The electronic spectra of aniline and nickel aniline complex (NAC) were recorded using DMSO as a solvent, and its spectra are shown in Figure 5.3. The absorption spectrum of aniline has a single band at 250 nm, which has been linked to benzene ring π-π* transitions [21]. The NAC spectra also showed this transition, but it shifted to lower frequencies, verifying the aniline's interaction with the nickel ion [22].

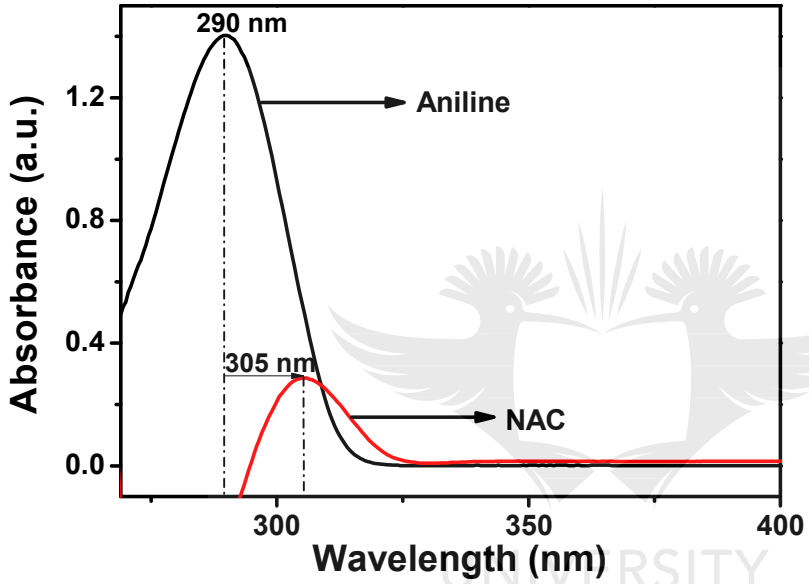

Figure 5.3: Electronic spectra of aniline and nickel aniline complex (NAC).

5.3.5 SEM analysis

The nickel coordination with the aniline moiety significantly affects the complex's surface morphology, which was examined by SEM studies. The SEM images of the nickel chloride salt and nickel aniline complex are presented in Figure 5.4. There was a clear difference between the SEM micrographs of the metal salt and the nickel aniline complex due to the introduction of aniline. The nickel chloride salt displays a fibrous morphology. At the same time, the NAC show agglomerated surface structure with smaller particles dispersed in a uniform matrix and creates the appearance of a platelet-like arrangement.

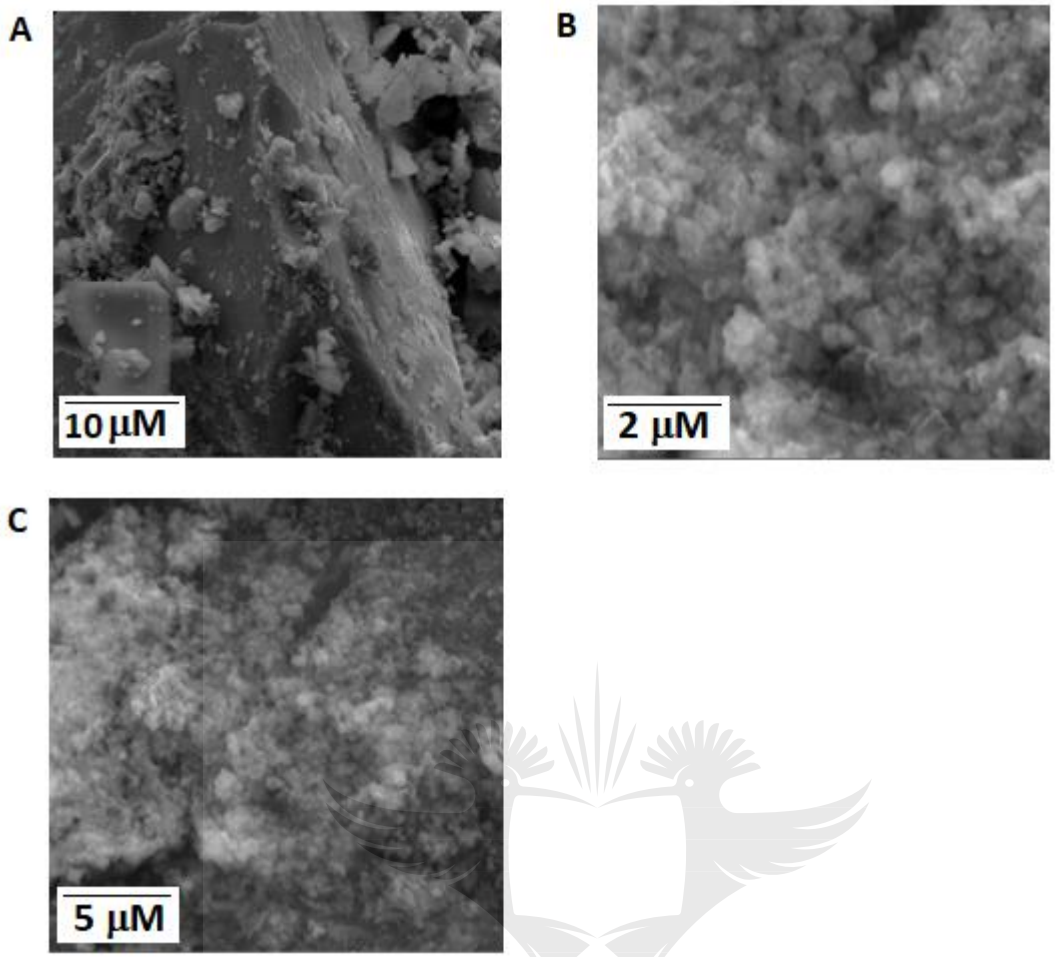

Figure 5.4: SEM images of (A) Nickel chloride salt (B and C) Ni (II) aniline complex.

5.3.6 XRD Study

XRD pattern of the starting material, NiCl salt, and the formed complex, NAC are displayed in Figure 5.5(A) and (B). Both samples exhibited crystallinity with reduced number of peaks for the NiCl. The diffraction pattern of the metal complex showed numerous diffraction peaks with a cubic structure. The major peaks were indexed as (101), (202), (004), (400), (022) which is in good agreement with literature value (JCPDS 78-0423). The XRD pattern of the NAC illustrates definite and sharp crystalline peaks signifying that the sample is crystalline in phase [23,24]. The occurrence of crystallinity in the NAC is attributed to the metallic compound's intrinsic crystalline form. The NAC's crystallite size, L, was calculated using Scherrer's formula [25] by measuring the entire length at half the maximum of the XRD peaks.

$$L = k\lambda / \beta (\cos \theta) \quad (5.1)$$

'k' in the above equation is called Scherrer's constant with a value equal to 0.94, 'λ' = 1.5406 Å (wavelength of the X-ray sources), 'β' stands for full width at half maximum known as FWHM (radians), and 'θ' stands for peak angle. Table S5.2 shows that the complex does have an average crystallite size of 27 nm, suggesting that it is nanocrystalline.

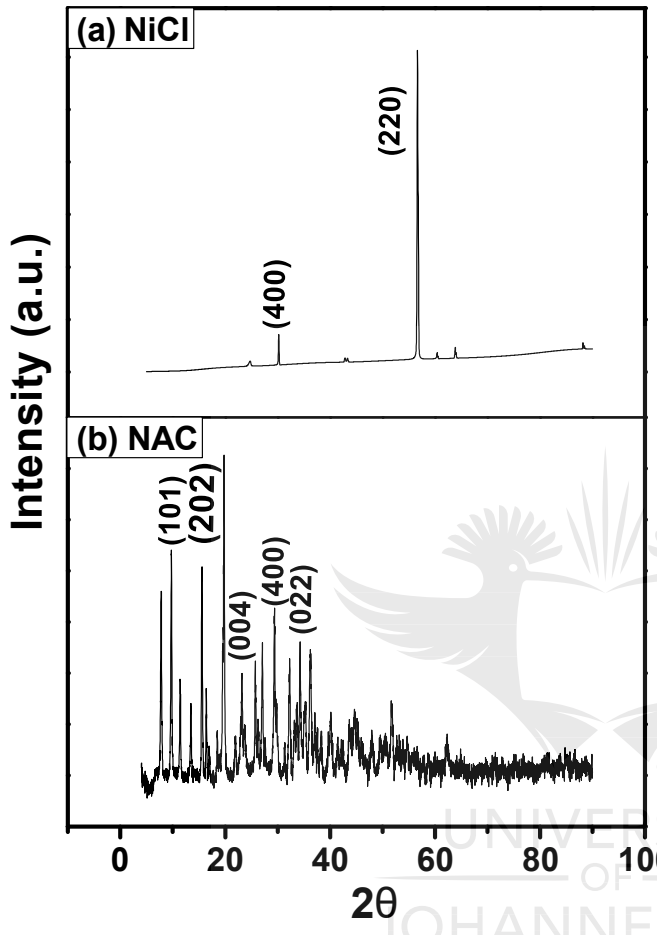

Figure 5.5: XRD pattern of (A) NiCl salt (B) Nickel (II) aniline complex.

5.3.7 Electrochemical behavior of NAC modified electrode

To analyze the electrochemical properties of the fabricated sensor, we used electrochemical impedance spectroscopy (EIS). In the EIS, an impedance spectrum is generated whereby it can be used to extract the electron transfer kinetics and diffusion properties. The electron transfer resistance is represented by the semicircle diameters, while the straight line depicts the electrochemical process' diffusion limiting phase. At a reference voltage of 0.225 V, the impedance spectra were recorded throughout a frequency range of 1 KHz to 7 MHz in 5 mM hexacyanoferrate (iii) with 0.1 M KCl. Figure 5.6 illustrates the spectra of the bare electrode (curve a) and the electrode modified with NAC (curve b). According to the Nyquist plots, a straight line was found at lower frequencies for the bare and NAC modified GCE, illustrating

that the electrochemical process has a diffusion limiting phase [26,27]. It can also be observed that the spectra for the modified electrode display a small radius circular arc than that of bare GCE. This indicates a decrease in the electron transfer impedance at the electrode's surface, suggesting that the NAC can promote $[Fe(CN)_6)]^{3-/4-}$ electron transport. The electron transport of the NAC is due to its conductivity. The intense interaction between the two unpaired electrons in the 3d orbital of Ni^{2+} and the aniline's antibonding orbitals could explain the conductivity. The interaction delocalizes the aniline's π-electronic charge, decreasing the energy gap and increasing the conductivity [28].

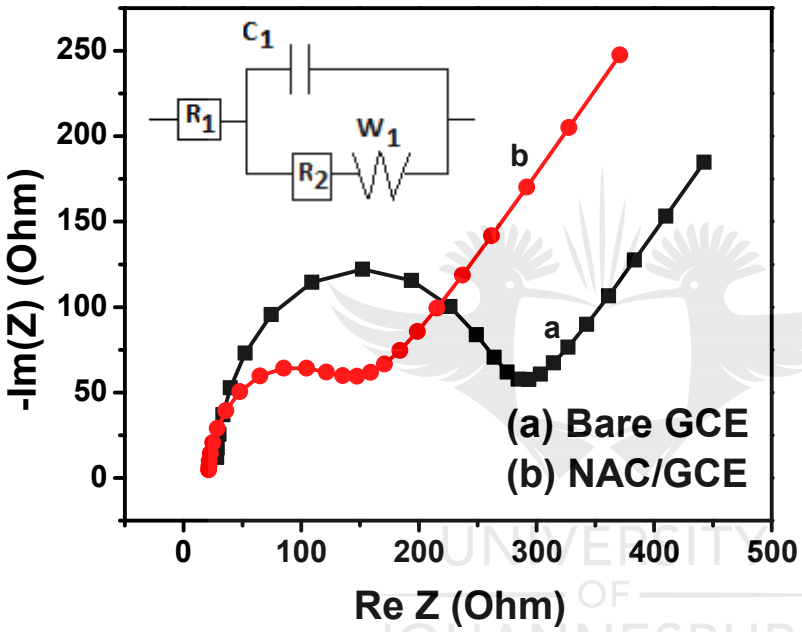

Figure 5.6: Impedance plots of (a) Bare GCE (b) NAC modified GCE. Inset: a model of an equivalent circuit based on the fitting curve.

5.3.8 Electrocatalytic effect of Ni-ani/GCE towards cysteine

The Ni (II) aniline complex modified electrode was used to examine cysteine's electrocatalytic oxidation. Before the implementation of the Ni (II) aniline complex modified electrode to cysteine's oxidation, a comparison of the electrochemical response of the bare and modified electrode was investigated both in the absence and presence of cysteine. The study was done using cyclic voltammetry (CV) in 10 mM PBS electrolyte at 50 mV/s scan rate, as represented in Figure 5.7A. In the absence of cysteine (Figure 5.7A, inset), the cyclic voltammetry curve at the bare electrode (curve 'a') shows a very weak current signal. However, the current signal was enhanced upon modifying the electrode (curve 'b') with the

complex material. There was also a significant change in the oxidation current value (curve 'b') upon the analyte's addition for the modified electrode compared to the bare one in Figure 5.7A, the main panel. The results indicate that the Ni (II)-aniline complex displayed excellent electrocatalytic behavior for the oxidation of cysteine. In addition, the complex material increased the electron transfer rate between cysteine and the bare electrode during the oxidation process. Such enhanced activity is due to the Nickel (II) ion and aniline moiety's synergistic effect.

The electrocatalytic oxidation of cysteine was probed by CV in 10 mM PBS electrolyte at 50 mV/s scan rate by varying the concentration (Figure 5.7B). The result shows that as cysteine concentration is increased, the anodic peak current increases, indicating that cysteine has been oxidized by the electrode modified with NAC. The maximum peak currents occurring at the voltammogram symbolize that the NAC modified electrode has a good electrochemical activity for cysteine oxidation with a rapid electron transfer and mass transport [29]. A possible oxidative mechanism of cysteine on the surface of solid electrodes can be proposed, as shown in Scheme 5.1.

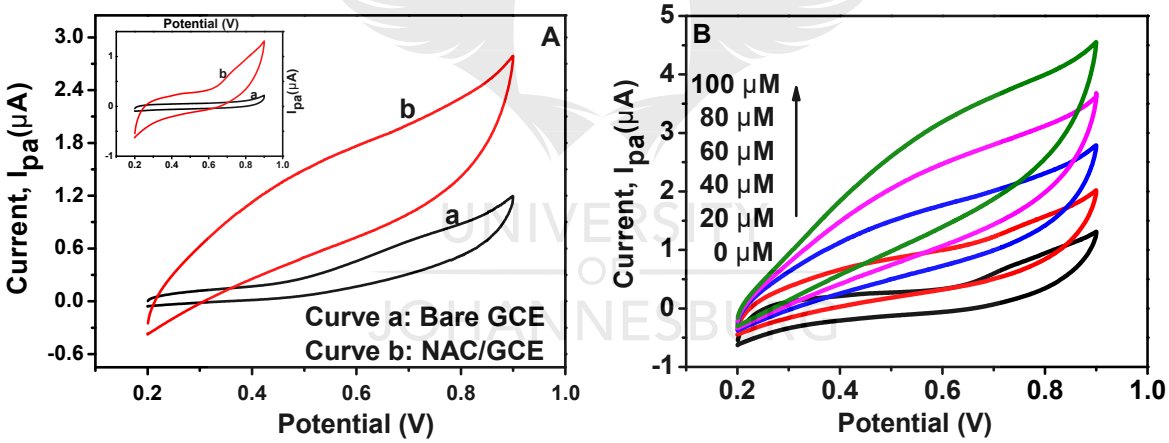

Figure 5.7: (A) Cyclic voltammetry response of bare GCE and NAC modified electrode with 0 μM cysteine (inset) and 40 μM cysteine (main panel) **(B)** Cyclic voltammetry response of NAC modified GCE containing different concentrations of cysteine (Using 10 mM PBS electrolyte with pH 7.4, scanned at a rate of 50 mV/s).

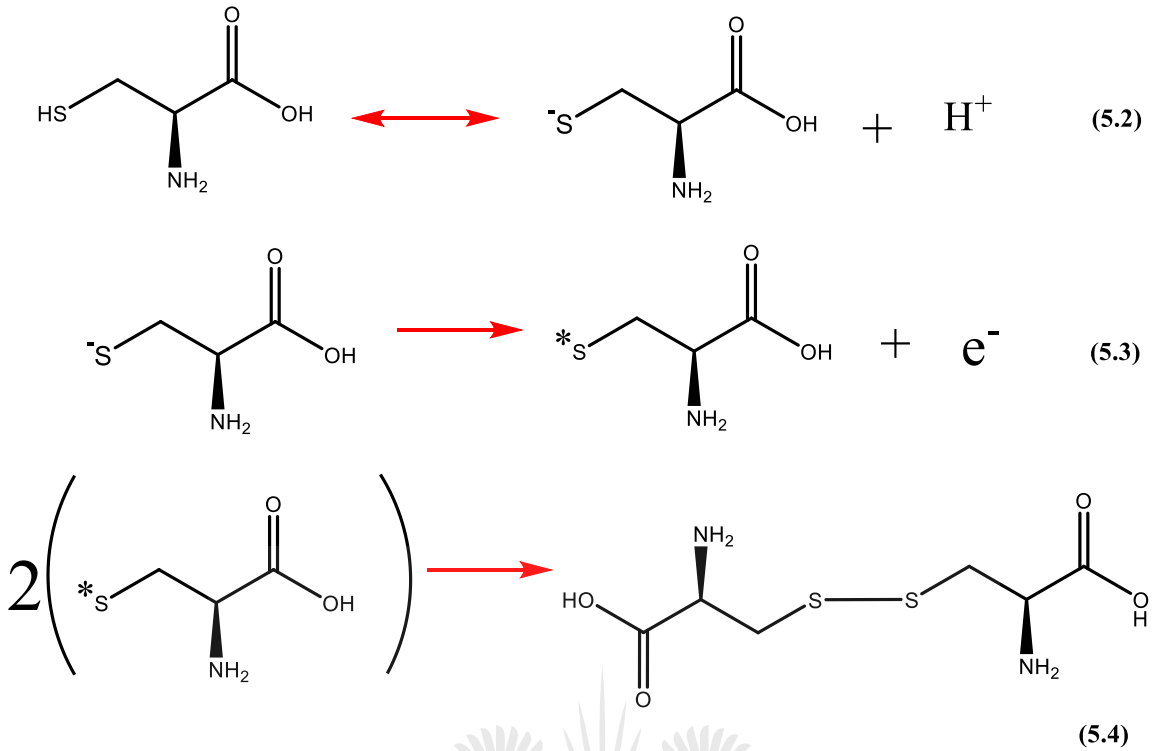

Scheme 5.1: Electrochemical oxidation of cysteine at the NAC modified electrode.

According to the scheme, the functional group SH of L-cysteine is oxidized according to Equation (5.3), and two molecules are absorbed in the electrode surface to form L-cystine, as shown in Equation (5.4). The electrochemical measurement (Figure 5.7B) verifies the oxidative mechanism of cysteine. From Figure 5.7B, the irreversible oxidation peak near 0.40 V could be ascribed to the oxidation of the –SH group of L-cysteine forming cysteine, which results in the formation of a disulfide bond. Similar mechanisms are reported in the literature [30,31].

5.3.9 Influence of scan rate on cysteine oxidation

CVs were run at various scan rates to investigate kinetic parameters on cysteine oxidation at the NAC/GCE modified electrode. Figure 5.8 A shows the CV curves of the oxidation of 40 µM cysteine within 50 mV/s to 400 mV/s. According to the result, peak current rises as the scan rate rises. As demonstrated in Figure 5.8B, the anodic peak current increases linearly as the scan rate increases. A linear relationship can also be shown when peak current is plotted against the scan rate's square root. The correlation between the logarithm of the peak current and the logarithm of the scan rate also exhibited linearity with a gradient value of 0.40. The results show that the mechanism occurring at the electrode's surface was diffusion controlled [32].

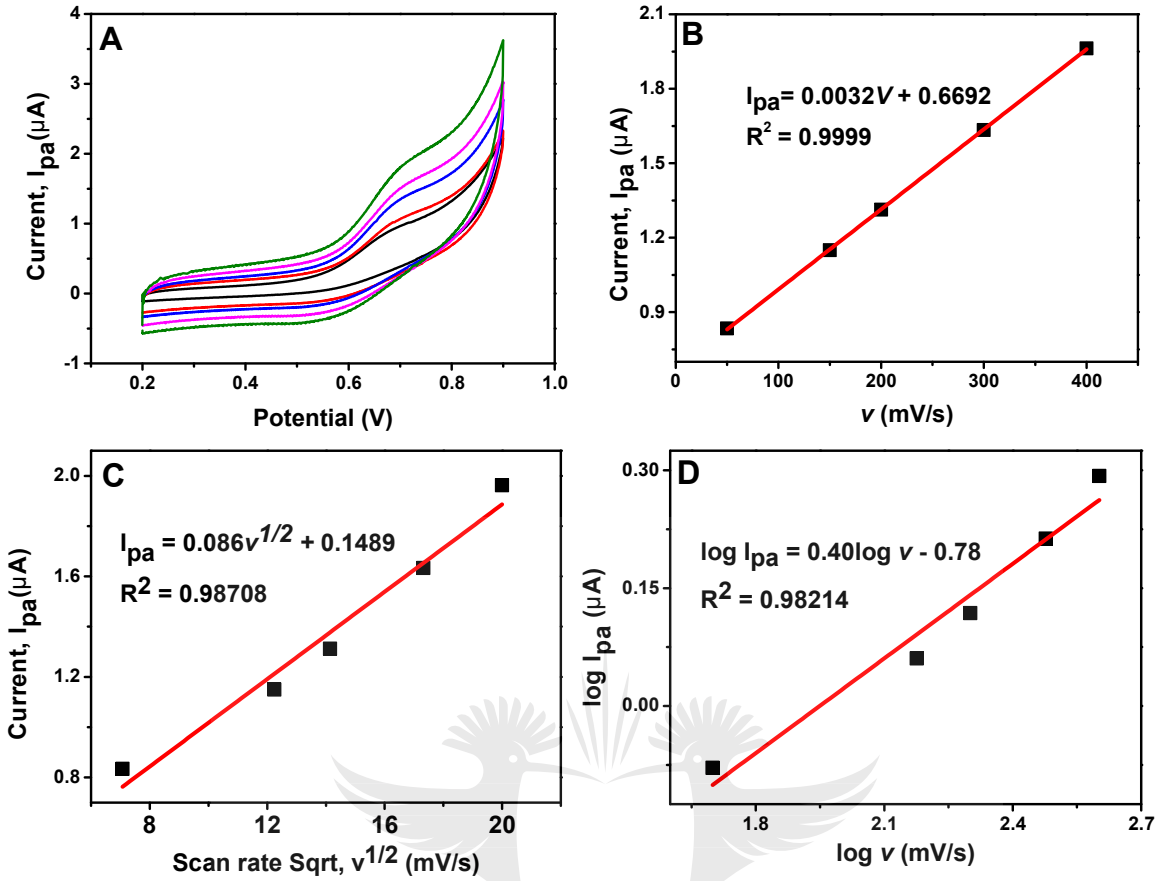

Figure 5.8: (A) CV responses of NAC/GCE containing 40 μM cysteine in PBS (pH 7.4) at different scan rates (50 mV/s to 400 mV/s). The line plot of (B) peak current vs. scan rate (C) peak current vs. scan rate's square root (D) logarithm of peak current vs. scan rate's logarithm.

5.3.10 Square wave voltammetric detection of cysteine

To check the cysteine sensor's analytical performance, we employed the method of squarewave voltammetric (SWV) detection. This technique would enable us to determine some parameters, including sensitivity and detection limit values. The SWV detection was done by a scan of the potential between 0.2 to 0.9 V at 10 Hz frequency, scanned at a rate of 50 $mVs^{-1,}$ and a pulse height of 25 mV in PBS electrolyte. The currents produced due to cysteine's electrocatalytic oxidation were recorded after an accumulation time of 10 s. Figures 5.9A and B show that, with cysteine concentrations, the oxidation peak currents increase linearly in the region of 2.5 μM to 25 μM and 40 μM to 220 μM, respectively. The result suggests that the electrode's electrochemical activity has improved upon modification. It is

worth noting that the oxidation peak moved to a higher potential range, indicating the electro-oxidation process's irreversibility [33]. The calibration curve was recorded for cysteine detection by plotting the oxidation peak currents against the concentration. The linear response of the modified electrode towards cysteine be expressed as i_{pa} (μA) = 0.1134 c (μM) + 0.8365 (R^2 = 0.98994) and = 0.04022 c (μM)+ 2.85342 (R^2 = 0.98811) where c is concentration. A detection limit of 2.09 μM was calculated based on a signal-to-noise ratio equal to 3.0. The sensitivities of the proposed sensor were calculated to be 1.6026 $\mu A \mu M^{-1} cm^{-2}$ and 0.5686 $\mu A \mu M^{-1} cm^{-2,}$ respectively, in the two linear ranges. The results illustrate that the proposed sensor has a low detection limit and broad linear range, which is considerably higher than many other sensors mentioned in the literature, as listed in Table 5.2. The comparison confirms that the nickel aniline complex is an effective medium for the electrochemical recognition of cysteine.

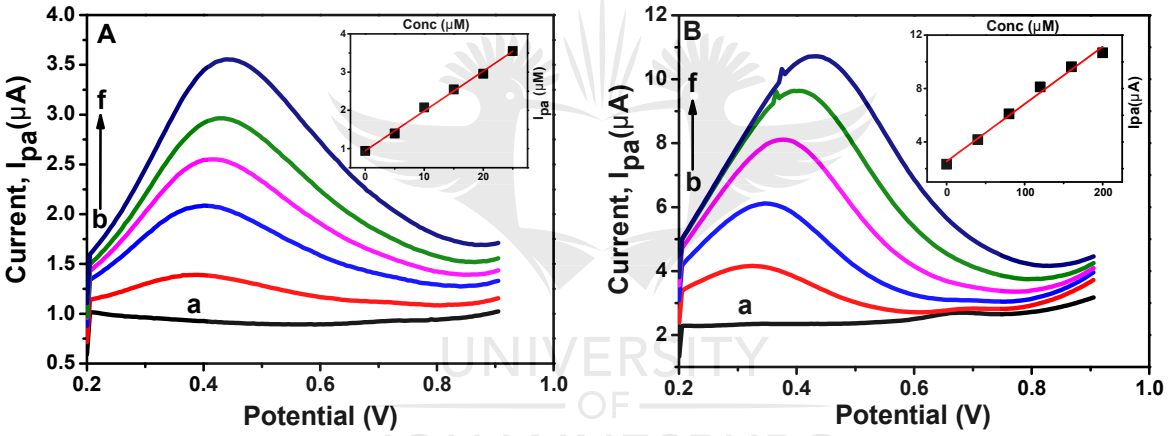

Figure 5.9: (A) Square wave voltammetric responses of NAC modified GCE in 10 mM PBS electrolyte (pH 7.5) with reduced concentrations of cysteine (from a to f: 0, 5, 10, 15, 20, 25 μM, respectively). Calibration plot is shown inset **(B)** Square wave voltammetric responses of NAC modified GCE in 10 mM PBS electrolyte (pH 7.4) with increasing concentrations of cysteine (from a to f: 0, 40, 80, 120, 160, 200 μM, respectively). The calibration plot is shown inset.

Table 5.2: Comparative analysis of the efficiency of electrochemical sensors for cysteine detection

Electrochemical sensors	Techniques	Detection Limit (µM)	Linear Range (µM	References
MWCNTs/PEI/AuNPs/DTNB	Amperometry	2.7	9-250	[34]
Iron tetrasulfonated phthalocyanine/MWCNTs	Amperometry	0.13	1.21 – 24.23	[35]
Glassy carbon electrode modified with MWCNT	Amperometry	5.4	10-500	[36]
Carbon electrode bulk modified with cobalt phthalocyanine	Amperometry	0.2	1-12	[37]
Brilliant-blue-modified Nafion-coated GCE	CV	0.5	10-100	[38]
$CuGeO_3$/10 with PANI nanowire modified GCE	CV	0.44	1-2	[39]
PAMT	DPV	3.36	20-180	[40]
Co(II) SMCP	Amperometry	0.4	2-20	[41]
CFE modified with Micro Au	Voltammetry	0.06	0.5-5	[42]
Ni (II)-aniline complex	SWV	2.09	2.5-25 40-220	This work

Multi-wall carbon nanotube (MWCNT), Carbon fiber electrodes (CFE), Polyethylenimines (PEI), salophen-modified carbon paste (SMCP), DTNB 5,5-Dthiobis-2-nitrobenzoic acid, Poly[5-amino-2-mercapto-1,3,4-thiadiazole] (PAMT), Polyaniline (PANI).

5.3.11 Selectivity and Reproducibility studies

The sensor's selectivity was investigated by studying the chronoamperometry determination of successive additions of cysteine at 0.4 V in the presence of 20 µM of each glucose, tryptophan, glycolic acid, glycine, glutathione, and histamine, as shown in Figure 5.10A. The interferents were chosen because their peak potentials are close to cysteine and within the

potential range under investigation. Upon the addition of cysteine, there was an obvious current response. On the contrary, the modified electrode was passive towards the electroactive interfering species with no noticeable current response. The result confirms that the fabricated Ni (II) aniline complex modified GCE is highly selective towards cysteine determination.

To ascertain the sensor's reproducibility, the electrochemical oxidation of cysteine (20 µM) was performed with cyclic voltammetry for four successive measurements. The tests were performed using five separate electrodes modified with the Nickel (II) aniline complex at 50 mV/s scan rate in an electrolyte of PBS (pH 7.4). The cysteine's oxidation peak current obtained with the four successive measurements of 5 different modified electrodes revealed a relative standard deviation of 7.44 %, implying that the results are reproducible (Figure 5.10B).

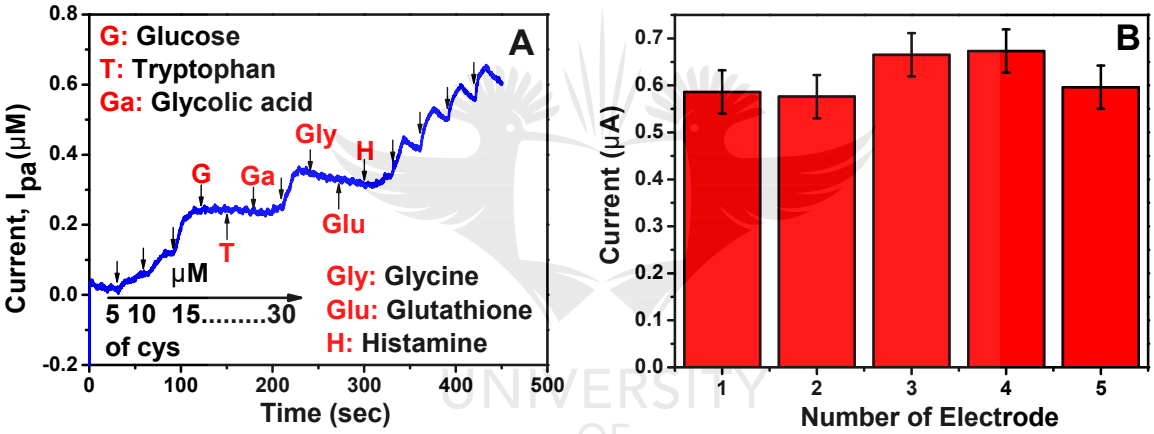

Figure 5.10: (A) Amperometric current response of cysteine in the presence of glucose, tryptophan, glycolic acid, glycine, glutathione, and histamine with a potential of 0.40 V (Using an electrolyte of PBS, 10mM concentration at 50 mV/s scan rate. (B) The current registered during electrooxidation of 20 µM cysteine on five different NAC/GCE surfaces prepared in the same condition.

5.4. Sub-conclusion

We have successfully prepared a nickel (II) aniline complex via a simple complexation method. Aniline performed as a ligand, complexing with the nickel-metal via the nitrogen group of the aniline. The FTIR, UV, NMR, and elemental analysis established the synthesis of the complex material. XRD analysis of the complex shows a crystallite size of 27 nm. Also, the surface morphology using SEM displayed that the particles of the complex were agglomerated. The complex material exhibited good electrocatalytic properties for cysteine

detection, as evidenced by its low detection limit and broad linear range. The sensor showed a fast response, appreciable sensitivity, and reproducibility results, indicating that NAC could also be a favorable material for constructing efficient electrochemical sensors.

5.5 References

[1] Go, Young-Mi, and Dean P. Jones. (2011). "Cysteine/cystine redox signaling in cardiovascular disease." *Free Radical Biology and Medicine*, 50(4): 495-509.

[2] Hignett, G., Threlfell, S., Wain, A. J., Lawrence, N. S., Wilkins, S. J., Davis, J., Compton, R.G & Cardosi, M. F. (2001). Electroanalytical exploitation of quinone–thiol interactions: application to the selective determination of cysteine. *Analyst*, *126*(3), 353-357.

[3] Li, S., Schöneich, C., & Borchardt, R. T. (1995). Chemical instability of protein pharmaceuticals: mechanisms of oxidation and strategies for stabilization. *Biotechnology and Bioengineering*, *48*(5), 490-500.

[4] Rezaei, B., & Mokhtari, A. (2007). A simple and rapid flow injection chemiluminescence determination of cysteine with Ru $(phen)_3^{2+}$–Ce (IV) system. *Spectrochimica Acta Part A: Molecular and Biomolecular Spectroscopy*, *66*(2), 359-363.

[5] Pazalja, M., Kahrović, E., Zahirović, A., & Turkušić, E. (2016). Electrochemical sensor for determination of L-cysteine based on carbon electrodes modified with Ru (III) Schiff base complex, carbon nanotubes, and Nafion. *Int. J. Electrochem. Sci*. *11*, 10939-10952.

[6] Stabler, S.P.; Marcell, P.D.; Rodell, E.R.; Allen, R.H.; Savage, D.G.; Lindenbaum, J. (1988). Elevation of total homocysteine in the serum of patients with cobalamin or folate deficiency detected by capillary gas chromatography-mass spectrometry. J. Clin. Investig. 81, 466–474.

[7] Yu, X., Wang, Q., Liu, X., & Luo, X. (2012). A sensitive chemiluminescence method for the determination of cysteine based on silver nanoclusters. *Microchimica Acta*, *179*(3-4), 323-328.

[8] Huang, S., Xiao, Q., Li, R., Guan, H. L., Liu, J., Liu, X. R., He, Z.K. & Liu, Y. (2009). A simple and sensitive method for L-cysteine detection based on the fluorescence intensity increment of quantum dots. *Analytica Chimica Acta*, *645*(1-2), 73-78.

[9] Fei, S., Chen, J., Yao, S., Deng, G., He, D., & Kuang, Y. (2005). Electrochemical behavior of L-cysteine and its detection at carbon nanotube electrode modified with platinum. *Analytical Biochemistry*, *339*(1), 29-35.

[10] Liu, L. P., Yin, Z. J., & Yang, Z. S. (2010). An l-cysteine sensor based on Pt nanoparticles/poly (o-aminophenol) film on glassy carbon electrode. *Bioelectrochemistry*, *79*(1), 84-89.

[11] Lee, P. T., Thomson, J. E., Karina, A., Salter, C., Johnston, C., Davies, S. G., & Compton, R. G. (2015). Selective electrochemical determination of cysteine with a cyclotricatechylene modified carbon electrode. *Analyst*, *140*(1), 236-242.

[12] Pei, L. Z., Cai, Z. Y., Pei, Y. Q., Xie, Y. K., Fan, C. G., & Fu, D. G. (2014). Electrochemical determination of L-cysteine using polyaniline/CuGeO 3 nanowire modified electrode. *Russian Journal of Electrochemistry*, *50*(5), 458-467.

[13] Adegunloye, A., Perla, V. K., Ghosh, S. K., Zinyemba, O., & Mallick, K. (2020). Electrochemical and electrical response of bismuth-aniline complex under the exposure of organic and inorganic environment. *SN Applied Sciences*, *2*(12), 1-10.

[14] Jahandari, S., Taher, M. A., Karimi-Maleh, H., & Mansouri, G. (2019). Simultaneous voltammetric determination of glutathione, doxorubicin and tyrosine-based on the electrocatalytic effect of a nickel (II) complex and of Pt: Co nanoparticles as a conductive mediator. *Microchimica Acta*, *186*(8), 493.

[15] Nie, H., Yao, Z., Zhou, X., Yang, Z., & Huang, S. (2011). Nonenzymatic electrochemical detection of glucose using well-distributed nickel nanoparticles on straight multi-walled carbon nanotubes. *Biosensors and Bioelectronics*, *30*(1), 28-34.

[16] Lee-Thorp, J. A., Rüede, J. E., & Thornton, D. A. (1978). The infrared spectra (3500-150 cm^{-1}) of aniline complexes of cobalt (II), nickel (II), copper (II), and zinc (II) halides. *Journal of Molecular Structure*, *50*(1), 65-71.

[17] Fuson, N., Josien, M. L., Powell, R. L., & Utterback, E. (1952). The NH Stretching Vibration and NH–N Hydrogen Bonding in Several Aromatic Compounds. *The Journal of Chemical Physics*, *20*(1), 145-152.

[18] Nour, E. M., Taha, A. A., & Alnaimi, I. S. (1988). Infrared and Raman studies of [UO2 (salen)(L)](L= H2O and CH3OH). *Inorganica Chimica Acta*, *141*(1), 139-144.

[19] Devi, T. P., & Singh, R. H. (2010). Complexes of nickel (II) with the Schiff bases derived from condensation of salicylaldehyde and Bis-Ni (AMUH) 2Cl2. *Rasayan J Chem*, *3*, 14.

[20] Skauge, T., Turel, I., & Sletten, E. (2002). Interaction between ciprofloxacin and DNA mediated by Mg2+-ions. *Inorganica Chimica Acta*, *339*, 239-247.

[21] Li, X. H., Wu, B., Huang, J. E., Zhang, J., & Liu, Z. F. (2003). Fabrication and characterization of well-dispersed single-walled carbon nanotube/polyaniline composites. *Carbon (New York, NY)*, *41*(8), 1670-1673.

[22] Friedel, R. A., & Orchin, M. (1958). Ultraviolet Spectra of Aromatic Compounds Chemistry.

[23] Souaya, E. R., Hanna, W. G., Ismail, E. H., & Milad, N. E. (2000). Studies on some acid divalent metal nitrilotriacetate complexes. *Molecules*, *5*(10), 1121-1129.

[24] Joseyphus, R. Selwin, and M. Sivasankaran Nair. "Synthesis, characterization and biological studies of some Co (II), Ni (II) and Cu (II) complexes derived from indole-3-carboxaldehyde and glycylglycine as Schiff base ligand." *Arabian Journal of Chemistry* 3, no. 4 (2010): 195-204.

[25] Robertson, J. H. (1979). Elements of X-ray diffraction by BD Cullity.

[26] Choudhary, M., Siwal, S., Nandi, D., & Mallick, K. (2016). Catalytic performance of the in situ synthesized palladium–polymer nanocomposite. *New Journal of Chemistry*, *40*(3), 2296-2303.

[27] Myeni, N., Perla, V. K., Ghosh, S. K., & Mallick, K. (2020). Organic matrix stabilized copper sulfide nanoparticles: Synthesis, characterization and application in glucose recognition. *Materials Today Communications*, *25*, 101291.

[28] El-Saved, B. A., Shaaban, S., Sallam, M. M., & Emara, A. A. A. (1996). Temperature dependence of the electrical conductivity of salicylaldehyde hydrazone and its transition metal complexes. *Journal of Materials Science Letters*, *15*(10), 883-885.

[29] He, W., Zhang, W., Zhang, L., Zhang, X., & Yang, F. (2017). A versatile sensor for determination of seven species based on NiFe nanoparticles. *Journal of Electroanalytical Chemistry*, *797*, 61-68.

[30] Liu Z., Wu G., (2006). The electro-oxidative activity of cysteine on the Au electrode as evidenced by surface enhanced Raman scattering. Spectrochim Acta A 64;251–254.

[31] Spataru N., Sarada BV., Popa E., Tryk DA., Fujishima A (2001). Voltammetric determination of L-cysteine at conductive diamond electrodes. Anal Chem 73:514–519.

[32] Gosser, D. K. (1993). *Cyclic voltammetry: simulation and analysis of reaction mechanisms* (Vol. 43). New York: VCH.

[33] Malem, F., & Mandler, D. (1993). Self-assembled monolayers in electroanalytical chemistry: application of. omega.-mercapto carboxylic acid monolayers for the electrochemical detection of dopamine in the presence of a high concentration of ascorbic acid. *Analytical Chemistry*, *65*(1), 37-41.

[34] Santhiago, M., Lima, P. R., Santos, W. D. J. R., & Kubota, L. T. (2010). An amperometric sensor for l-cysteine based on nanostructured platform modified with 5, 5′-dithiobis-2-nitrobenzoic acid (DTNB). *Sensors and Actuators B: Chemical*, *146*(1), 213-220.

[35] Devasenathipathy, R., Mani, V., Chen, S. M., Kohilarani, K., & Ramaraj, S. (2015). Determination of L-cysteine at iron tetrasulfonated phthalocyanine decorated multiwalled carbon nanotubes film modified electrode. *Int. J. Electrochem. Sci*, *10*, 682-690.

[36] Salimi, A.; Hallaj, R. Catalytic oxidation of thiols at preheated glassy carbon electrode modified with abrasive immobilization of multiwall carbon nanotubes: Applications to amperometric detection of thiocytosine, L-cysteine and glutathione. *Talanta*, *66*(4), 967-975.

[37] Filanovsky, B. (1999). Electrochemical response of new carbon electrodes bulk modified with cobalt phthalocyanine to some thiols in the presence of heptane or human urine. *Analytica Chimica Acta*, *394*(1), 91-100.

[38] Chen, S. M., Chen, J. Y., & Thangamuthu, R. (2008). Electrochemical preparation of brilliant-blue-modified Poly (diallyldimethylammonium Chloride) and nafion-coated glassy carbon electrodes and their electrocatalytic behavior towards oxygen and l-cysteine. *Electroanalysis: An International Journal Devoted to Fundamental and Practical Aspects of Electroanalysis*, *20*(14), 1565-1573.

[39] Pei, L. Z., Cai, Z. Y., Pei, Y. Q., Xie, Y. K., Fan, C. G., & Fu, D. G. (2014). Electrochemical determination of L-cysteine using polyaniline/CuGeO 3 nanowire modified electrode. *Russian Journal of Electrochemistry*, *50*(5), 458-467.

[40] Kalimuthu, P., & John, S. A. (2009). Nanostructured electropolymerized film of 5-amino-2-mercapto-1, 3, 4-thiadiazole on glassy carbon electrode for the selective determination of L-cysteine. *Electrochemistry Communications*, *11*(2), 367-370.

[41] Amini, M. K., Khorasani, J. H., Khaloo, S. S., & Tangestaninejad, S. (2003). Cobalt (II) salophen-modified carbon-paste electrode for potentiometric and voltammetric determination of cysteine. *Analytical Biochemistry*, *320*(1), 32-38.

[42] Wang, L. H., & Huang, W. S. (2012). Electrochemical oxidation of cysteine at a film gold modified carbon fiber microelectrode its application in a flow through voltammetric sensor. *Sensors*, *12*(3), 3562-3577.

CHAPTER 6

ELECTROCHEMICAL RECOGNITION OF URIC ACID AND DOPAMINE USING COBALT-ANILINE COMPLEX WITHIN AN ORGANIC AND INORGANIC MATRIX

6.1 Introduction

For many years, cobalt-based compounds have captured a strong interest in research owing to their physiochemical properties, including ferromagnetism, high melting point, multivalence states, and high stability [1]. Cobalt compounds have found usefulness in applications such as biomedicine [2], catalysis [3], inks and pigments [4], biological systems [5], hybrid supercapacitors [6], and sensors [7]. Cobalt is one of the most promising ones among the transition metals due to its extensive range of spectroscopic and unique properties. It can also form complexes by covalently binding to other molecules or ions. Cobalt research is still ongoing since it has a wide range of functions and uses, particularly in sensors.

Some electrochemical cobalt-based sensors have been reported for sensing applications, and they all exhibited promising performances. For example, cobalt oxide/reduced graphene composite exhibited good selectivity and fast and stable response to hydrogen peroxide [8]. Ternary nickel-cobalt sulfide nanoparticles have also been used for nonenzymatic sensing of glucose [9]. Wu *et al.* also documented cobalt sulfide application for the electrocatalytic detection of glucose and hydrogen peroxide [10]. The design of a bipyridine cobalt (ii) complex sensor has also been reported for the electrochemical sensing of acetaminophen and naproxen [11]. In another recent report, cobalt tetraaminebenzamidephthalocyanine complex was developed for dopamine detection [12]. Hu *et al.* also reported the fabrication of single-atom cobalt-based uric acid sensor [13].

To enhance the sensitivity and selectivity of biological molecules, the design of chemically modified electrodes has extensively been reported. The analysis of uric acid (UA) and dopamine (DA) biomolecules is essential owing to their physiological processes to living organisms. Uric acid is an essential biomolecule and an oxidation product of purine metabolism [14,15]. Dopamine is a crucial neurotransmitter that performs a significant function in human metabolism, cardiovascular, circulatory, and central nervous systems [16]. Studies concerning electrochemical oxidation of UA and DA have extensively been conducted [17].

This study describes UA and DA's electrocatalytic oxidation by a cobalt-aniline metal complex synthesized using a chemical complexation method. The covalent interaction of aniline with cobalt gave rise to a complex with a novel catalytic and luminescent property similar to what was described in our previous work [18,19,29]. The formation of those complexes could be ascribed to the partially filled d-orbital on the transition metal ions. The cobalt aniline complex was further reacted with a sulfur source and yielded no meaningful change in the property of the intermediate product. Various characterization methods have been used to validate the successful synthesis of the product. No article has been reported as regards the utilization of cobalt aniline complex for sensing biological molecules to the author's knowledge. The complex material displayed good electrochemical signals for UA and DA recognition.

6.2 Experimental

6.2.1 Materials

Cobalt sulfate heptahydrate, aniline, sulphuric acid, ethanol, uric acid, and dopamine were purchased from Sigma-Aldrich, obtained as an analytical grade, and utilized without additional purification. All received chemicals and solvents that were used are of analytical quality.

6.2.2 Material characterization

Transmission electron microscopy (TEM) was performed using JEOL (JEM-2100) analytical instrument to determine the complex's microscopic property. The structural characterization was performed using PANanalytical X'pert pro diffractometer system that has CuKα radiation (k = 0.1542). Fourier transform infrared (FTIR) spectra were measured using a Shimadzu IRAffinity-1 with a spectral resolution of $0.5cm^{-1}$. A potentiostat (bio-logic SP-200) coupled to a data acquisition system was used for all electrochemical tests. In the experiment, a glassy carbon electrode (GCE) was utilized as the working electrode, an Ag/AgCl electrode filled with saturated KCl was utilized as the reference electrode, and a platinum wire (0.5mm) was utilized as the counter electrode. An aqueous phosphate buffer solution (10 mM) was used as an electrolyte.

6.2.3 Synthesis of cobalt-aniline complex and characterization techniques

In a standard experiment, 0.0098 g of cobalt sulfate heptahydrate was dissolved in 10 ml of sulphuric acid. The dissolved cobalt sulfate solution was added dropwise to aniline solution dissolved in ethanol (0.48 g of aniline in 10 mL of ethanol) under stirring conditions. A pink precipitate was observed due to the complexation between cobalt and aniline (COAC).
To improve the property or activity of the complex material, sodium sulfide (0.1 M) was added to the pink precipitate of the cobalt aniline complex under the stirring condition and left overnight. As a result, the color of the precipitation changed to reddish-brown. A fraction of the solid material was stored for the TEM study, while the rest was filtered, washed, and dried under vacuum for additional characterization.

The dried synthesized materials were characterized by various methods to establish optical and surface properties. They were also used as electrode materials to assess the electrochemical efficiency of uric acid and dopamine sensing.

6.3 Results and discussion

The mechanism for the formation of Co (II)-aniline can be proposed as follows (Scheme 6.1).

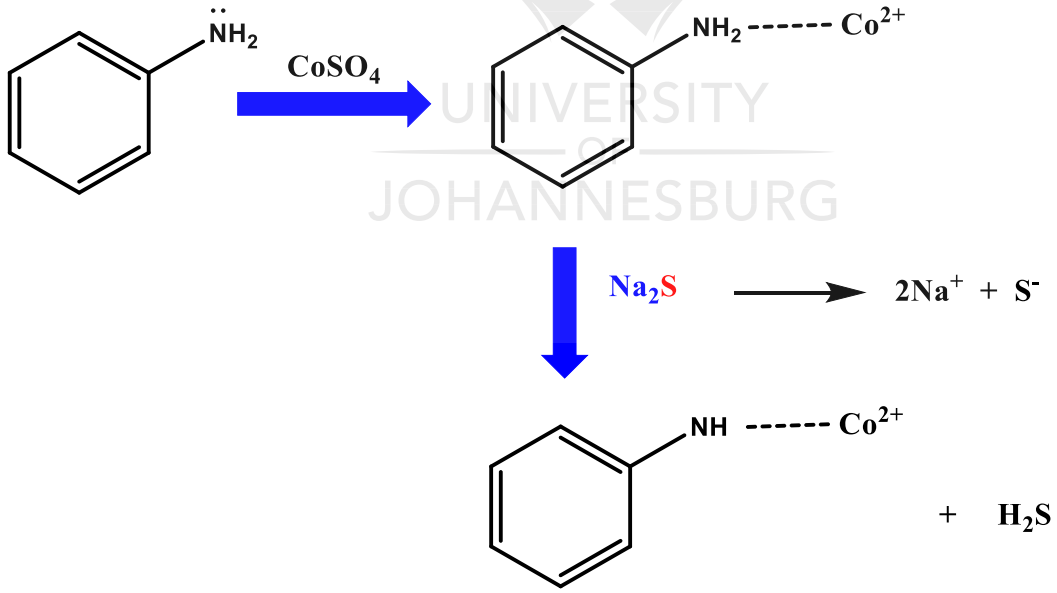

Scheme 6.1: Mechanism of the formation of Cobalt aniline complex.

During the reaction between aniline and copper sulfate, the organic molecule (aniline) acts as a ligand that coordinated with copper sulfate through the lone pair of electrons on nitrogen on atom and forms the Co (II)-aniline complex. After the addition of Na_2S, the anion species of

Na_2S (S^-) attacked the NH_2 group on the complex to reduce it to NH with the evolution of hydrogen sulfide. The result from the elemental analysis and NMR can evidence the reduction of the NH_2 to NH. However, the final product was still a cobalt aniline complex because the sulfur from the sodium sulfide did not attach with the cobalt ion in the reaction. For clarity purposes, the intermediate product was named cobalt aniline complex-1 (COAC-1), and the final product was named cobalt aniline complex-2 (COAC-2).

6.3.1 Elemental Analysis

The elemental analysis of the complex's carbon, hydrogen, nitrogen, and nickel contents was studied further to validate the stoichiometry and structure of the synthesized COAC-2. Table 6.1 summarizes the information gathered. The determined compositions were similar to the elemental compositions. The aniline was found to be coordinated to the Co (II) ion in a 1:1 mole ratio of cobalt to aniline, resulting in a tetrahedral geometry. The coordination sphere was made up of three water molecules, and the counterions were sulfate. The complex's proposed structure is shown in Figure 6.1, based on this analysis and other spectroscopic studies performed on the complex.

Table 6.1: Elemental analysis data of the Cobalt aniline complex-1 (COAC-2)

Compound	**Molecular formula (molar mass)**	**Microanalysis: found (calculate) %**				
		C	**H**	**N**	**S**	**Co**
[Co-aniline] SO_4	$C_6H_{12}CoNO_7S$ (351.8829)	24.61 (23.93)	3.84 (4.02)	4.98 (4.65)	11.55 (10.65)	20.12 19.57

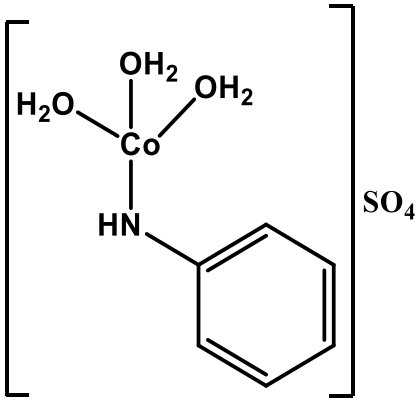

Figure 6.1: Proposed structure of the Co (II) aniline complex (COAC-2).

6.3.2 Morphological studies

The structural morphology of the complex materials was characterized by TEM analysis. The HR-TEM images of COAC-1 and COAC-2 are presented in Figure 6.2(A) and (B), respectively. The HR-TEM image from Figure 6.1A clearly shows that the cobalt metal is complexing with the aniline monomer material with a little agglomeration. After introducing sodium sulfide, the material became more agglomerated without forming a nanoparticle or polymer (Figure 6.2B). A similar kind of morphology has been observed in our former reports [20]. However, in that report, the introduction of sodium sulfide to a bismuth aniline complex led to nanoparticles' formation stabilized by the aniline moiety. In Figure 6.2C, the SEM micrograph of the COAC-2 is shown. It could be seen from the figures that the complex exhibits a platelet-like structure.

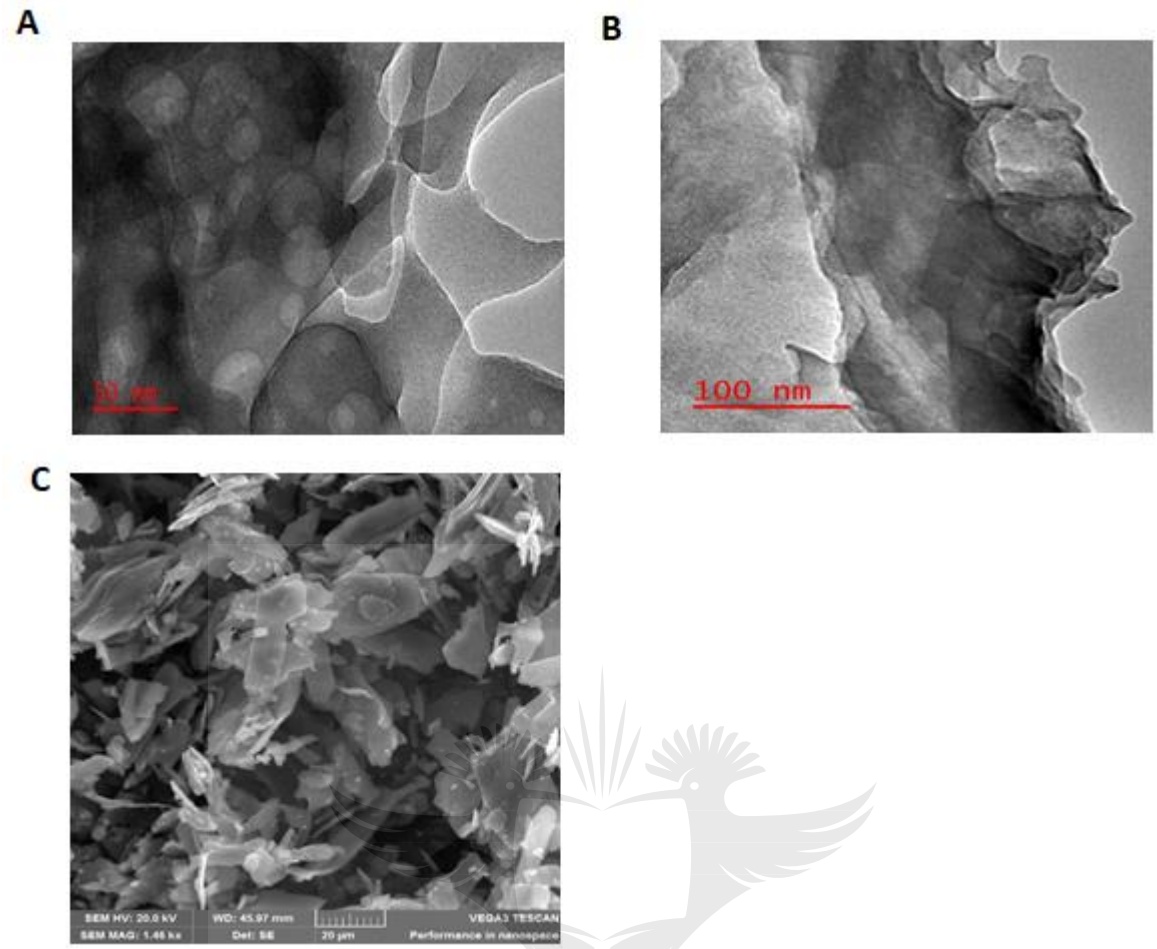

Figure 6.2: HRTEM images of (A) cobalt aniline complex (COAC-1) (B) cobalt aniline complex (COAC-2) (C) SEM image of COAC-2.

6.3.3 FTIR spectroscopy

The prepared complex was further verified with FTIR spectroscopy, as displayed in Figure 6.3. The IR spectrum of the COAC-1 is quite very similar to the COAC-2. The spectra of the aniline complexes are comparatively rich in bands that arise in the amino group's internal vibrations. The complexes are characterized by N-H stretching frequencies at 3265 cm^{-1}, a band lower than that of the aniline moiety, occurring at 3341 cm^{-1}. This stretching frequency indicates the metal coordination with the nitrogen group present in the aniline structure to form a complex [21]. A peak noticed at 3258 cm^{-1} in the complexes is due to the OH bending vibration. The stretching frequency of the C-N bonds in both complexes was confirmed by the prominent signal at 1082 cm^{-1}. The C=C stretching vibration for the benzenoid ring in the two complexes is visible at 1487 cm^{-1} and 1592 cm^{-1}. There are, however, very weak C-H bending on the complexes. The IR spectrum of COAC-2 displayed the regeneration of all the

aniline vibrational bands in COAC-1. The resurgence indicates no new product formation when sulfur was introduced through sodium sulfide rather than a more agglomerated complex through the extra N-H bending at 1735 cm^{-1}. Also, another difference between the two complexes is in their peak intensities. One can observe that the IR peak intensities of the COAC-1 are higher or longer than the COAC-2, meaning the coordination between cobalt and the nitrogen atom on the aniline ring was further strengthened as sulfur was added, leading to more aggregation, hence indicating a complex formation.

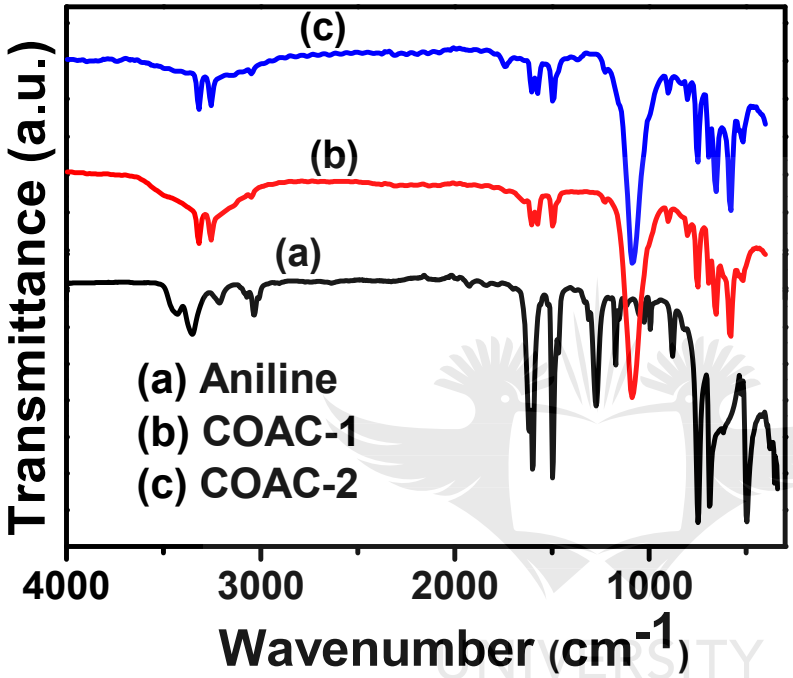

Figure 6.3: FTIR spectra of aniline and COAC-1 and COAC-2 complexes.

6.3.4 NMR study

^{1}HNMR of the ligand and the COAC-2 was performed in DMSO-d_6. The ^{1}H NMR spectrum of the ligand and the complex is displayed in Figures S6.1 and S6.2, respectively. The ^{1}H and spectral information of aniline and the cobalt aniline complex in DMSO-d_6 are presented in Table S6.1. As shown in Figures S6.1 and S6.2, the peaks assigned for the aromatic protons in aniline appear at 7.20-7.23 ppm as triplets and to 6.89-6.91 ppm as duplets. The amine shifted from a peak of 4.97 ppm in aniline to a downfield at 7.79 ppm in the COAC-2 as NH. The spectral analysis indicates that the aromatic protons and amine shift confirm the formation of a complex product [22].

6.3.5 Electronic Spectra

The absorption spectrum of aniline and the cobalt aniline complexes (COAC-1 and COAC-2) were measured in DMSO, and its spectra are presented in Figure 6.4. The aniline spectra have a single energy band of about 290 nm originating from the benzene ring's π–π* transition [23]. This transition was also visible in the COAC-1's UV-vis spectrum but red-shifted from 290 nm to 301 nm. Likewise, there was also a redshift in the COAC-2 spectrum from 290 nm to 296 nm. This redshift confirms the formation of the complex [24].

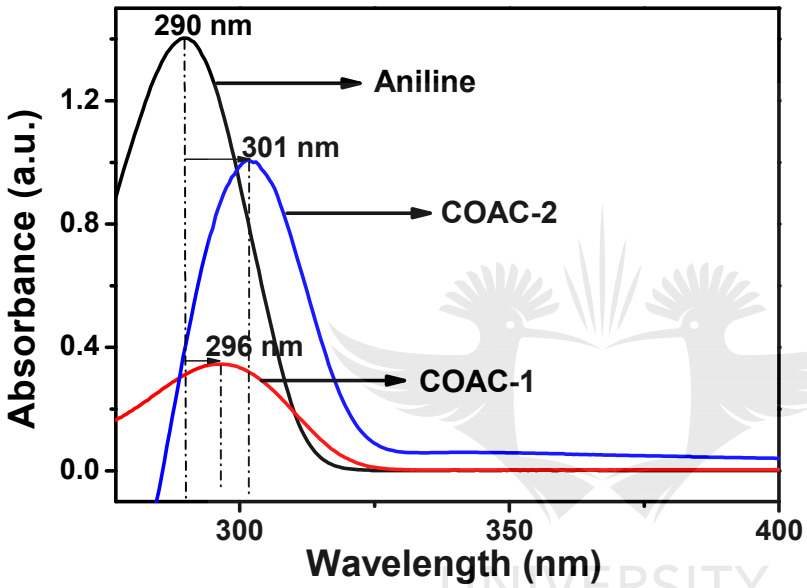

Figure 6.4: Absorption spectra of aniline and cobalt aniline complexes.

6.3.6 XRD analysis

XRD study was used to examine the complex's structures. The diffraction spectrum of the starting material, cobalt sulfate metal and the complexes are compared in Figure 6.5. The cobalt salt spectrum has a reduced number of broad peaks while the complexes have greater number. The spectrum of the COAC-1 and COAC-2 are very similar. The COAC-1 spectrum indicates that most of its peaks are rough or un-sharped peaks, implying that the complex material is more amorphous than crystalline. The peak intensity at 19.49º (200), 20.21º (211), and 22.03º (213) reduced after introducing sulfur, thus corroborating the FTIR results. Longer peaks emerged in COAC-2 complex architecture at 24.58º (220), 28.22º (222) and 30.59º (331) upon sulfur introduction. The prominent broader peaks for COAC-2 compared to COAC-1 could be attributed to the crystal size suppression by the sulfate anions.

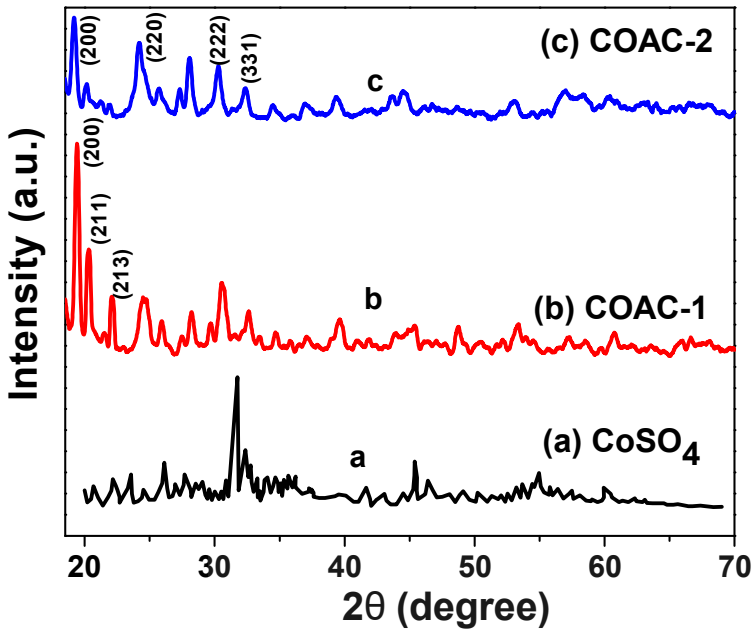

Figure 6.5: X-ray diffraction pattern of (A) Cobalt sulfate salt (B) Cobalt aniline complex (COAC-1) (C) Cobalt aniline complex (COAC-2).

6.3.7 Electrochemical characterization of the sensor

The developed sensor was characterized using electrochemical impedance spectroscopy (EIS) to investigate its electrochemical behavior. Nyquist plots obtained from electrochemical measurements usually provide useful information on electron transfer kinetics at the electrode's surface. The Nyquist diagram often includes a semicircle part that depicts charge transfer resistance (inversely proportional to conductivity) and a linear part representing a diffusion limiting process. For example, the Nyquist figure in Figure 6.6 displays a straight line for bare electrode, COAC-1, and COAC-2 modified GCE at lower frequencies. This line denotes an electrochemical process diffusion limiting phase. COAC-1 has a semi-circle with a diameter smaller than the COAC-2 and the bare electrode. The small semi-circle signifies that COAC-1 has a higher conductivity than the other two electrodes and can promote electron transfer of $[Fe(CN)_6]^{3-/4}$ and facilitate the detection of UA and DA. The heavy interaction between the three unpaired electrons in the 3d orbital of Co^{2+} and the antibonding π-orbitals of the aniline may be attributed to the material's conductivity. The interaction causes delocalization of the π-electronic charge on the aniline, lowering the energy gap and increasing conductivity [25]. The conductivity can also be ascribed to the charge hopping mechanism between the metal ion and the aniline moiety [26].

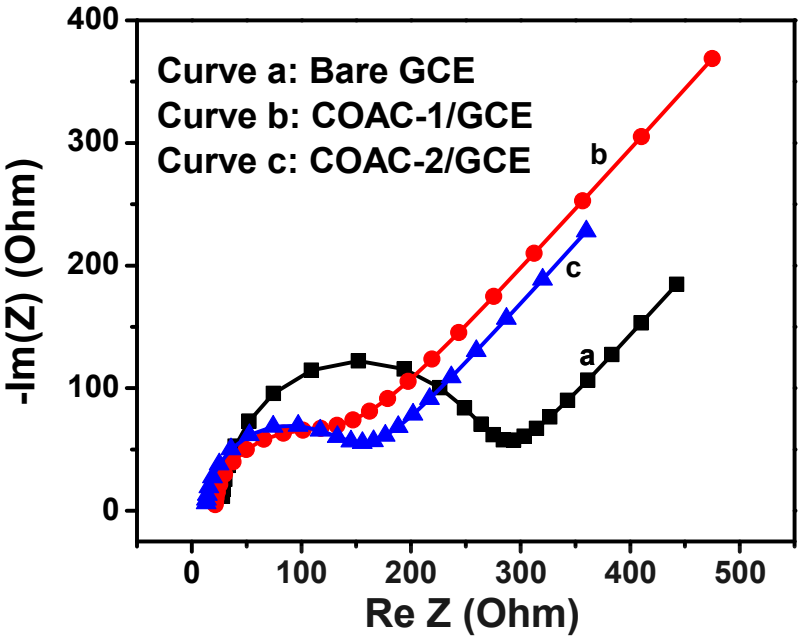

Figure 6.6: Nyquist plot of bare electrode and modified electrodes.

6.3.8 Electrochemical oxidation of UA and DA

The electrochemical response of bare GCE, COAC-1/GCE, and COAC-2/GCE was examined using cyclic voltammetry (CV). The cyclic voltammograms for the bare electrode in the presence of 60 µM of UA within a potential region of -0.2 V and 0.6 V at a 50 mV/s scan rate are exemplified in Figure 6.7A. The figure shows that upon UA's addition, the COAC-1/GCE's displayed a higher oxidation peak response than the bare GCE owing to its large surface area. Upon addition of sulfur (COAC-2), the current value reduced a little. Therefore, the COAC-1 was used for further studies. The cyclic voltammogram for the COAC-1/GCE modified electrode upon variation of UA's concentration from 20 µM to 180 µM shows a steady increase in current values (Figure 6.7B). The oxidation process of UA at the electrode also indicates a change in the peak current position to the region of larger potential values indicating that the oxidation process is irreversible.

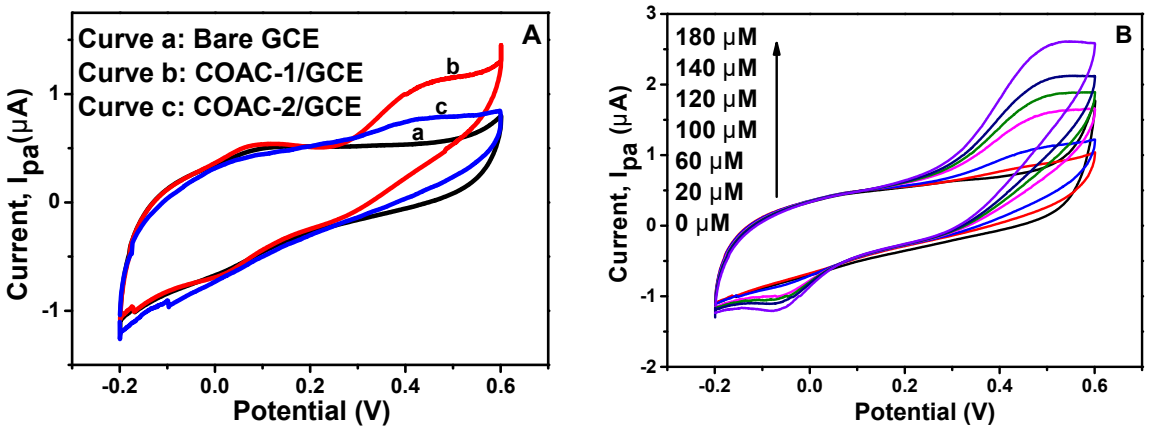

Figure 6.7: (A) Cyclic voltammograms of bare GCE and COAC-1/GCE in the presence of 60 µM uric acid **(B)** Cyclic voltammograms of COAC-1/GCE upon an increase in UA's concentration.

Figure 6.8A shows the electrocatalytic response of the bare GCE, COAC-1/GCE, and COAC-2/GCE in the presence of 40 µM DA. It could be noticed that the COAC-1/GCE exhibited a higher peak current response than both bare GCE and COAC-2/GCE in the presence of dopamine. Therefore, further studies were carried out using COAC-1/GCE. The decrease in the current value for UA and DA's detection with COAC-2/GCE could result from its more agglomerated form with the introduction of sulfur.

Investigation of the electrochemical response of COAC-1/GCE in the presence of varying DA concentrations is as shown in Figure 6.8B. A steady rise of the current response was noticed upon increasing the DA concentration from 20 µM to 220 µM, which can be ascribed to the enhanced electron transfer in the electrode's surface. A probable mechanism for UA and DA oxidation is as shown in Scheme 6.2 [27].

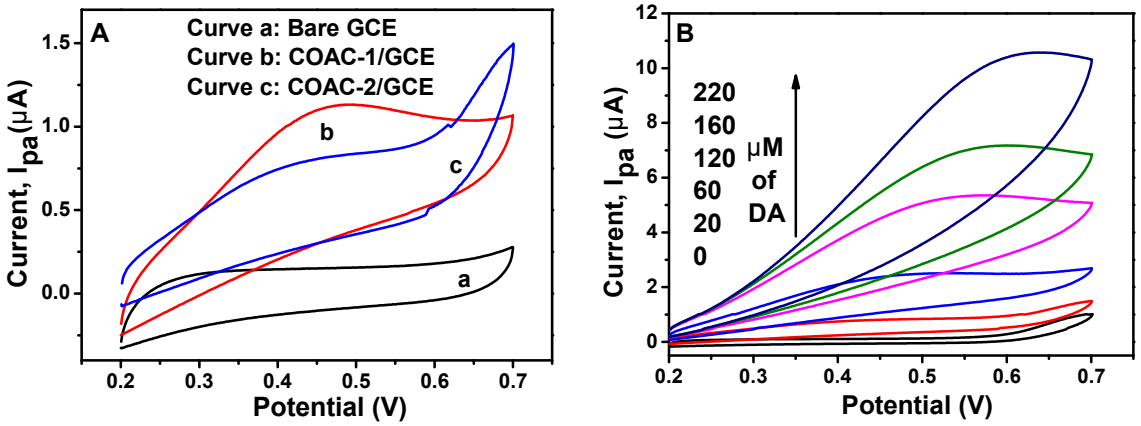

Figure 6.8: (A) Cyclic voltammograms of 40 µM DA at bare GCE, COAC-1/GCE, and COAC-2/GCE **(B)** Cyclic voltammograms of COAC-1/GCE with increasing concentration of DA (Using 10 mM PBS at a 50 mV/s scan rate.

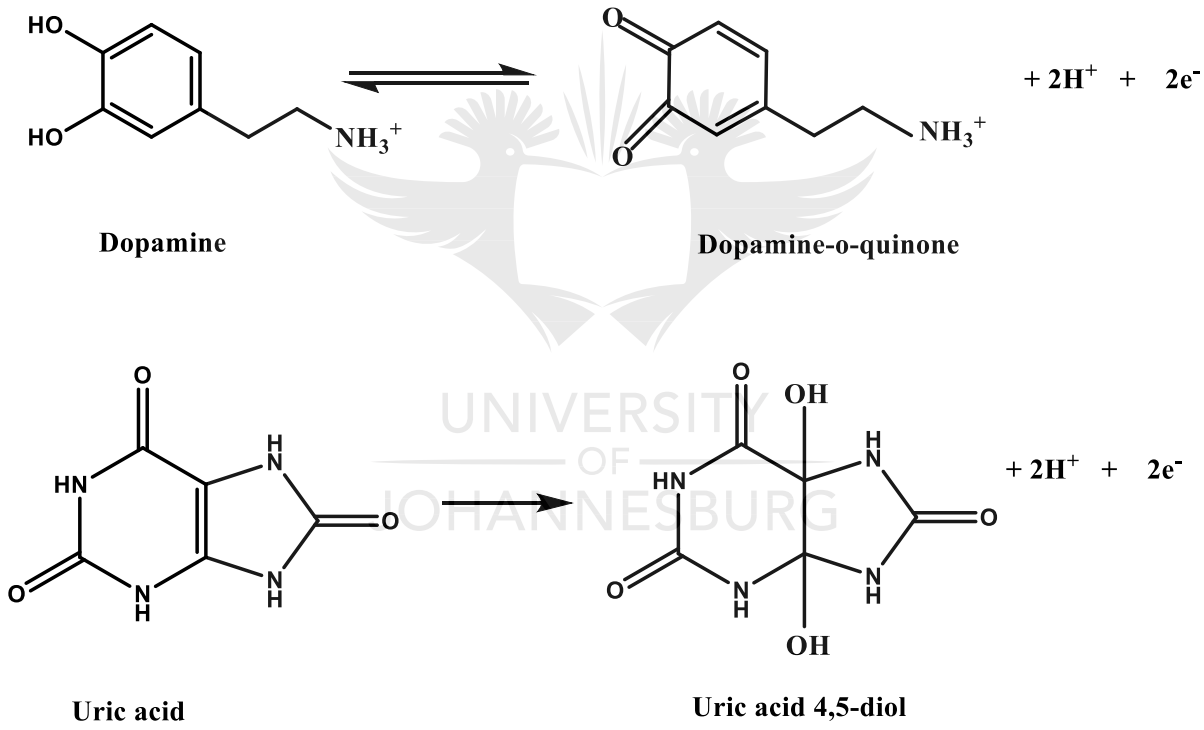

Scheme 6.2: Probable mechanism of oxidation of dopamine and uric acid at COAC-1/GCE.

From the above scheme, the exchange of two protons and electrons occurs both for the oxidation of UA and DA. Thus, the functional group -OH of the dopamine is oxidized to a ketonic group to form dopamine-o-quinone while uric acid is oxidized to uric acid 4,5-diol.

6.3.9 Square wave voltametric detection of UA and DA

COAC-1 electrocatalytic performance for UA and DA sensing was also investigated by square wave voltammetry technique under a scan rate of 50 mV/s, a frequency of 10 Hz, and

a pulse width of 25 mV. The graph showing the square wave voltammetric detection in Figure 6.9 (A) and (B) indicates a steady rise in current response as each UA and DA's concentration increased. The current increase proves that the COAC-1 modified electrode's electrocatalytic response for UA and DA sensing is linearly dependant on their concentrations. In the absence of the analytes, no typical oxidation peak was found within the potential window implemented. The calibration curves (concentration of UA and DA as a function of current) with regression coefficients 0.99885 and 0.99637 were plotted to derive the detection limit and sensitivity (LOD) from their square wave voltammograms. The sensitivity of UA was calculated to be 0.0834 μA $\mu M^{-1}cm^{-2}$ and a LOD of 9.26 μM under a linear range of 20 – 280 μM. The sensitivity of DA was achieved to be 0.2121 μA $\mu M^{-1}cm^{-2}$ and a LOD of 9.52 μM under a linear range of 10 – 200 μM. The detection limit and linear range of the developed sensor for UA and DA detection were compared with reports in the literature as displayed in Table 6.2. The comparison demonstrates that the analytical variables are better than or similar to those of previous studies.

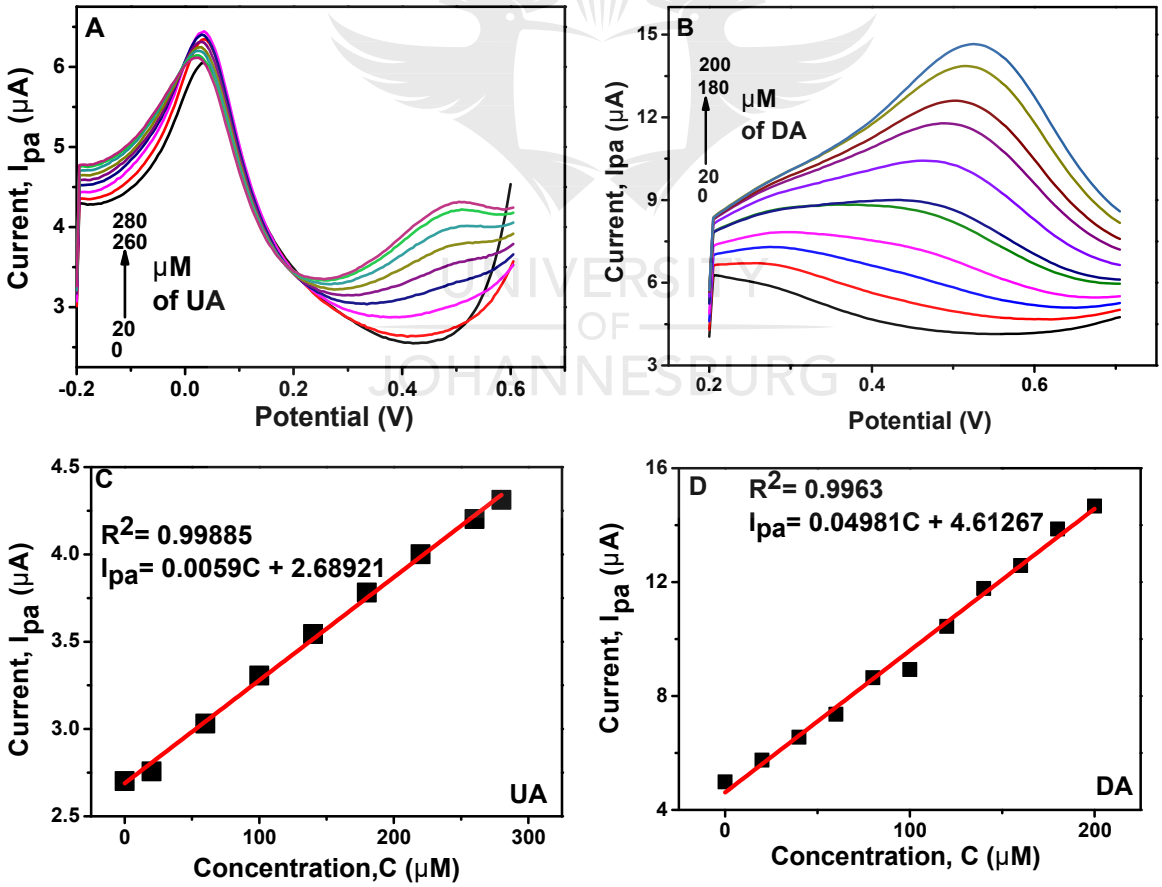

Figure 6.9: Square wave voltammetric response of COAC-1/GCE with varying concentrations of **(A)** Uric acid **(B)** Dopamine. **(C)** calibration plot for peak current against UA's concentration. **(D)** calibration plot for peak current against DA's concentration.

Table 6.2: Comparison of the proposed sensor with other modified electrodes

Modified electrode	Linear range (µM)		Detection limit (µM)		References
	UA	DA	UA	DA	
RGNA[a]	20-170	30 -190	6.4	7.5	[28]
AuNP@MoS_2/GCE	10 -7 x 10^3	0.05 - 4 x 10^3	10	0.05	[29]
CS[b]/GR[c]	2.0 - 45	1.0 - 24	2	1	[30]
GR	6.0 - 1330	5.0 - 710	0.82	2.0	[31]
Pt-Au hybrid	21-336	24-384	21	24	[32]
Trp-GCE[d]	10-1000	0.5-110	12.9	0.29	[33]
CNNS-GO[e]	10-200	1-20	10	10	[34]
ZnO NWA/GFE[f]	0.5-40	0.5-40	0.5	0.5	[35]
COAC[g]	20-280	10 -200	9.26	9.52	This work

[a] Recessed gold nanoelectrode array

[b] Chitosan

[c] Graphene

[d] Tryptophan-functionalized graphene nanocomposite modified glassy carbon electrode

[e] Graphitic carbon nitride nanosheets doped graphene oxide

[f] ZnO nanowire arrays modified 3D graphene foam electrode

[g] Cobalt aniline complex

6.3.10 Selectivity test

The amperometric technique was adopted to investigate the COAC-1 electrode's selectivity towards UA and DA. This was performed by the sequential addition of the separate analyte and some potential interfering species, as shown in Figure 6.10 (A) and (B). Uric acid's selectivity was performed by interfering with tryptophan, cysteine, histamine, ascorbic acid, alanine, and glucose in UA's presence. The catalyst selectivity towards DA recognition was studied by adding interferences such as glucose, ascorbic acid, cysteine, tryptophan, and histamine. The result in Figures 6.10(A) and (B) indicates that the interferences were irresponsive towards UA and DA's amperometric signal. The unresponsiveness implies that the developed sensor exhibits high specificity towards the recognition of UA and DA.

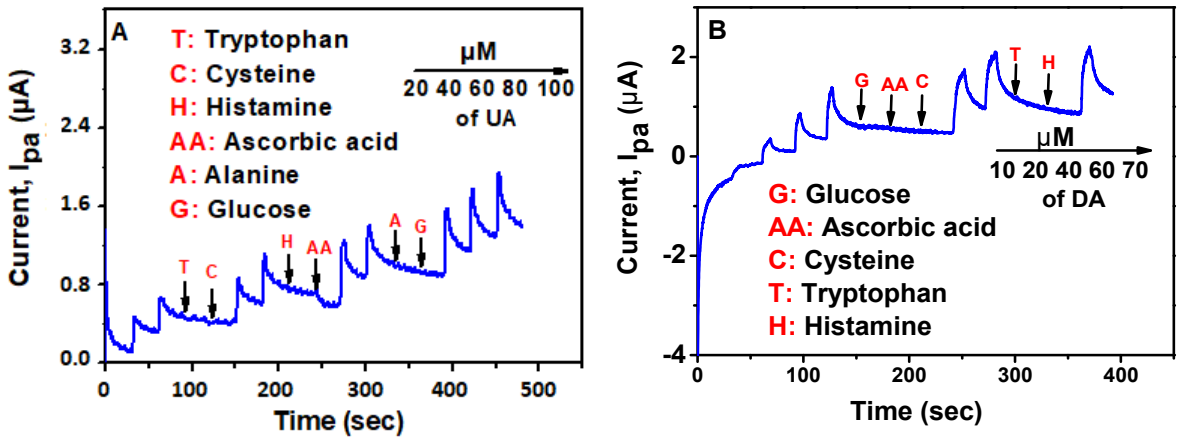

Figure 6.10: Amperometric current response of **(A)** Uric acid in the presence of tryptophan, cysteine, histamine, ascorbic acid, alanine, and glucose under an applied potential of 0.45. **(B)** Dopamine at a potential of 0.40 V in the presence of glucose, ascorbic acid, cysteine, tryptophan, and histamine (Using 10 mM PBS solution at 50 mV/s scan rate.

6.4 Sub-conclusion

In conclusion, the Co-aniline complex was successfully synthesized using a simple complexation procedure. On further reaction with sulfur, the complex material yielded no change but rather a more agglomerated complex. The agglomerated complex materials were confirmed with various characterization techniques, including UV, ^{1}HNMR, SEM, TEM, FTIR, XRD, and elemental analysis. The comparative study of the material with bare GCE shows the material's excellent property ascribed to the electrical conductivity due to the delocalization of the π-electric charges within the complex. The Co-aniline complex material was employed as an electrochemical sensing platform for the detection of UA and DA. The modified electrode sensor exhibited remarkably electrocatalytic activity towards UA and DA, including good sensitivity and selectivity, detection limit, and broad linear range. The Co-aniline complex material's response to UA and DA's electrochemical detection indicates its possibility for other biological molecule recognition, including nucleic acids, enzymes, and proteins, if the catalyst could be modified. These biomolecules or surfactants could also be used to modify the complex materials to enhance biomolecule recognition in future studies.

6.5 References

[1] Manzak, A., & Yildiz, Y. (2019). Introductory Chapter: Cobalt Compounds and Applications. *Cobalt Compounds and Applications*, 3.

[2] Pankhurst, Q. A., Connolly, J., Jones, S. K., & Dobson, J. (2003). Applications of magnetic nanoparticles in biomedicine. *Journal of Physics D: Applied physics*, *36*(13), R167.

[3] Askarinejad, A., Bagherzadeh, M., & Morsali, A. (2010). Catalytic performance of Mn3O4 and Co3O4 nanocrystals prepared by sonochemical method in epoxidation of styrene and cyclooctene. *Applied Surface Science*, *256*(22), 6678-6682.

[4] Eshkalak, S. K., Khatibzadeh, M., Kowsari, E., Chinnappan, A., & Ramakrishna, S. (2018). New functionalized graphene oxide based on a cobalt complex for black electrophoretic ink applications. *Journal of Materials Chemistry C*, *6*(32), 8726-8732.

[5] Sanpo, N., Berndt, C. C., Wen, C., & Wang, J. (2013). Transition metal-substituted cobalt ferrite nanoparticles for biomedical applications. *Acta Biomaterialia*, *9*(3), 5830-5837.

[6] Shinde, V. R., Mahadik, S. B., Gujar, T. P., & Lokhande, C. D. (2006). Supercapacitive cobalt oxide (Co3O4) thin films by spray pyrolysis. *Applied Surface Science*, *252*(20), 7487-7492.

[7] Wahab, R., Ahmad, N., Alam, M., & Ahmad, J. (2021). The development of cobalt oxide nanoparticles-based electrode to elucidate the rapid sensing of nitrophenol. *Materials Science and Engineering: B*, *265*, 114994.

[8] Kubendhiran, S., Thirumalraj, B., Chen, S. M., & Karuppiah, C. (2018). Electrochemical co-preparation of cobalt sulfide/reduced graphene oxide composite for electrocatalytic activity and determination of H_2O_2 in biological samples. *Journal of Colloid and Interface Science*, *509*, 153-162.

[9] Xu, S., Su, C., Wang, T., Ma, Y., Hu, J., Hu, J., Hu, N., Su, Y., Zhang, Y., & Yang, Z. (2018). One-step electrodeposition of nickel cobalt sulfide nanosheets on Ni nanowire film for hybrid supercapacitor. *Electrochimica Acta*, *259*, 617-625.

[10] Wu, W., Yu, B., Wu, H., Wang, S., Xia, Q., & Ding, Y. (2017). Synthesis of tremella-like CoS and its application in sensing of hydrogen peroxide and glucose. *Materials Science and Engineering: C*, *70*, 430-437.

[11] Biscaglia, S., Ceconi, C., Malagù, M., Pavasini, R., & Ferrari, R. (2016). Uric acid and coronary artery disease: an elusive link deserving further attention. *International Journal of Cardiology*, *213*, 28-32.

[12] Kondori, T., Tajik, S., Akbarzadeh-T, N., Beitollahi, H., Graiff, C., Jang, H. W., & Shokouhimehr, M. (2021). Synthesis and characterization of bipyridine cobalt (ii) complex modified graphite screen printed electrode: an electrochemical sensor for simultaneous detection of acetaminophen and naproxen. *RSC Advances*, *11*(5), 3049-3057.

[13] Sajjan, V. A., Mohammed, I., Nemakal, M., Aralekallu, S., Kumar, K. H., Swamy, S., & Sannegowda, L. K. (2019). Synthesis and electropolymerization of cobalt tetraaminebenzamidephthalocyanine macrocycle for the amperometric sensing of dopamine. *Journal of Electroanalytical Chemistry*, *838*, 33-40.

[14] Hu, F. X., Hu, T., Chen, S., Wang, D., Rao, Q., Liu, Y., Dai, F., Guo, C., Yang, H.B. & Li, C. M. (2021). Single-atom cobalt-based electrochemical biomimetic uric acid sensor with wide linear range and ultralow detection limit. *Nano-micro Letters*, *13*(1), 1-13.

[15] Lima, W. G., Martins-Santos, M. E. S., & Chaves, V. E. (2015). Uric acid as a modulator of glucose and lipid metabolism. *Biochimie*, *116*, 17-23.

[16] Heien, M. L., Khan, A. S., Ariansen, J. L., Cheer, J. F., Phillips, P. E., Wassum, K. M., & Wightman, R. M. (2005). Real-time measurement of dopamine fluctuations after cocaine in the brain of behaving rats. *Proceedings of the National Academy of Sciences*, *102*(29), 10023-10028.

[17] Choudhary, M., Brink, R., Nandi, D., Siwal, S., & Mallick, K. (2017). Gold nanoparticle within the polymer chain, a multi-functional composite material, for the electrochemical detection of dopamine and the hydrogen atom-mediated reduction of Rhodamine-B, a mechanistic approach. *Journal of Materials Science*, *52*(2), 770-781.

[18] Islam, R. U., Taher, A., Choudhary, M., Siwal, S., & Mallick, K. (2015). Polymer immobilized Cu (I) formation and azide-alkyne cycloaddition: A one potreaction. *Scientific Reports*, *5*(1), 1-8.

[19] Ghosh, S. K., Perla, V. K., & Mallick, K. (2020). Organic molecule stabilized bismuth iodide nanoparticles: a hybrid system with multifunctional physical properties. *Physical Chemistry Chemical Physics*, *22*(6), 3345-3351.

[20] Devi, N., Ghosh, S., & Mallick, K. (2019). Supercapacitive performance of highly dispersed bismuth sulfide nanoparticles in organic matrix: The role of sulphur source. *Inorganic Chemistry Communications*, *103*, 93-99.

[21] Lee-Thorp, J. A., Rüede, J. E., & Thornton, D. A. (1978). The infrared spectra (3500—150 cm-1) of aniline complexes of cobalt (II), nickel (II), copper (II) and zinc (II) halides. *Journal of Molecular Structure*, *50*(1), 65-71.

[22] Skauge, T., Turel, I., & Sletten, E. (2002). Interaction between ciprofloxacin and DNA mediated by Mg^{2+} -ions. *Inorganica Chimica Acta*, *339*, 239-247.

[23] Li, X. H., Wu, B., Huang, J. E., Zhang, J., & Liu, Z. F. (2003). Fabrication and characterization of well-dispersed single-walled carbon nanotube/polyaniline composites. *Carbon (New York, NY)*, *41*(8), 1670-1673.

[24] Friedel, R. A., & Orchin, M. (1958). Ultraviolet Spectra of Aromatic Compounds Chemistry.

[25] El-Saved, B. A., Shaaban, S., Sallam, M. M., & Emara, A. A. A. (1996). Temperature dependence of the electrical conductivity of salicylaldehyde hydrazone and its transition metal complexes. *Journal of Materials Science Letters*, *15*(10), 883-885.

[26] Fischer, P., & Seanor, D. A. (1982). Dielectric breakdown phenomena in polymers. In *Electrical Properties of Polymers* (pp. 320-327). New York: Academic Press.

[27] da Silva, R. P., Lima, A. W. O., & Serrano, S. H. (2008). Simultaneous voltammetric detection of ascorbic acid, dopamine and uric acid using a pyrolytic graphite electrode modified into dopamine solution. *Analytica Chimica Acta*, *612*(1), 89-98.

[28] Zhang, Y., Zhou, Q., Zhao, W., Chu, W., & Zheng, J. (2016). Array of recessed gold nanoelectrodes formed with polymethylmethacrylate for individual detection of ascorbic acid, dopamine and uric acid. *Electrochimica Acta*, *212*, 25-31.

[29] Sun, H., Chao, J., Zuo, X., Su, S., Liu, X., Yuwen, L., Fan, C., & Wang, L. (2014). Gold nanoparticle-decorated MoS_2 nanosheets for simultaneous detection of ascorbic acid, dopamine and uric acid. *RSC Advances*, *4*(52), 27625-27629.

[30] Han, D., Han, T., Shan, C., Ivaska, A., & Niu, L. (2010). Simultaneous determination of ascorbic acid, dopamine and uric acid with chitosan-graphene modified electrode. *Electroanalysis*, *22*(17-18), 2001-2008.

[31] Qi, S., Zhao, B., Tang, H., & Jiang, X. (2015). Determination of ascorbic acid, dopamine, and uric acid by a novel electrochemical sensor based on pristine graphene. *Electrochimica Acta*, *161*, 395-402.

[32] Thiagarajan, S., & Chen, S. M. (2007). Preparation and characterization of PtAu hybrid film modified electrodes and their use in simultaneous determination of dopamine, ascorbic acid and uric acid. *Talanta*, *74*(2), 212-222.

[33] Lian, Q., He, Z., He, Q., Luo, A., Yan, K., Zhang, D., Lu, X., & Zhou, X. (2014). Simultaneous determination of ascorbic acid, dopamine and uric acid based on tryptophan functionalized graphene. *Analytica Chimica Acta*, *823*, 32-39.

[34] Zhang, H., Huang, Q., Huang, Y., Li, F., Zhang, W., Wei, C., Chen, J., Dai, P., Huang, L., Huang, Z., & Kang, L., (2014). Graphitic carbon nitride nanosheets doped graphene oxide for electrochemical simultaneous determination of ascorbic acid, dopamine and uric acid. *Electrochimica Acta*, *142*, 125-131.

[35] Yue, H. Y., Huang, S., Chang, J., Heo, C., Yao, F., Adhikari, S., ... & Lee, Y. H. (2014). ZnO nanowire arrays on 3D hierachical graphene foam: biomarker detection of Parkinson's disease. *ACS Nano*, *8*(2), 1639-1646.

CHAPTER 7
CONCLUSIONS AND RECOMMENDATIONS

7.1 Summary of Findings and Conclusions

This project successfully illustrated the synthesis of aniline-based transition metal complexes using a simple complexation method and their application to detect some bioactive molecules. The synthesis approach allows aniline to precipitate the metal salts by complexation between aniline moiety and the transition metals. The ambient reaction conditions, followed by centrifugation and drying, highlight this synthesis method. The complexes material's identity were elucidated by SEM, IR, ^{1}H, ^{13}C-NMR, UV-Vis, FTIR, XRD, XPS, and elemental analysis. The electrochemical behaviour of the complexes were studied upon modification on a glassy carbon working electrode using cyclic voltammetry and EIS. The complexes potential as electrochemical sensors for biologically active molecules has also been evaluated. It can be concluded that an organic matrix such as aniline proved to be a great complexing agent for the transition metals Bi, Co, and Ni. The ability of aniline to form a complex with those metals is a result of the single pair of electrons on the nitrogen atom present in the aniline structure.

It has been found that the synthesized complexes show good electrocatalytic activity for the recognition of biologically active molecules, including dopamine, iodine, uric acid, and cysteine. EIS studies prove that the material is conductive enough to facilitate the detection of the analytes of interest. Cyclic voltammetry primarily showed the bismuth aniline complex's potential to detect DA and iodine, cobalt aniline complex to detect UA and DA, and nickel aniline complex to detect cysteine. Furthermore, SWV illustrated that the three complexes were sensitive towards the listed molecules as they responded linearly towards the continual addition of the molecules in the different modified electrochemical systems. Lastly, chronoamperometry elucidated the three complexes' selective nature as they could create a linear response towards the continual addition of the individual molecules of interest. The CA studies showcased the selectivity of these complex materials to the analytes of interest in the presence of interferent species.

According to the electroanalytical data, the aniline transition metal complexes modified electrode outperforms the bare electrode and other complexes or nanomaterials reported in the literature. The sensors acted as suitable platforms for the detection of the different analytes with wide linear range ranging from 25 – 250 μM for iodine, 2.5 μM-220 μM for

cysteine, 20 – 280 μM for uric acid, 10 – 200 μM for dopamine. The sensors possess reasonable detection limits of 23.17 μM for iodine, 12.3 μM and 9.26 μM for dopamine, 2.09 μM for cysteine, and 9.52 μM for uric acid. The electrochemical studies showed that the transition metals and aniline had a synergistic catalytic effect on the oxidation of iodine, dopamine, cysteine, and uric acid. The significantly increased peak currents and reduced peak potentials greatly improved the analytical performance of the prepared sensors.

The aniline-based Bi, Co, and Ni metal complex materials possess the qualities of a credible sensing system for sensitive and selective detection of biologically active molecules. The use of these metal complexes will open up exploring other transition metals, complexing with aniline and its derivatives as modified electrodes for electroanalysis.

7.2 Recommendations for Future Work

This research revealed that the synthesis of aniline complexes with transition metals such as Bi, Ni, and Co using the simple complexation method is suitable for electrochemical sensor development. Aniline, which might, in the future, have the potential to contribute to advanced applications within the biomedical field, should be explored and optimized. Further research to chemically reduce the Bi, Ni, and Co metal in the complexes to their metallic states should be looked at, which would improve the material's conductivity. The complex material could also be modified with other materials to form a composite, further enhancing the sensitivity. This work could also be taken to the next level by conducting a real sample analysis of the biomolecules in samples such as urine and blood to check their suitability of the complex materials for electroanalysis. It would be essential to develop nano-complexes that will simultaneously detect multiple biological molecules at the same platform. It would also be interesting to explore other transition metals directly with aniline and study the ensuing complex for biomolecules' electrochemical sensing.

APPENDIX

Supplementary information

Chapter 4

Table S4.1: ^{1}H NMR data of the ligand and Bi (III) aniline complex

Ligand/complex	^{1}H and ^{13}C NMR data (ppm)
Aniline	^{1}H NMR = 7.08-7.05 (2H, t, *J* = 7.5 Hz, Ar), 6.65 (2H, d, *J* = 8.0 Hz, Ar), 6.57-6.55 (1H, t, *J* = 7.0 Hz, Ar), 4.97 (2H, br, NH_2)
Bi–Aniline	^{1}H NMR =7.04-7.01 (2H, t, *J* =7.5 Hz, Ar), 6.54-6.51 (2H, d, *J* = 6.25 Hz, Ar), 5.07 (2H, br, NH_2)

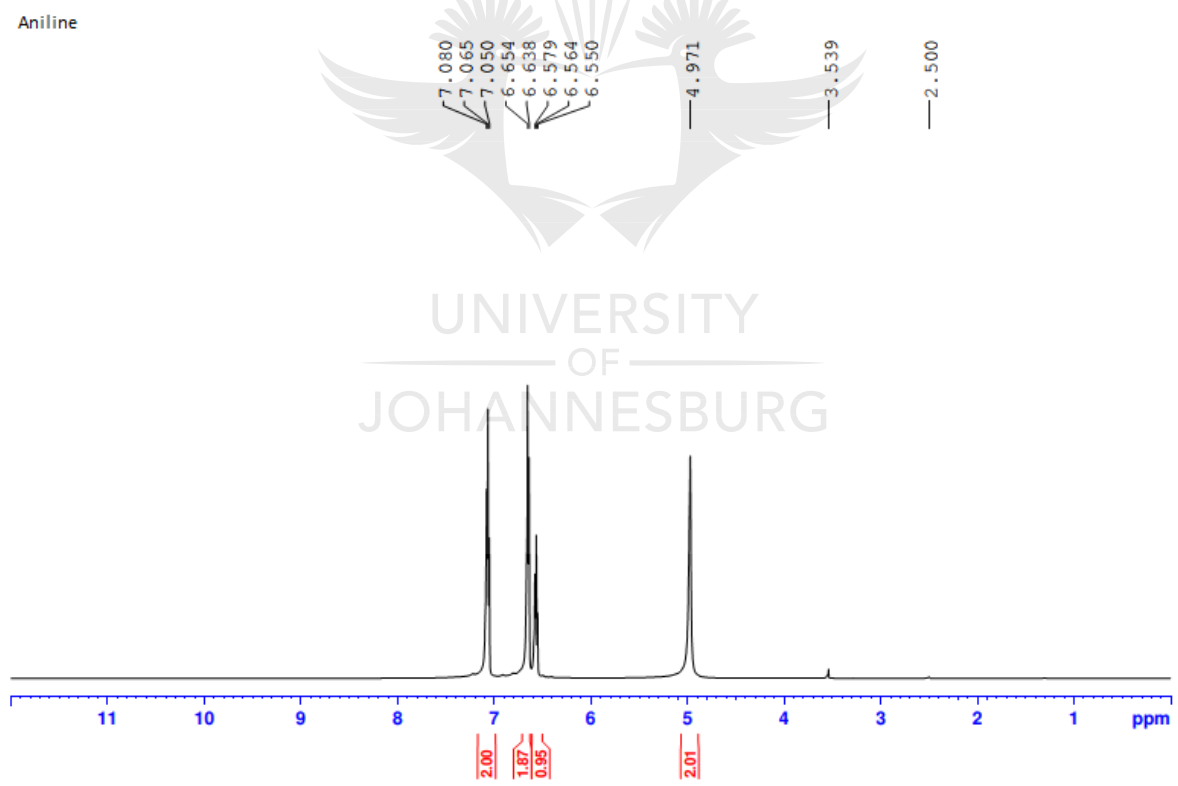

Figure S4.1: ^{1}H NMR spectrum of **Aniline** in DMSO

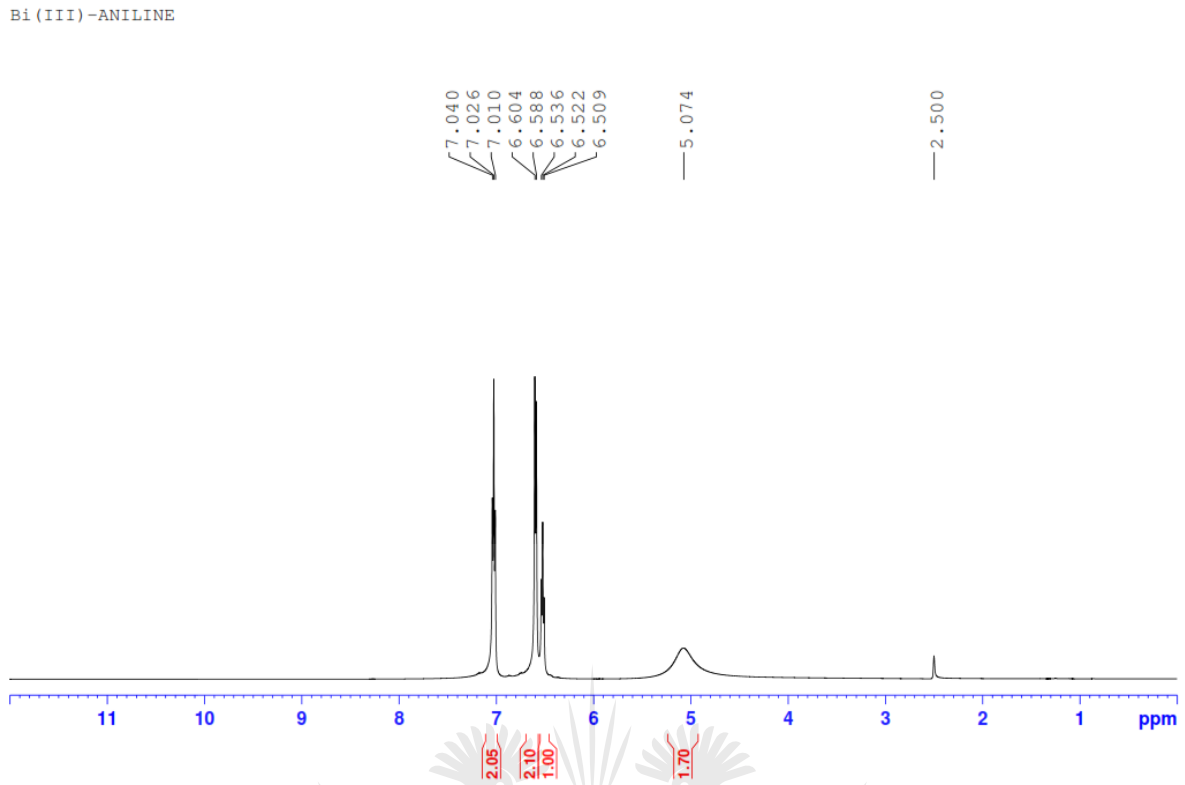

Figure S4.2: ^{1}H NMR spectrum B**i–Aniline** complex in DMSO-d_6

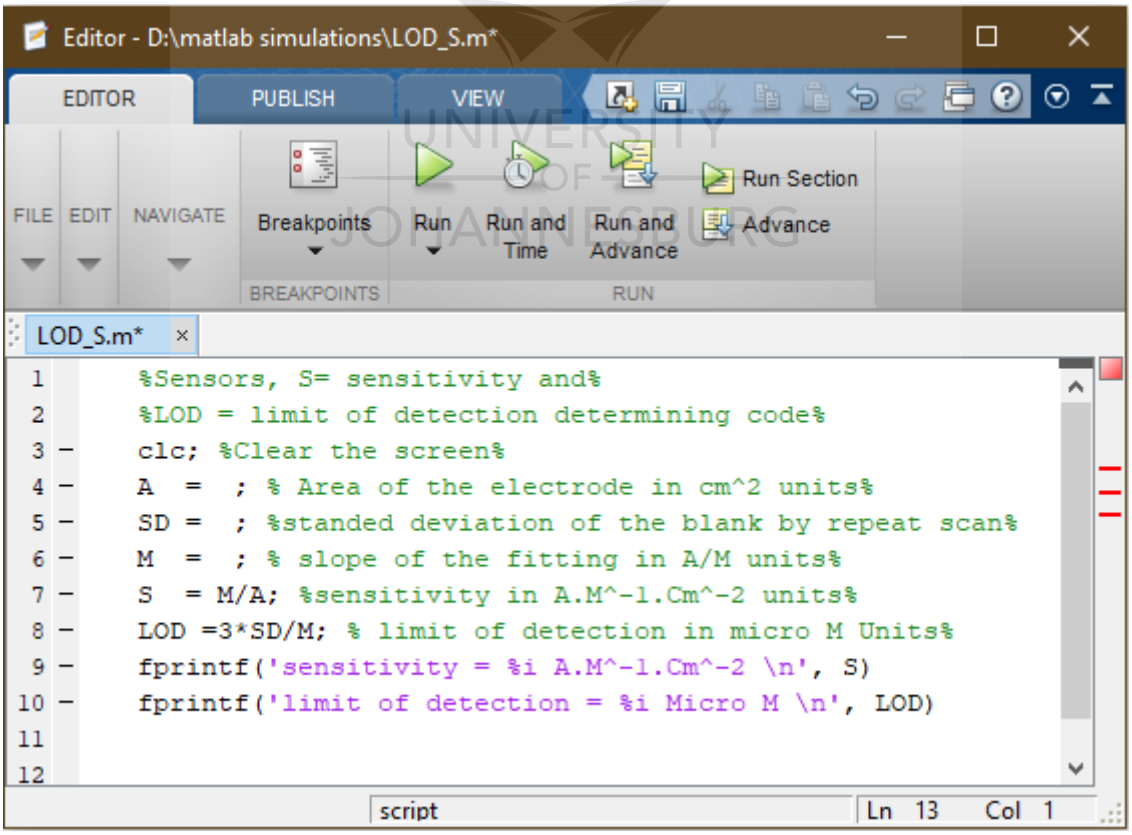

Figure S4.3: MATLAB code for the calculation of sensitivity and limit-of-detection

Chapter 5

Table S5.1: ^{1}H and ^{13}C NMR data of the ligand and Ni (II) aniline complex

Ligand/complex	^{1}H and ^{13}C NMR data (ppm)
Aniline	^{1}H NMR = 7.08-7.05 (2H, t, *J* = 7.5 Hz, Ar), 6.65 (2H, d, *J* = 8.0 Hz, Ar), 6.57-6.55 (1H, t, *J* = 7.0 Hz, Ar), 4.97 (2H, br, NH_2) $^{13}C\{H\}$NMR= 114.01, 115.87, 128.80, 148.45
Ni–Aniline	^{1}H NMR =7.12 (2H, s, Ar), 5.32 (3H, d, *J* = 7.5 Hz, Ar), 3.19 (2H, br, NH_2) $^{13}C\{H\}$NMR= 119.41, 129.21, 129.50, 139.93

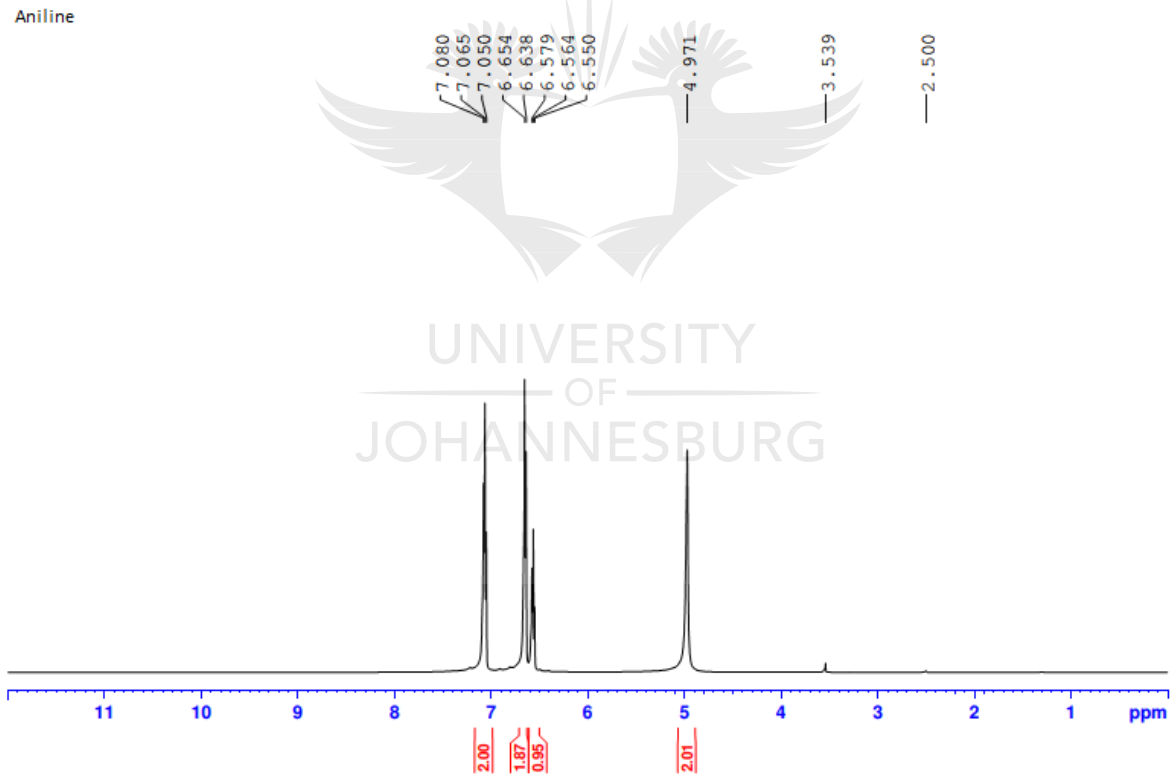

Figure S5.1: ^{1}H NMR spectrum of **Aniline** in DMSO

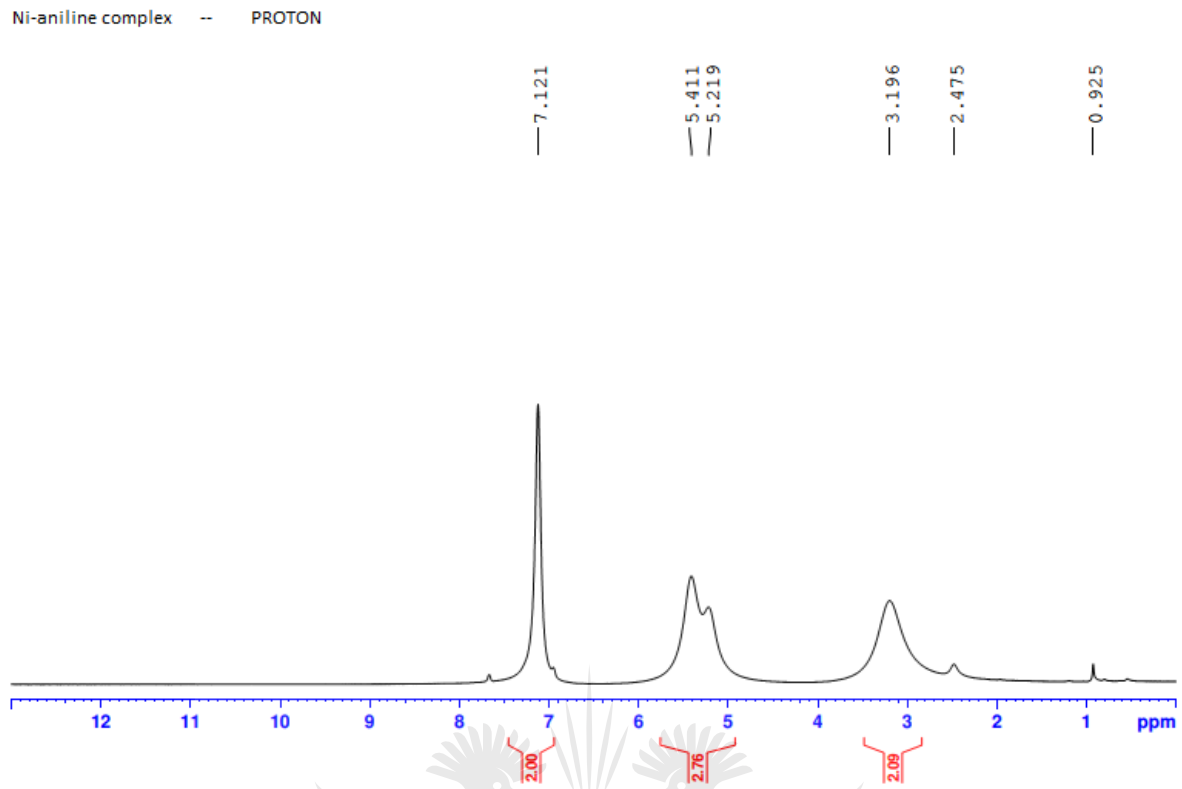

Figure S5.2: ^{1}H NMR spectrum of Ni–Aniline complex in DMSO-d_6

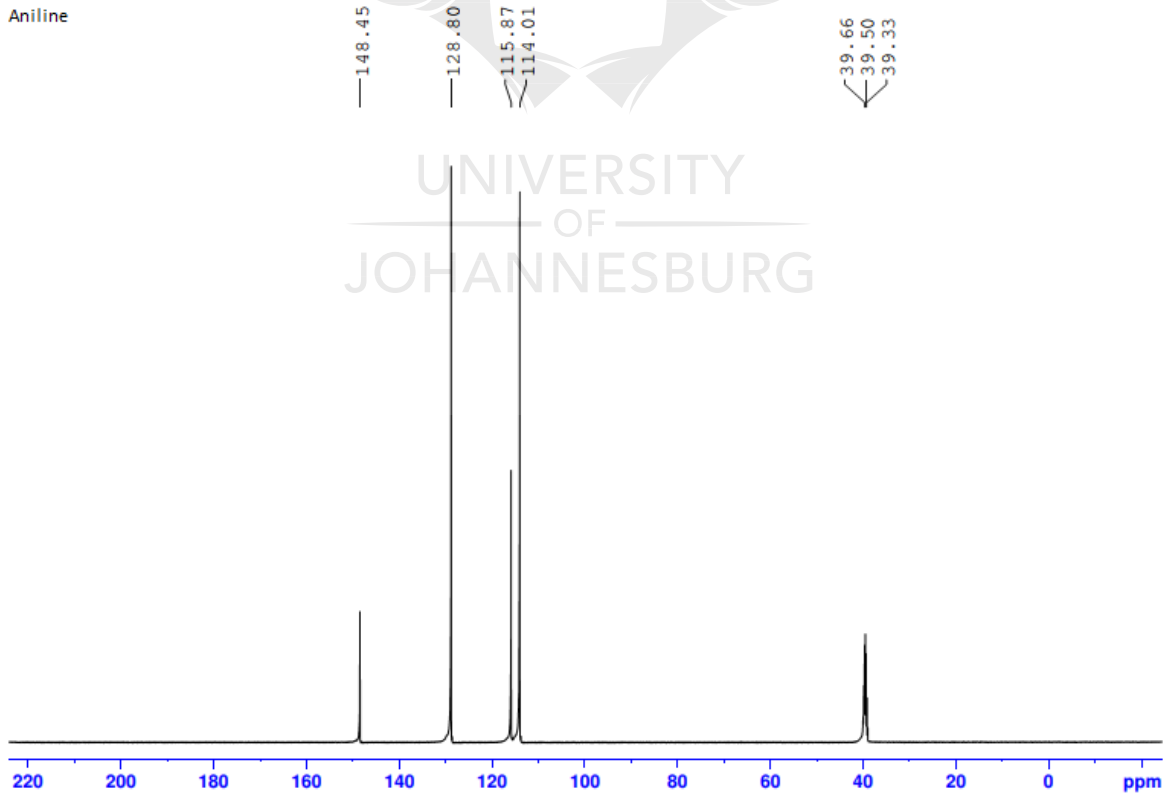

Figure S5.3: ^{13}C{H} NMR spectrum Aniline in DMSO-d_6

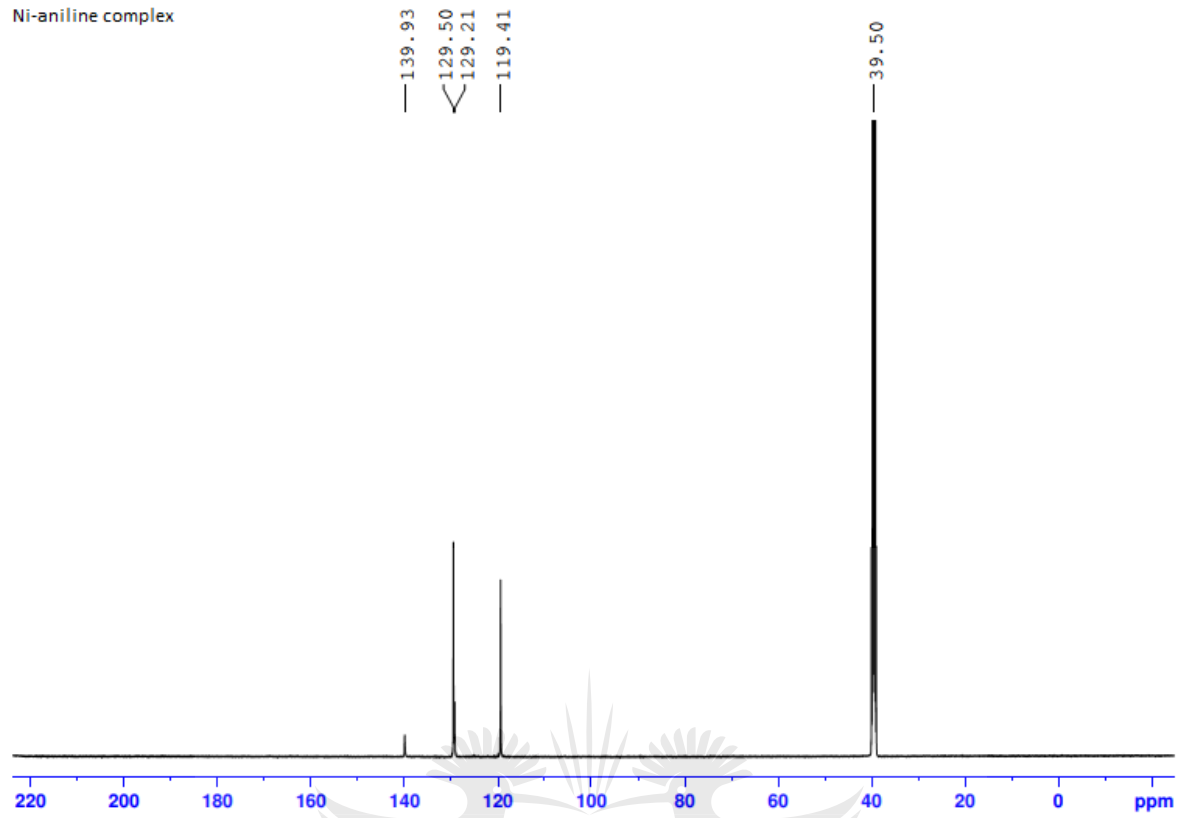

Figure S5.4: $^{13}C\{H\}$ NMR spectrum **Ni–Aniline** complex in DMSO-d_6

Table S5.2: Some structural parameters of Nickel (II) aniline complex

K	λ (Å)	Peak position 2θ (°)	FWHM B_{size} (°)	L (nm)	L (nm)Average
0,94	1,54178	7,78346	0,22579	36,86131229	27,34015056
0,94	1,54178	9,72534	0,22108	37,69549042	
0,94	1,54178	15,55985	0,20159	41,5738225	
0,94	1,54178	19,74247	0,32793	25,70214192	
0,94	1,54178	23,22609	0,83816	10,11412852	
0,94	1,54178	25,74984	0,26662	31,94761504	
0,94	1,54178	27,06986	0,30451	28,04810137	
0,94	1,54178	13,45277	0,18407	45,42443618	
0,94	1,54178	29,42216	0,54037	15,8875524	
0,94	1,54178	36,23364	0,30785	28,38024359	
0,94	1,54178	34,7398	3,73227	2,331152254	
0,94	1,54178	32,25315	0,26798	32,25560047	
0,94	1,54178	51,7328	0,48063	19,20036035	
0,94	1,54178	40,04899	0,64834	13,6317585	
0,94	1,54178	44,66376	2,07757	4,320920015	
0,94	1,54178	62,28485	0,61242	15,84194234	
0,94	1,54178	16,39215	0,15632	53,66820142	
0,94	1,54178	11,4106	0,19474	42,85232645	

Chapter 6

Table S6.1: ^{1}H NMR data of the ligand and Cobalt aniline complex

Ligand/complex	^{1}H and ^{13}C NMR data (ppm)
Aniline	^{1}H NMR = 7.08-7.05 (2H, t, *J* = 7.5 Hz, Ar), 6.65 (2H, d, *J* = 8.0 Hz, Ar), 6.57-6.55 (1H, t, *J* = 7.0 Hz, Ar), 4.97 (2H, br, NH_2)
Co–Aniline (COAC-2)	^{1}H NMR = 7.23-7.20 (2H, t, *J* = 7.75, Ar), 6.90 (3H, d, *J* = 7.5 Hz, Ar), 7.79 (1H, br, NH)

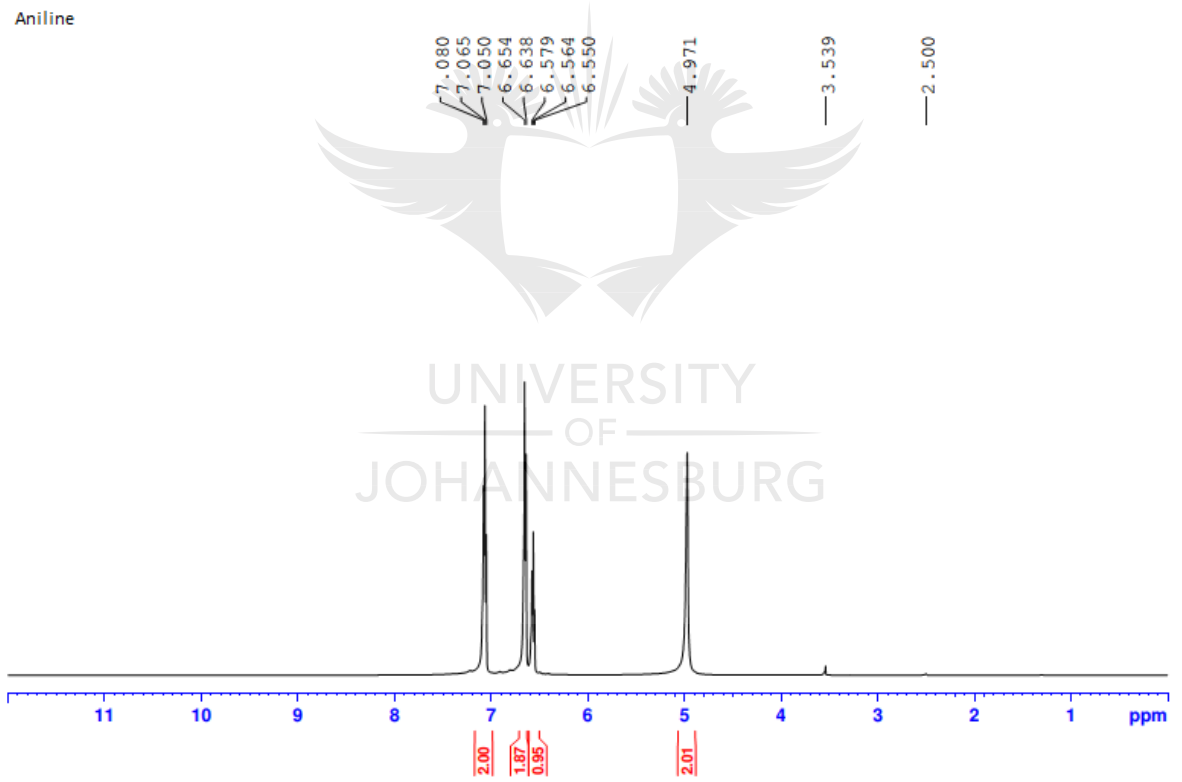

Figure S6.1: ^{1}H NMR spectrum of **Aniline** in DMSO

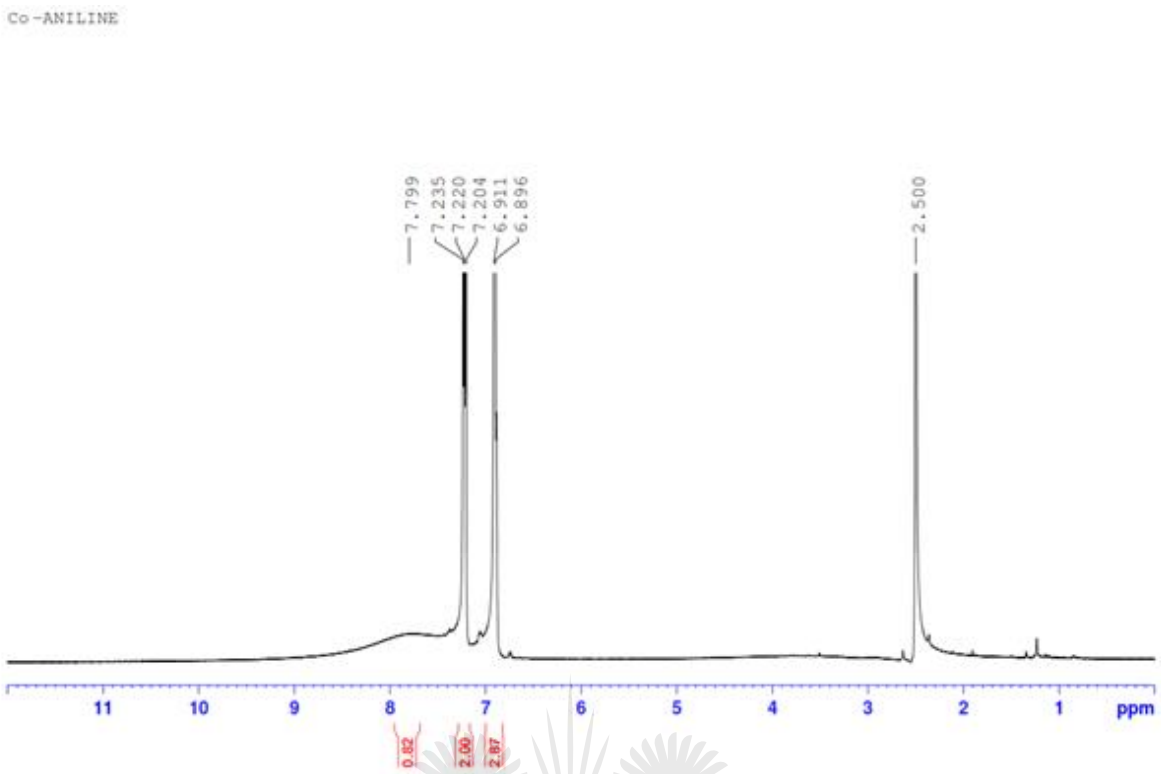

Figure S6.2: ^{1}H NMR spectrum **Co–Aniline** complex in DMSO-d_6